

Investigations for Fuel Recycling in LWRs

by

Ludwig Send

A diploma thesis
presented to the Forschungszentrum Karlsruhe (FZK)
in fulfillment of the
thesis requirements for the degree of
Diploma
in
Mechanical Engineering

Karlsruhe, Germany, October 2005

©Ludwig Send, 2005

I hereby declare that I am the sole author of this thesis.

I authorize the Forschungszentrum Karlsruhe (FZK) to lend this thesis to other institutions or individuals for the purpose of scholarly research.

Ludwig Send

I further authorize the Forschungszentrum Karlsruhe (FZK) to reproduce this thesis by photocopying or other means, in total or in part, at the request of other institutions or individuals for the purpose of scholarly research.

Ludwig Send

Abstract

This thesis is addressed to investigations on the effects of high and very high burn-ups in modern Light Water Reactor (LWR) fuels. The impact of two different LWR system parameters on the isotopic fraction buildup during depletion process have been profoundly investigated, namely the soluble boron concentration in Pressurized Water Reactors (PWRs) and the moderator to fuel ratio as a lattice parameter. The emphasis lies on the buildup of minor actinides and plutonium, especially plutonium Pu^{238} which is of particular interest for issues of fuel cycle's back-end and proliferation.

These investigations analyze in detail the impact of the two aforementioned parameters, and discuss the potential difficulties when burn-up is raised. Results are plotted into graphs which are also part of this work. As for the fuel, a uranium-oxide fuel with 5% enrichment in U^{235} has been used for all investigations.

The calculations have been accomplished by using the KARBUS module of the Karlsruhe Program System (KAPROS). The KARBUS module calculates fuel burn-up applying a model of a one-dimensional tree-zone Wigner-Seitz fuel cell.

In the first part of this work a validation of the KARBUS code has been done. This became necessary after the code had undergone various changes and adjustments. The validation work was a recalculation of the Isotope Correlation Experiment (ICE) accomplished in the nuclear power plant of Obrigheim, Germany, in the late seventies. The experimental data was used for evaluation. Validation results are also included in this thesis.

Acknowledgments

First of all I would like to express my deepest gratitude to my supervisor, Dr. C.H.M. Broeders, for his scientific guidance, for sharing his impressive knowledge of science and his copious support. I very much appreciated that his door was literally always open for consultations. Moments of difficulties and ignorance typically vanished immediately when entering his office. Usually, the given explanations and his advice finally clarified all obscurities, opening the wide field of nuclear power reactors to me. His patience always gave me a warm welcome! I believe that in many cases it might have not been easy to introduce me to the basics of scientific working.

I am very grateful to Prof. Dr. Volker Heinzl and Dr. C.H.M. Broeders for the opportunity to perform that work at the Institute for Reactor Safety (IRS). I also kindly acknowledge their encouragement and support for my taking part in the Frédéric Joliot and Otto Hahn summer school which was a great experience and especially helpful for my work.

I would also like to express my thanks to the Institute for Reactor Safety, for letting me become part of the team. In particular I would like to mention Dr. Victor Sanchez-Espinoza, Dr. Bruno Merk and Dr. Ron Dagan with whom I shared my problems in fruitful discussions. I also gratefully acknowledge the work of our secretaries.

I would like to mention Wolfgang Stamm for introducing and supporting me with \LaTeX , this welcome alternative to conventional word-processors, and Robert Send for his careful revision, correcting minor linguistic deficiencies.

I want to give my special thanks to the Fuchs family for giving me accommodation, Mrs Fuchs for her lovely cooking and Mr Fuchs for sharing his profound knowledge in power-plant technique with me in many discussions. Thank you Uta Fuchs for bearing with me, for your love and patience. To all those I did not mention, to my friends, colleagues and all those I might have forgot: Many many thanks!

I dedicate this diploma thesis with particular esteem to my parents, for their love and support throughout my life, guiding me to what I achieved until today.

Ludwig Send

Contents

List of Tables	vii
List of Figures	ix
1 Introduction	1
2 Principles of Burn-up Calculation	5
2.1 The k - Factor Model	5
2.2 The Time-dependent Boltzmann-Equation	10
3 Validation of the KAPROS / KARBUS Code	19
3.1 Introductory Remarks on Validation	19
3.2 Remarks on Software and Calculation Model	20
3.2.1 The KAPROS System	20
3.2.2 The KARBUS Procedure	22
3.2.3 The Burn-up Model	27
3.3 Validation Work Accomplishment	28
3.3.1 Validation settings	28
3.3.2 Validation results	31
3.4 Summary	38
4 Basic Requirements of High Burn-up fuels in LWRs	41
4.1 Economic Benefits of High Burn-ups	42
4.2 Implications on the Core System	44
4.3 High Burn-up Fuels	46
4.4 Soluble and Solid Burnable Poisons	47
4.5 Isotope Fraction Buildup	49
4.6 Spent Nuclear Fuel	50

4.7	Summary:	51
5	Parametric Investigations on High Burn-ups in LWRs	53
5.1	Impact of Boric Acid Concentration on High Burn-ups	54
5.1.1	Introductory Remarks on Boric Acid	54
5.1.2	Input Adjustments for Calculations	58
5.1.3	Calculations on Soluble Boron Concentrations	62
5.1.4	Results and Discussion	64
5.2	Impact of wider Lattices	75
5.2.1	Input Adjustments for Calculations of Wider Lattices	75
5.2.2	Lattice Effects on Soluble Boron	75
5.2.3	Results for Lattice Variation	79
5.3	Buildup of Pu^{238}	80
5.4	Summary	84
6	Conclusion and Prospects	85
A	Appendix of Chapter No.3	A1
A.1	ksuxgo	A1
A.2	input.karbus	A2
A.3	ICE Validation Charts	A15
A.4	ICE Calculated Charts	A31
B	Appendix of Chapter No.5	B1
B.1	LWR High Burn-ups, constant boron modeling	B1
B.2	LWR High Burn-ups, variable boron modeling No.1	B5
B.3	LWR High Burn-ups, variable boron modeling No.2	B12
B.4	LWR High Burn-ups, variation of lattices	B22

List of Tables

2.1	Signs and symbols for Boltzmann's Equation	13
3.1	Basic Settings for the ICE/KWO-project.	29
3.2	KWO-ICE geometric settings	30
3.3	KWO-ICE thermohydraulic settings	30
3.4	KWO-ICE variable boron concentration	31
3.5	KWO-ICE power history	34
3.6	KWO-ICE Evaluations No.1	35
3.7	KWO-ICE Evaluations No.2	36
3.8	KWO-ICE Evaluations No.3	37
5.1	Set of Isotopes used for criticality analysis	60
5.2	Symbol legend of Equation (5.1)	61
5.3	LWR geometric settings for boron investigations	64
5.4	LWR thermohydraulic settings for boron investigations	64
5.5	Variable boron concentration 400 ppm	65
5.6	PWR soluble boron concentrations	66
5.7	Comparison of 188 ppm and 80 ppm constant approximation no.1	73
5.8	Comparison of 188 ppm and 80 ppm constant approximation no.2	74
5.9	LWR geometric settings for lattice investigations	76

List of Figures

2.1	Model of K_{eff}	8
3.1	Power-rating history	25
3.2	Moderator-Fuel Cell	27
4.1	Levelized fuel costs versus burn-up	44
5.1	Boron Concentration during burn-up	62
5.2	k_{∞} , influence of soluble boron	67
5.3	Influence of soluble boron on plutonium	67
5.4	Influence of soluble boron on the plutonium-uranium ratio	68
5.5	Am^{241} , influence of soluble boron	68
5.6	k_{∞} for constant and variable boron concentrations	69
5.7	k_{∞} for three different lattices	76
5.8	k_{∞} variable for three different lattices	77
5.9	k_{∞} for tight lattice	77
5.10	k_{∞} for wider MOX lattice	78
5.11	k_{∞} for wide lattice	78
5.12	Pu^{238} , influence of boron	82
5.13	Pu^{238} , variable and constant modeling	82
5.14	Pu^{238} , influence of lattices	83
A.1	Am^{241} , KWO validation	A15
A.2	Am^{243} , KWO validation	A16
A.3	Cm^{242} , KWO validation	A16
A.4	Cm^{244} , KWO validation	A17
A.5	Kr^{83}/Kr^{86} ratio, KWO validation	A17
A.6	Kr^{84}/Kr^{83} ratio, KWO validation	A18

A.7	Kr^{84}/Kr^{86} ratio, KWO validation	A18
A.8	Nd^{143}/Nd^{148} ratio, KWO validation	A19
A.9	Nd^{144}/Nd^{148} ratio, KWO validation	A19
A.10	Nd^{145}/Nd^{148} ratio, KWO validation	A20
A.11	Nd^{146}/Nd^{145} ratio, KWO validation	A20
A.12	Nd^{146}/Nd^{148} ratio, KWO validation	A21
A.13	Pu^{238} , KWO validation	A21
A.14	Pu^{239} , KWO validation	A22
A.15	Pu^{240} , KWO validation	A22
A.16	Pu^{241} , KWO validation	A23
A.17	Pu^{242} , KWO validation	A23
A.18	Pu^{242}/Pu^{241} ratio, KWO validation	A24
A.19	Pu^{240}/Pu^{239} ratio, KWO validation	A24
A.20	Pu^{241}/Pu^{240} ratio, KWO validation	A25
A.21	Pu^{242}/Pu^{240} ratio, KWO validation	A25
A.22	Pu/U ratio, KWO validation	A26
A.23	U^{235} , KWO validation	A26
A.24	U^{236} , KWO validation	A27
A.25	U^{238} , KWO validation	A27
A.26	U^{235}/U^{238} ratio, KWO validation	A28
A.27	Xe^{131}/Xe^{134} ratio, KWO validation	A28
A.28	Xe^{132}/Xe^{131} ratio, KWO validation	A29
A.29	Xe^{132}/Xe^{134} ratio, KWO validation	A29
A.30	Xe^{136}/Xe^{134} ratio, KWO validation	A30
A.31	Nd buildup in comparison with power history	A30
A.32	Am^{242} , KWO validation	A31
A.33	Am^{242M} , KWO validation	A32
A.34	Np^{237} , KWO validation	A32
A.35	Np^{239} , KWO validation	A33
A.36	U^{234} , KWO validation	A33
A.37	Zr^{91} , KWO validation	A34
A.38	Zr^{93} , KWO validation	A34
A.39	Zr^{96} , KWO validation	A35
B.1	Cm^{242} , influence of soluble boron	B1
B.2	Gd^{155} and Gd^{157} , influence of soluble boron	B2

B.3	Nd^{143} , influence of soluble boron	B2
B.4	Np^{237} , influence of soluble boron	B3
B.5	Sm^{149} and Sm^{151} , influence of soluble boron	B3
B.6	Xe^{135} , influence of soluble boron	B4
B.7	Am^{241} , variable and constant boron concentrations	B5
B.8	Am^{242} , variable and constant boron concentrations	B6
B.9	Am^{243M} , variable and constant boron concentrations	B6
B.10	Cm^{242} , variable and constant boron concentrations	B7
B.11	Eu^{155} , variable and constant boron concentrations	B7
B.12	Gd^{155} , variable and constant boron concentrations	B8
B.13	Pu^{239} , variable and constant boron concentrations	B8
B.14	Pu^{241} , variable and constant boron concentrations	B9
B.15	Pu/U ratio, variable and constant boron concentrations	B9
B.16	Pu , variable and constant boron concentrations	B10
B.17	Rh^{103} , variable and constant boron concentrations	B10
B.18	Sm^{149} , variable and constant boron concentrations	B11
B.19	Sm^{151} , variable and constant boron concentrations	B11
B.20	Am^{243} , variable and constant boron concentrations	B12
B.21	Cm^{244} , variable and constant boron concentrations	B13
B.22	Eu^{153} , variable and constant boron concentrations	B13
B.23	Gd^{157} , variable and constant boron concentrations	B14
B.24	Np^{237} , variable and constant boron concentrations	B14
B.25	Np^{239} , variable and constant boron concentrations	B15
B.26	Pm^{147} , variable and constant boron concentrations	B15
B.27	Pu^{240} , variable and constant boron concentrations	B16
B.28	Pu^{242} , variable and constant boron concentrations	B16
B.29	Sm^{147} , variable and constant boron concentrations	B17
B.30	Sm^{148} , variable and constant boron concentrations	B17
B.31	Sm^{150} , variable and constant boron concentrations	B18
B.32	Tc^{99} , variable and constant boron concentrations	B18
B.33	U^{234} , variable and constant boron concentrations	B19
B.34	U^{235} , variable and constant boron concentrations	B19
B.35	U^{238} , variable and constant boron concentrations	B20
B.36	U^{236} , variable and constant boron concentrations	B20
B.37	k_{∞} , constant and variable boron concentrations	B21
B.38	Pu , variable and constant modeling for $V_m/V_s = 1.283$	B22

B.39 Pu , variable and constant modeling for $V_m/V_s = 1.796$	B23
B.40 Pu , variable and constant modeling for $V_m/V_s = 2.565$	B23
B.41 Pu^{238} , comparison of three lattices	B24
B.42 Pu^{239} , comparison of three lattices	B24
B.43 Pu^{240} , comparison of three lattices	B25
B.44 Pu^{241} , comparison of three lattices	B25
B.45 Pu^{242} , comparison of three lattices	B26

Chapter 1

Introduction

Up to now, a longterm solution for the treatment of spent nuclear fuel (SNF) has not been agreed upon, large amounts of fuel components have to be stored in repositories. In particular the transuranics complicate storage and handling due to their long lasting high radio-toxicity, which makes it necessary to exclude these isotopes from the biogeochemical cycle. Current issues aggravate the situation: On the one hand, storage capacities are limited and nuclear power reactor operation continuously adds to the amount of spent nuclear fuel. On the other hand, the ongoing dramatical price increases of fossil primary energy carriers¹ will increase the share of the worlds nuclear energy production. A rising world energy consumption counteracting the effort to reduce CO₂ emission will furthermore strengthen the attempt to extend nuclear energy production.

These aspects lead to very simple consequences for energy consumption. First of all, energy consumption has to be reduced to save the limited resources. Considering the technical aspect of energy production, the efficiency of energy production has to be raised. Focusing on nuclear energy generation, the consequences are the following:

Unlike the fossil fired power plants, resources for nuclear energy production have to be saved on either side. The amount of uranium ore and storage capacities in the repositories are limited. Both aspects lead to the need of reduced fuel throughput in nuclear power plants.

Reduced fuel consumption can be realized by different techniques. Fresh fuel can be saved by recovery and reprocessing of the fissile components in spent nuclear fuel. This is put into practice at the plutonium recycling in Mixed Oxide (MOX) fuel.

¹Not only the price of fossil energy carriers increased, also the price for uranium ore more than doubled within the last few months of 2005.

Reprocessing at the same time allows the separation of problematic components from deposition, such as minor actinides. An obstacle could be the interdiction of SNF reprocessing, as it is the case in Germany.

A second possibility to save resources is offered by alternative fuel cycle concepts leading away from the common uranium based cycle. Two major techniques should hereby be mentioned: The alternative thorium based uranium fuel cycle and the concept of uranium-plutonium based breeder reactors. Both reactor types use a surplus of neutrons for breeding non fissile fuel components into fissiles. The in situ² combustion of these generated fissiles contributes to the energy output of the reactor, thus saving fresh fuel.

The opposite site of the fuel cycle, the back end, is getting more and more important, as the amounts of SNF and nuclear waste grows. This leads to enhanced efforts, on the one hand to reduce the production of SNF which corresponds to reduced fuel throughput and on the other hand to the development of waste treatment techniques. The development of so called accelerator driven systems (ADS) should hereby be mentioned. These systems are focused to the combustion of SNF components that are not usable under LWR thermal neutron conditions, such as the minor actinides. A further possibility to reduce the spent fuel volume is the application of re-enriched reprocessed uranium fuel.

Currently, major efforts are focused on the increase of burn-up in LWRs for different reasons. Burn-up is the relation between fuel energy output in the unit of [GWd] and the fuel mass in the unit of tons initial heavy metal [tHM]. In other words, the burn-up represents the specific energy production of the fuel. To reduce the fuel throughput and thus the spent fuel volume, burn-up should be raised. A further topic of increased burn-up is a commercial one. Higher burn-ups are related to longer cycle times, lowering the time of refueling outage, thus contributing to higher savings. These aspects are discussed in detail in Chapter 4.

The consequences of increased burn-ups in fuels are of particular interest for future developments. This aspect became the central issue during working on the main topic of fuel recycling in LWRs. Namely the focus turned on investigations on the buildup and related effects of different isotope groups with particular impact on the burn-up process and the subsequent SNF-processing. Burn-up investigations are hence the guideline and basis not only for fuel development but also for subsequent SNF processing, and might be the key for the development of a closed nuclear fuel cycle.

²For some breeders the combustion of breded fissiles passes the step of reprocessing.

To perform such burn-up investigations, a program system KAPROS with a special burn-up module KARBUS was applied and carefully validated beforehand. This validation was rather time consuming but necessary to provide a reliable investigation environment for subsequent burn-up investigations. The basic principles of these investigations are introduced in the following chapter.

Chapter 2

Principles of Burn-up Calculation

Major processes and reactions in nuclear reactors are decisively defined by the neutrons. For calculation and prediction of neutron influenced processes it is therefore inevitable to know the parameters influencing neutron reactions. On the one hand, the number of neutrons in a defined volume element effects the incidence of reactions, on the other hand, the variation of neutron population is of particular interest for the transient behavior of a system. Changes of fuel and structure matter during irradiation are associated with the spatial flux distribution. Basic principles of neutron physics corresponding to nuclear reactors will be discussed in the following.

2.1 The k - Factor Model [3] [6] [39]

Considering a neutron population only to be influenced and changed by nuclear reactions, i.e. interactions between neutrons and nuclei, a simple balancing model can be applied. It describes the alteration of consecutive neutron populations using multiplying factors to account for gains and losses caused by the neutron reactions. Deviation of these multiplying factors from 1 point out the share of neutrons which are produced or removed by the corresponding reaction. Foremost any kind of losses through boundaries are ignored in a model case of a core volume extended to infinity.

In the most common nuclear power reactor type, the Light Water Reactor (LWR), fission of U^{235} fuel takes place in the thermal spectrum ¹ of neutron energies. Neutrons generated through fission correspond to an average energy level of around 2 MeV.

¹THERMAL SPECTRUM is defined as the energy range where particles are in energetic equilibrium with the energy state of their surrounding matter. The neutrons mean kinetic energy \bar{E}_K , which corresponds to the neutrons total Energy \bar{E}_N , equals $\bar{E}_N = 3/2k_B T$. For LWRs values of about $\bar{E}_N = 0.025$ eV are reached. The neutron energy spectrum follows a Maxwell Distribution.

Thus neutrons have to cross a huge energy range of several orders of magnitude to reach the thermal spectrum. The k -Factor model balances the neutron number, considering effects that occur while neutrons cross this energy band.

A starting population of N_0 fast neutrons out of fission increases its number by subsequent fast fission reactions with U^{238} . The corresponding factor is called *Fast Fission Factor* ϵ . Usually in LWRs, ϵ is smaller than 1.05.

By colliding with light nuclei neutrons loose energy and slow down. They reach the isotope dependent resonance range which expands, for the most important U^{238} , from several eVs up to KeVs. In this energy band, especially for U^{238} , absorption cross-sections are partly very high due to sharp resonances. The magnitude of the resonance range as well as the resonance characteristic differs with isotopes and is thus depending on the fuel composition. Resonance absorption decreases the neutron population by a factor of 0.97 to 0.85. This factor is called the *Resonance Escape Probability Factor*, labeled p . If a neutron reaches thermal energies, the diffusion² process starts and prolongs until this neutron is absorbed, with the core volume being infinite as assumed.

Thermal neutrons are not only absorbed in the fuel but also in the structure material such as cladding, moderator or comprised fission products. This leads to another factor called *Thermal Utilization* f which specifies the share of “parasitic” absorption. The remaining thermal neutron population will be absorbed in the fuel, but only a fraction of the captured neutrons cause fission. The competing process is neutron capture with the result of breeding the fuel to higher isotopes. This happens for any isotope in case of neutron capture. To close the neutron generation cycle, the average number of fission neutrons generated per fission and fuel atom, named production rate ν , needs to be known. For LWR uranium fuel, ν has a value of approximately 2.5. Multiplying the quotient of fission causing neutrons to fuel absorbed neutrons, with the production rate ν gives the last factor in the cycle, called the *Neutron Yield* η . It indicates the number of fission neutrons per in the fuel absorbed neutron.

Multiplication of the initial population N_0 with the four factors described above results the population of the successor generation N_1 , shown by Equation (2.1).

²DIFFUSION denotes a way of particle motion, characterized through random collisions among particles -here nuclei and neutrons- in thermal equilibrium, see above. Every neutron interaction, marked as a vertex of their zigzag trajectory, can provoke energy and thus velocity increase, as well as a decrease of energy. The average energy of neutrons during the diffusion process stays constant: $\bar{E} = 3/2k_B T$.

All factors are merged in the so called *Infinite Medium Multiplication Factor* k_∞ for an infinite core Volume, see Equation (2.2). k_∞ is herein independent of geometric parameters but determined by means of material properties.

$$N_1 = N_0 \epsilon p f \eta \quad (2.1)$$

$$k_\infty = \epsilon p f \eta \quad (2.2)$$

For real core geometries, which means finite boundaries, neutron leakage out of the core has to be included in the multiplication factor. Two more factors for the probability of neutrons staying inside the core were set, one for each major energy range. The fast non-leakage factor P_{FNL} for high energies, and the thermal non-leakage factor P_{TNL} for thermal energies. Including these two factors in the k_∞ model yields a new parameter for the effective multiplication of neutrons k_{eff} in a real core, that now accounts for geometric influences such as shape and extension, shown by Equation (2.3).

$$k_{eff} = k_\infty P_{FNL} P_{TNL} = \epsilon p f \eta P_{FNL} P_{TNL} \quad (2.3)$$

Describing the neutron cycle by multiplying factors as done here, is preferred, since the single steps of the cycle are back-to-back processes and not parallel. The single factors in Figure 2.1 are either calculated from statistics or experimentally measured. The k -model does not consider any inhomogeneities of the core structure. Yet, since inhomogeneous cores with separation between fuel, moderator and structure are common practice, Figure 2.1 shows the k -factors for each of the basic structural components and was taken from Reference [12].

Hence, the quantity k_{eff} provides a measure to evaluate the stability of fission chain reactions in nuclear reactors. As k_{eff} is called the effective multiplication factor, it is obvious that only a system with a $k_{eff} = 1$ will be stable or static. This is the steady state operating condition for all reactors. For $k_{eff} = 1$ a core is called critical, reactors are therefore regulated toward this state. For $k_{eff} < 1$, a so called sub critical reactor, the neutron population dies out, the reactor turns off. Vice versa for $k_{eff} > 1$ in a supercritical reactor, neutron population and reactor power will in principle grow to infinity. This excursion continues until system parameters are again changed critical or sub critical. In technical cores this happens reversible due to insertion of control and shutdown rods as well as by thermal interaction³, or irreversible by destruction

³The technical design of reactor cores follows the principle of negative feedback coefficients. These coefficients (the effects described by the coefficients) act on the cause of the unwanted perturbation, see also Chapter 5.1.1.

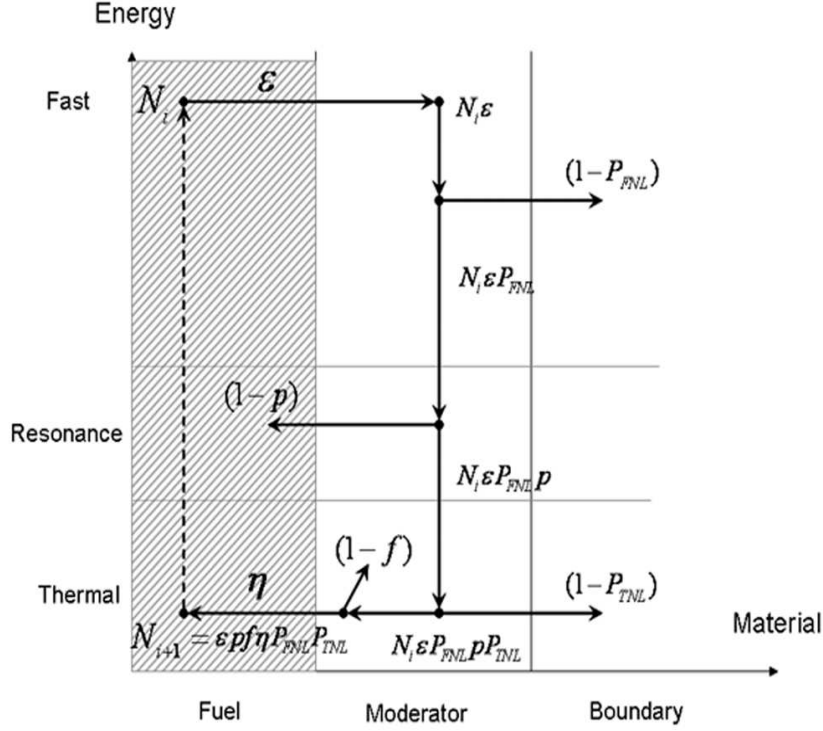


Figure 2.1: Neutron generation model of k_{eff} ,

and disarrangement of the core structure.

In the k -model approach no conclusion about the time-dependent development of the neutron populations is made. The crucial parameter to evaluate time dependence would be the mean lifetime of a neutron generation Λ .

In practice, k_{eff} is a significant control parameter that evaluates the steady state condition of a system in a global manner. In matters of calculations, k_{eff} is the result of full core investigations. An estimated k_{eff} value is a reference value to calculate steady state solutions of core flux. Furthermore, the k -model helps to understand basic neutron processes in cores.

A quantity which is derived from k describes the related surplus of neutrons per generation [23]. It is called the reactivity ρ and carries the unit $1\$ = 100\text{cent}$. $1\$$ represents the reactivity which is produced by the effective delayed neutron fraction with $1\$ = \beta_{eff}$. As in practice $k \cong 1$, ρ is defined by the following equation:

$$\rho = \frac{k - 1}{k} \quad [\$]. \quad (2.4)$$

The lifetime of a fission neutron starts when the neutron causing the fission is absorbed by the nucleus [28]. An intermediate, excited nucleus with a surplus of one neutron compared to the absorbing nucleus is build. Except for neutron capture, fission occurs after a short time and the nucleus splits into two highly excited fission products that immediately emit ν *Prompt Neutrons*. Neutron emission occurs if the excitation energy of the product nucleus exceeds the binding energy of a neutron. The lifetime of a fission neutron ends, when it is absorbed. Assumed all neutrons to be generated in such a prompt way, an average generation lifetime of the order 10^{-5} s would be the consequence. Intervention in the growth of the neutron population by feedback control would be impossible.

A small fraction, less than 1% of the neutrons are generated differently. After undergone fission and prompt emission, the emitters excitation energy is insufficient for an additional neutron emission. A small number of these fission products will decay by a β -decay into a *Daughter Nuclei* with higher excitation energy than the *Parent Nuclei*. In some cases, excitation of the daughters is again larger than the binding energy of a neutron with the aforementioned consequences, neutron emission. Unlike the prompts, these neutrons are delayed by the time it takes to undergo the β -decay. According to the lifetime definition, this results in the comparatively long lifetime of the so called *Delayed Neutrons*. The β -decay can extend the lifetime of delayed neutrons from about a second up to several tenth of seconds. The delayed mean lifetime e.g. for U^{235} lies at around 13 s. Depending on their precursor decay constants delayed neutrons are separated into *Delayed Groups*⁴ with similar time-constants.

If a β -decay leads to an excitation that enables neutron emission, γ -decay is also possible, however those decays are of minor interest. To separate clearly, only parent nuclei whose daughter nuclei undergo a neutron emission, delayed by a β -decay, are called *Precursors*.

Weighted with their shares of population, the mean lifetime of a neutron generation grows up to 10^{-2} s which is a thousand times the mean lifetime of prompt neutrons. Therefore, delayed neutrons offer the possibility of intervention for regulation purposes in the nuclear fission process. Even though their fraction is comparatively small, delayed neutrons play a dominant role in most dynamic⁵ processes. The k_{eff} -model does not distinguish between delayed and prompt neutrons, since for static problems neutron lifetime is indiscriminated.

⁴Normally the delayed neutrons are separated into six different Delayed Groups.

⁵According to [28], *kinetics* describe processes wherein the core-system's feedback is negligible, *dynamic* problems involve system feedback.

Power generation in nuclear reactors is realized by steady state operation conditions for $k_{eff} = 1$. As mentioned above, for $K_{eff} = 1$ production and loss are balanced for the total neutron population. Considering only the share of the prompt neutron fraction $1 - \beta$, the reactor would be subcritical. Criticality is reached by adding the share of the delayed neutron fraction. Hence, the reactor is operating on *Delayed Criticality*, which is the desirable state of operation. Delayed Criticality is of particular relevance for non steady state operation during reactivity perturbations or reactor transients. As long as the reactor remains delayed critical, in case of perturbation, the neutronic response will be dominated by the time-constant of the delayed neutrons. As mentioned above, the average lifetime of these neutrons is approximately equal to the decay time of the precursors, which is in the range of seconds, thus allowing feedback control.

Inserting a positive reactivity smaller than 1\$⁶ will primarily result in a *prompt jump*. This jump corresponds to the surplus of “added” prompt neutrons. It is referred to as a jump due to the effect of the prompt neutrons time-constant which makes the increase look like a step-function. At this point, the delayed neutron population is still constant. The increased prompt neutron population will increase the buildup of precursors and thus result in more delayed neutrons, rising the multiplication factor above one. The effect of reactivity insertion in delayed critical systems is an increasing population with a time-constant dominated by precursor decays.

Reactivity insertion above 1\$ makes the reactor prompt supercritical. Thus the delayed neutron fraction is of no more relevance for multiplication. The neutron population increases exponentially, dominated by the time-constant of the prompt neutrons lifetime, which is around 10^{-5} seconds. This corresponds to an uncontrolled chain reaction since no feedback parameters respond within this time-scale.

Delayed criticality is therefore very important for reactor operation. To determine the dynamic behavior of a core, the equations of Point Kinetics are applied. See e.g. References [6] and [28].

2.2 The Time-dependent Boltzmann-Equation

The previous section deals with the neutron cycle and its effects in a global manner, ignoring neutrons spatial distribution, time-dependence or inhomogeneities in the structure of the core. However, the latter aspects are of crucial relevance for profound investigations of neutronic systems.

⁶i.e. less neutrons than the share of the delayed neutron fraction β .

Information in this chapter is mainly based on References [1], [6], [22], [28]. To account for the mentioned drawbacks this section introduces a neutron balancing model which allows a complete description comprising the spatial distribution of neutrons, the neutron energy, direction of motion and time-dependence. The change of neutron density is described by the gains and losses in an arbitrary volume element of a system. This comprehensive equation is called the *Neutron Transport Equation*.

The Transport Equation for neutrons was derived from gas kinetics and the theory of rarefied gases where, according to the motion of neutron gases, the mean free path for particle motion is assumed to be large compared to the dimensions of the interacting particles. Since the mean free path of neutrons has the same dimension as the homogeneous areas in the core, e.g. the diameter of the fuel pins or the moderator regions between fuel rods, the core can be considered as quasi-homogeneous. For fast neutrons, the mean free path is usually in the order of centimeters.

Unlike the gas kinetics equation, no interaction among the neutrons is implied in the neutron Transport Equation. In contrast to the original, nonlinear Boltzmann Equation, the neutron Transport Equation is linear. Since the fundamental equation for dilute gases (Boltzmann's Equation) was proposed by Ludwig Boltzmann, the derived equation for neutron transport is called the *time-dependent Boltzmann Equation*. The latter will be discussed in the following two versions: a common one, Equation (2.5) for *non-multiplying media* as well as a version for *multiplying media*, Equation (2.6).

$$\begin{aligned}
 \underbrace{\frac{1}{v} \frac{\partial \Phi(\vec{r}, E, \vec{\Omega}, t)}{\partial t}}_{\text{time-dep. change}} &= \underbrace{S(\vec{r}, E, \vec{\Omega}, t)}_{\text{Source}} \\
 &\quad - \underbrace{\Sigma_t(\vec{r}, E) \Phi(\vec{r}, E, \vec{\Omega}, t)}_{\text{Removal}} - \underbrace{\nabla \cdot (\vec{\Omega} \Phi(\vec{r}, E, \vec{\Omega}, t))}_{\text{Leakage}} \\
 &\quad + \underbrace{\int_{E'=0}^{\infty} \int_{\vec{\Omega}'=0}^{4\pi} \Sigma_s(\vec{r}, E') f(\vec{r}; E', \vec{\Omega}' \rightarrow E, \vec{\Omega}) \Phi(\vec{r}, E', \vec{\Omega}', t) d\vec{\Omega}' dE'}_{\text{In - Scattering}}
 \end{aligned} \tag{2.5}$$

For neutron transport the two mentioned cases, have to be separated: multiplying and non-multiplying media. In non-multiplying media, neutrons are added by an external neutron source $S(\vec{r}, E, \vec{\Omega}, t)$ to the system. Apart from this, no neutron interaction occur which may rise the number of neutrons. In multiplying media, fission as well as (n,2n) and (n,3n) reactions may contribute to increase the neutron population.

This requires a further neutron source expression, implemented in Equation (2.6) for multiplying media.

The influence of the delayed neutron interaction was already pointed out in the previous section of this chapter. However, for dynamic investigations it is inevitable to separate prompt and delayed neutron generation. This is done in Equation (2.6) by introducing two further source-terms, the source expression S in the equation is analog for non-multiplying media. All variables and quantities used within the Boltzmann Equations are explained in Table 2.1.

$$\begin{aligned}
\underbrace{\frac{1}{v} \frac{\partial \Phi(\vec{r}, E, \vec{\Omega}, t)}{\partial t}}_{\text{time-dep. change}} &= \underbrace{S(\vec{r}, E, \vec{\Omega}, t)}_{\text{external Source}} + \underbrace{\sum_i \lambda_i C_i(\vec{r}, t) D \chi_i(E)}_{\text{Source of del. Neutrons}} \\
&\quad - \underbrace{\Sigma_t(\vec{r}, E) \Phi(\vec{r}, E, \vec{\Omega}, t)}_{\text{Removal}} - \underbrace{\nabla \cdot (\vec{\Omega} \Phi(\vec{r}, E, \vec{\Omega}, t))}_{\text{Leakage}} \\
&\quad + \underbrace{\int_{E'=0}^{\infty} \int_{\vec{\Omega}=0}^{4\pi} (1 - \beta) \chi(E) \nu(E') \Sigma_f(\vec{r}, E) \Phi(\vec{r}, E', \vec{\Omega}', t) d\vec{\Omega}' dE'}_{\text{Source of prompt Neutrons}} \\
&\quad + \underbrace{\int_{E'=0}^{\infty} \int_{\vec{\Omega}=0}^{4\pi} \Sigma_s(\vec{r}, E') f(\vec{r}; E', \vec{\Omega}' \rightarrow E, \vec{\Omega}) \Phi(\vec{r}, E', \vec{\Omega}', t) d\vec{\Omega}' dE'}_{\text{In - Scattering}}
\end{aligned} \tag{2.6}$$

The central problem of nuclear reactor theory is to determine the distribution of neutrons in the reactor core. This neutron distribution is characterized by the quantity of neutron density, $N(\vec{r}, t)$. The product of neutron density $N(\vec{r}, t)$ and neutron speed v frequently occurs in reactor theory and is therefore called the neutron flux Φ , which is shown in Equation (2.7).

$$\Phi = N(\vec{r}, t) \cdot v \tag{2.7}$$

It is convenient to work with the neutron flux Φ rather than the neutron density N , since neutron velocity need not be included e.g in the reaction rates. The Boltzmann Equations (2.5) and (2.6) are therefore noted in neutron flux and not in neutron density.

Time-dependent Changes

The left hand side of Equations (2.5) and (2.6) describes the time-dependent changes of the neutron flux. Within a phase space volume-element dQ , gains and losses are balanced for a differential time-step on the equation's right hand side (see also next item).

Variables:

r	Point in spherical coordinates
\vec{r}	Position vector pointing r
t	Time
E	Energy
$\vec{\Omega}, \vec{\Omega}'$	Unit vector of neutron direction

Quantities:

v	Neutron velocity
Φ	Neutron flux
S	Neutron source intensity
λ_i	β -decay constant for precursors of the i -th group
C_i	Concentration of precursors leading to neutrons of i -th group
$D\chi_i(E)$	Delayed neutrons energy distribution of the i -th group
β	Fraction of delayed neutron
Σ_t	Total macroscopic cross-section
Σ_f	Macroscopic fission cross-section
Σ_s	Macroscopic scattering cross-section
$\chi(E)$	Fission neutrons energy distribution
$\nu(E)$	Energy dependent neutron production rate
f	Normalized probability function for neutron transition from $E', \vec{\Omega}' \rightarrow E, \vec{\Omega}$
v	Neutron speed
N	Neutron density

Table 2.1: Explanation of the variables and Quantities used in the Boltzmann Equations (2.5) and (2.6)

The effects accounting for the time-dependent change of neutron flux are explained in particular below.

External Sources

According to Reference [1], external sources are more accurately denoted by *Independent Sources*. Since the expression “independent” takes sources into account whose emission rate is not correlated with the neutron flux, namely neutron emission not

arising through fission events⁷. Independent sources merged by S include (α, n) reactions, spontaneous fission but also the aforementioned external sources. For instance, sub-critical and so called accelerator driven systems (ADS) are powered by external neutron sources. The intensity of the source $S(\vec{r}, E, \vec{\Omega}, t)$ represents the incidence probability per unit time for neutrons to appear in the phase space volume dQ . This comprises neutrons entering the volume element dV around \vec{r} appearing under the angular increment $d\vec{\Omega}$ in the direction $\vec{\Omega}$ within the energy interval dE around E . The phase space volume element dQ is defined in the following:

$$dQ = dV dE dt = d\vec{\Omega} d\vec{r} dE dt$$

Delayed Neutron Source

As mentioned above, delayed neutrons are separated in groups by the decay time of their precursors. The production rate of delayed neutrons is given by the product of the precursor nuclei concentration $C(\vec{r}, t)$ times the corresponding decay constant λ . Thus determining the total number of generated neutrons in a volume per unit time, no conclusion about the neutrons energy is made. The neutron energy distribution is introduced by a probability function $D\chi(E)$ which denotes the energy-dependent neutron yield. Depending on the model, different numbers i of delayed groups are applied. The total amount of delayed neutrons corresponds to the sum of the i delayed groups. This leads to the following expression for the delayed neutron generation:

$$+ \sum_i \lambda_i C_i(\vec{r}, t) D\chi_i(E)$$

Neutron Removal

The effect which is described by the removal-term is the loss of neutrons out of the considered phase space element, characterized by the values of the variables $\vec{r}, E, \vec{\Omega}, t$. Obviously the neutron flux is reduced by any absorption, which can be expressed by the absorption reaction rate $\Sigma_a \cdot \Phi$. Considering the parameters of the phase space volume element dQ , neutrons also vanish out of the phase space when changing their energy or their direction of motion E and $\vec{\Omega}$. Both parameters are changed during collision of neutrons with nuclei, thus comprising neutron scattering. As the total microscopic

⁷To be accurate, in multiplying media neutrons could be generated through $(n, 2n)$ and $(n, 3n)$ reaction as well which are also proportional to the flux. However, this could be involved in Equation (2.6) by modifying the parameters ν and Σ .

cross-section σ_t is the sum of the absorption cross-section σ_a and the scattering cross-section σ_s , neutron losses, summarized within “removal”, are expressed the following:

$$-\Sigma_t(\vec{r}, E) \Phi(\vec{r}, E, \vec{\Omega}, t)$$

The negative sign denotes the loss or a reduction of the flux Φ .

Leakage

Leakage is called the difference between the influx and outflux of neutrons into and out of a phase space volume. Since the neutron flux Φ is a scalar quantity, the denotation flux is very misleading. The quantity which is needed for balancing is the oriented flux or neutron current $\vec{J}(\vec{r}, t)$. The neutron current is defined as the product of the neutron flux and the orientation vector: $\vec{J}(\vec{r}, t) = \Phi(\vec{r}, t) \cdot \vec{\Omega}$. Thus the difference between in- and outflux can be mathematically expressed by the divergence of the flux in the direction of $\vec{\Omega}$. The expression has a negative sign for a “loss”:

$$-\nabla \cdot (\vec{\Omega} \Phi(\vec{r}, E, \vec{\Omega}, t))$$

Prompt Fission Neutron Source

The reaction rate for fission is expressed as the product of the flux Φ and the macroscopic fission cross-section Σ_f , $R_f = \Sigma_f \Phi$. The reaction fission rate for times the average number of neutrons generated per fission ν leads to the number of neutrons produced per volume. Considering only the prompt neutrons, the delayed neutron fraction β has to be subtracted from the total number of neutrons which is done by multiplying with the factor $(1 - \beta)$. To account for the energy distribution of the fission neutrons, the neutron population is weighted with the probability function $\chi(E)$. To account for all prompt neutrons generated in the phase space volume, the production term has to be integrated over the whole energy range and over all orientations, resulting in the expression:

$$+ \int_{E'=0}^{\infty} \int_{\vec{\Omega}=0}^{4\pi} (1 - \beta) \chi(E) \nu(E') \Sigma_f(\vec{r}, E) \Phi(\vec{r}, E', \vec{\Omega}', t) d\vec{\Omega}' dE'$$

In-Scattering

In-scattering accounts for all neutrons transferred into the phase space volume dQ due to scattering. The outside conditions are marked by a dash, denoting conditions that are unlike the phase space volume conditions $\vec{r}, E, \vec{\Omega}, t$. In-scattering means, that a

neutron after scattering fits the phase space conditions and occurs at time t in the volume element dV at \vec{r} with the Energy E under the direction $\vec{\Omega}$. This effect is calculated by the reaction rate for the in-scattering reaction. Therefore, the incidence probability for scattering, which leads from energies E' and orientations $\vec{\Omega}'$ to E and $\vec{\Omega}$, is needed. In terms of cross-sections, this is the macroscopic scattering cross-section $\Sigma_s(\vec{r}, E', \vec{\Omega}' \rightarrow \vec{r}, E, \vec{\Omega})$. Since the cross-sections are normally⁸ independent from the orientation $\vec{\Omega}$, they only depend on energy and the local material. Therefore one distinguishes probabilities that depend on the cross-sections from those that do not, by introducing a further probability function $f(\vec{r}, E', \vec{\Omega}' \rightarrow \vec{r}, E, \vec{\Omega})$. This function describes the probability of scattering reactions leading from $E', \vec{\Omega}'$ to $E, \vec{\Omega}$ with the cross-section dependency $\Sigma_s(\vec{r}, E)$. Multiplying the probability functions with the flux leads to the expression for neutron in-scattering. To account for all neutron energies and directions this expression has to be integrated over the whole energy range ($0 \dots \infty$) and all orientations $0 \dots 4\pi$ resulting in the expression:

$$+ \int_{E'=0}^{\infty} \int_{\vec{\Omega}=0}^{4\pi} \Sigma_s(\vec{r}, E') f(\vec{r}; E', \vec{\Omega}' \rightarrow E, \vec{\Omega}) \Phi(\vec{r}, E', \vec{\Omega}', t) d\vec{\Omega}' dE'$$

Balancing the above mentioned single terms results in the general form of the Neutron Transport Equation (2.6). This equation is an integro-differential equation of the second order, depending on seven independent variables. These dependencies include three variables of space in the position vector \vec{r} , one for the time t , and four for the description of neutron velocity \vec{v} . For calculative purposes, the latter is split up into the energy E and the orientation vector for neutron motion, $\vec{\Omega}$. The Boltzmann Equation thus provides a very good description of the physical processes during neutron transport, however, it can generally not be solved analytical. This is only possible for very few exceptions. In consequence, different approximation methods have been developed to handle the multiple dependency on variables. The objective of most approximation methods therefore is, to solve the Boltzmann Equation numerically.

Starting from the Boltzmann Equation which is continuous in $\vec{r}, E, \vec{\Omega}, t$, particularly two variables are used to simplify the equation, namely the energy E and the orientation vector $\vec{\Omega}$. Each variable can be treated with different ansatzes, a brief introduction to these will be given in the following.

Four different general approximations for the orientation vector $\vec{\Omega}$ are applied, depending on the anisotropy of scattering. If, for the model-case, scattering can be considered isotropic, the angular dependency can be resolved by integration over the full angular

⁸For strictly oriented crystal structures a dependence on the incidence direction may occur.

range. This leads to an approximation called the *Diffusion Equation*. If scattering is non isotropic, the equation can be either treated by deterministic methods, or by statistical methods, the so called *Monte Carlo Simulation*. Monte Carlo applies Random Sampling and probability functions to determine neutron motion during transport. Deterministic methods use either the *discrete ordinate approximation*, referred to as S_N -methods, or apply spherical harmonics via *series expansion methods* which are the so called P_N -methods. Both methods are applied to reduce the continuous dependency of the orientation vector to discrete values. For discrete ordinate methods, the index N denotes the number of discretized angular ranges, for P_N -methods, N denotes the number of series used for expansion approximation. It is obvious that for steady state problems the time-dependence can also be removed for approximation purposes.

A further approximation is to simplify the energy dependence of the Boltzmann Equation. This can be done by assuming the neutrons to be monoenergetic which results in average values for the energy dependence of both, cross-sections and flux. As for neutron transport, neutrons cannot be assumed to be monoenergetic. To reduce the complexity of the calculation, energy groups are introduced to the Transport Equation discretizing the energy range. Therefore, the Transport Equation is split up into a quasi-monoenergetic system of differential equations, using scattering-terms for exchange and neutron transfer into other energy groups. All energy dependent parameters are averaged for every energy increment. This results in so called group-constant databases containing the energy-dependent material properties. Energy discretizing can be accomplished for user-defined numbers of energy groups and both equation types, the Transport Equation as well as the Diffusion Equation. The derived system of differential equations are thus called either the *Multigroup Transport Equation* or the *Multigroup Diffusion Equation*.

Chapter 3

Validation of the KAPROS / KARBUS Code

The previous chapter described the basic principles of neutron physics as an introduction to the calculation methods used in the software program. The first part of this chapter focuses on the software system itself, explaining the need of extra code validation work as well as the components, configurations and modules. The second part deals with the validation work on the basis of the Isotope Correlation Experiment (ICE) [18], which was accomplished in the late 70th in the PWR power plant of Obrigheim (KWO), Germany. Starting from experimental data, the reliability of the code system was proven again after having undergone major modifications and adjustments since the original evaluations. A comparable validation was successfully examined before on the basis of the same ICE-database in 1992, [3]. Results of the validation and difficulties which appeared during the investigations are discussed in the following.

3.1 Introductory Remarks on Validation

The **KA**rlsruhe **P**rogram **S**ystem **KAPROS**, which was used for the investigations, has its roots in the early stages of computer development back in 1973. In its first version, it was mainly based on assembler programming. Since those days, many developments have been made and generations of computers came into the market to be replaced by new ones. This process was always accompanied by modifications and new developments in hardware system architecture and the system software. The KAPROS system has undergone these steps of developments as well, to adjust to

current standards of computer technologies and stay operative. One of the last big development steps was a UNIX version adjusted to IBM computers running since 1989 namely KAPROS3 [3], [38].

However, these have not been the only innovations and modifications the systems has seen. Starting from the alignment to fast reactors, especially fast breeders, KAPROS was modified for investigations of advanced pressurized water reactor (AWPR), comprising new cross-section databases and the development of new modules and procedures. The most important procedure for the following investigations was the KAPROS procedure KARBUS. This procedure allows investigations on light water reactor systems (LWR) and fuel cycle problems as well, e.g. for burn-up.

Multiple changes and adjustments in the KAPROS software have been made. Those modifications were not only concerning new fields of activities, but in particular new software interfaces, e.g. FORTRAN compilers and computer hardware architectures. This necessitates to repeat the code validation. The ICE experimental data provides very well known boundary conditions to be reconstructed by calculations. A comparable code validation was accomplished in Reference [3] for an earlier KAPROS version with older cross-section libraries. The results of this validation work will further support the evaluation of the new ones. Validation of the latest version of KAPROS and the procedure KARBUS, comparing different cross-section libraries, is done in this chapter.

3.2 Remarks on Software and Calculation Model

This section will give a brief introduction to the KAPROS program and the procedure KARBUS, mainly used for the burn-up investigations. The burn-up model applied in the calculations is also described, including a sketch of the moderator-fuel-cell. Furthermore, boundary conditions and approximations to real core designs are shortly discussed.

3.2.1 The KAPROS System

According to [3] and [38], the UNIX version of KAPROS consists of two main parts interacting for calculations: The first part is the system “kernel”, which is of rather general nature. It is used for any task requiring a flexible sequence of program calls and associated organization of data-flow. The second part is given by the modules and the application libraries. Modules are programs working on special tasks, such as

calculating the neutron diffusion. The libraries contain among others, the cross-section data for burn-up calculations.

KAPROS enables the user to call modules for calculation in an optional manner, organizing the data flow between these modules and libraries in the so called program lifeline. The KAPROS Kernel is also used to store data blocks of calculated results in archives, thus allowing subsequent calculations and data post-processing.

The recent version of KAPROS used for validation and calculation is the KAPROS LNX-2.16 Kernel, a LINUX-operating system version running on PC. Programming language of the whole KAPROS system including the modules is FORTRAN77 with only few exceptions, such as calls for executables in the LINUX environment that are carried out by C-routines.

As mentioned above, calculations are subdivided into single tasks which are thereafter assigned to the corresponding modules. Some of the most frequently used modules and libraries of the KAPROS procedure KARBUS are listed in the following:

Modules:

- Determination of atomic number densities
- Calculation of multigroup cross-sections
- Cell calculations and heterogeneity corrections
- Neutron Diffusion
- Neutron Transport
- Burn-up and Depletion calculations
- Auxiliary modules for manipulating datablocks for post processing etc.

Libraries:

- Cross-section libraries
- Burn-up libraries

3.2.2 The KARBUS Procedure

Information in this section was taken from References [3], [4], [38]. The abbreviation **KARBUS** stands for **K**Arlsruhe **R**eactor **B**urnup **S**ystem, since it is layed out for investigations on reactor core burn-up in a wide range. This module combines the advantages of well established procedures for thermal and fast reactors, calculations are based on deterministic methods. A flow-chart in Reference [3] p.150 gives an overview about the KARBUS calculational structure.

When Running a KARBUS job for burn-up calculations and subsequent evaluation, three different tasks are performed: the calculations, the evaluation and the graphical elaboration. Within the program, tasks are further structured into three components with a run-file executing the main calculation steps. Specifications for calculations are taken from input-files and the results are written into output-files.

In the following the main steps of working out a KARBUS job will briefly be described, considering the calculations, the evaluations and the graphical presentation:

1. The first step of a KARBUS job are the calculations. Specifications for fuel, lattice, power etc. have to be defined in the *input.karbus* file. The second file that is needed to start calculations is the run-file *run.karbus*, executing the calculations. Both files are described in detail below. Executing the calculations generates two new files denoted *OUTPUT.karbus* and *ARCHIVE.karbus*. Calculation results are written into the *OUTPUT.karbus* file, in the *ARCHIVE.karbus* file, data of the calculation procedure is stored for subsequent calculations.
2. The next step is the evaluation of the main results. This involves the module MIXIMA which creates tables and plot-files, storing them into an *OUTPUT.mixima* file and four *ft*-files, namely *ft03* *ft04* *ft30* and *ft35*. This requires two basic files: the *run.mixima* file to execute the module and the *input.mixima* file for specifications. Source data is partly taken from the *OUTPUT.karbus* file. In the present investigation only the *ft35* file was used for subsequent data elaboration. This file contains data for the ancient PLOTEASY plot system, which is also part of KAPROS, requiring further post-processing, as described below.
3. The last of the three steps is data post processing for graphical elaboration and presentation. Therefore, an external program is used to generate files containing ASCII data tables for a scientific plot program called XMGRACE. The XMGRACE plot-tables are generated by the auxiliary *pelist2* program, which writes tabulated isotope data in a separate file for each isotope. Thereby, the

program uses the ancient *ft35* plot-data mentioned above. Graphs are eventually generated and plotted with the XMGRACE program.

Another module is provided for archiving purposes. It consists of a *run.archive* and an *input.archive* file. Executing the module prints out calculation procedure data into the *ARCHIVE.karbus* file for subsequent calculation, e.g. partial restart of calculations.

run.karbus

The *run.karbus* file is the main file of the KARBUS procedure, organizing the data storage and starting the calculation procedures. In the following, a typical *run.karbus* file is shown, explanations are given below by the comments (//Pos.):

```
#!/bin/sh
rm core KSUX.* ft* fort.* ARCHIV.karbus //Pos.1
touch ARCHIV.karbus
ln -s ARCHIV.karbus KSUX.$USER.FT31 //Pos.2
touch ft04 //Pos.3
ln -s ft04 KSUX.$USER.FT04
touch ft13
ln -s ft13 KSUX.$USER.FT13
touch ft14
ln -s ft14 KSUX.$USER.FT14
touch ft15
ln -s ft15 KSUX.$USER.FT15
touch ft18
ln -s ft18 KSUX.$USER.FT18
ln -s $KAPROS_PATH/data/KORFI3.NDLITE KSUX.$USER.FT36 //Pos.4
ln -s $KAPROS_PATH/data/KORFI3.NDACT KSUX.$USER.FT37
ln -s $KAPROS_PATH/data/KORFI3.NDFPS KSUX.$USER.FT38
ksuxgo input.karbus SIZE= 65536000 PL= 80 //Pos.5
mv KSUX.$USER.FT07 OUTPUT.karbus
exit
```

//Pos.1: When running the KARBUS procedure all existing data blocks which are produced in the procedure are deleted, to assure that no old datablocks from earlier calculations can disturb the program results.

//**Pos.2:** For data storage, the *ARCHIVE.karbus* data file is set and linked to the KAPROS unit *FT31*, which is the standardized archiving unit in KARBUS. Thus, any procedures can read this archive after completion of a KARBUS run.

//**Pos.3:** The commands following Pos.3 set the auxiliary *ft*-files. These are used for temporary data storage, storing procedure results etc. .

//**Pos.4:** The following three commands linking the KARBUS procedure to the burn-up libraries *ft36..38* of the BURNUP module are described in Reference [3], see also below.

//**Pos.5:**The *ksuxgo* command starts the main calculation procedure needing the input filename *input.karbus* as an argument. *SIZE* and *PL* specify the memory size and distribution to be used during the calculations. See also Appendix A.1.

BURNUP

BURNUP is the KAPROS module used for cell burn-up calculations in this application. It is assumed, that for the different core zones, in small sections materials are homogeneously distributed and material constants are not varying. In this case BURNUP calculates the cell burn-up depending on the mean absolute neutronflux $\bar{\Phi}_{tot}$ on the basis of three different one-group cross-section libraries containing data for light elements, fission products and heavy isotopes. BURNUP was developed from the successful KORIGIN code to establish a central burn-up module. KORIGIN [7] itself was the improved Karlsruhe version of the american Oak Ridge Laboratory ORIGEN code. Information was taken from Reference [3].

input.karbus

Specifications for the calculations are set in the *input.karbus* file. This input-file comprises different input data-blocks, which are independent from each other. In this application no sequence is of relevance. All data-blocks begin with the *KSIOX command card and are ended by a “*\$*\$” command. Comments can be inserted by the “*\$ ” command (star, Dollar, blank) anywhere in the file. The input file ends with “*GO” commands . A typical input-file used e.g. for the KWO ICE validation work, is shown in the Appendix A.2. Explanations of the input-file entries - entry data-blocks - are given below, linked by a “//Pos.” number to the reference in the appendix.

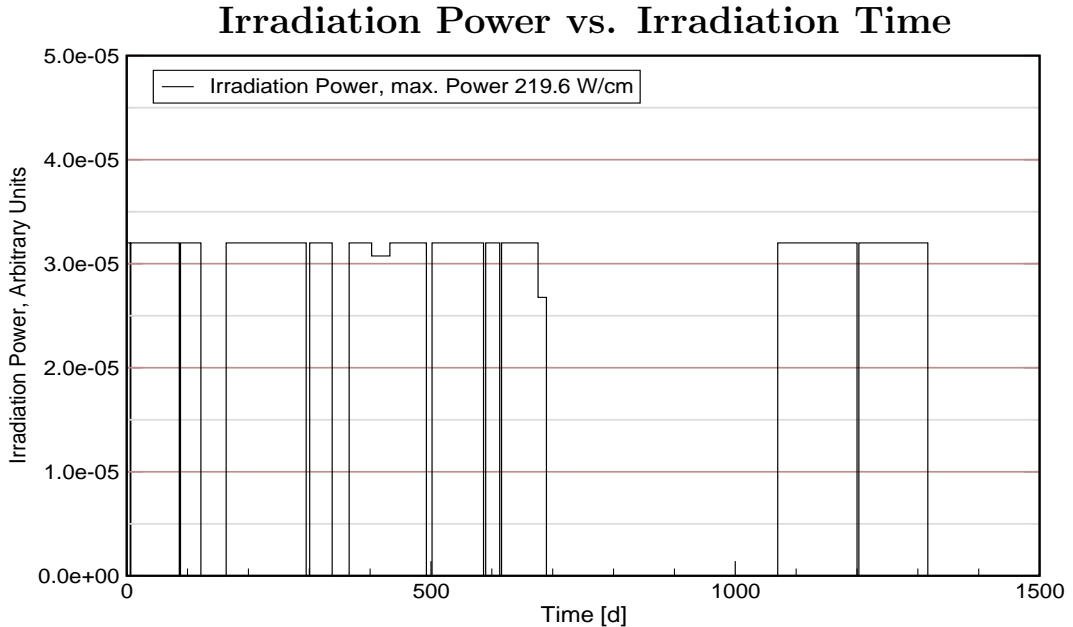


Figure 3.1: Irradiation power-rating history of the KWO ICE project. Power-rating in arbitrary units plotted versus irradiation time in days.

//**Pos. 1** This data-block creates an *ARCHIVE* file which is initialized by a *GO* command at the end of the input-file, see also Pos.12.

//**Pos. 2** The 'BU1D' card defines the irradiation procedure for burn-up. The number next to the 'BU1D' specifies the number of macro time steps of the irradiation. Every macro time step is defined by three lines. The number of the first line denotes the number of micro time-steps forming a macro time step. The second line specifies the days of irradiation for each micro time step and the last line denotes the irradiation power in absolute values for each micro time step in the unit of [W/cm]. A typical power-rating history for the KWO ICE project is shown in Figure 3.1.

//**Pos. 3** In this data block the lattice parameters are specified by the module NDCALC. A three-zones Wigner-Seitz cell is applied, with zones being the moderator, the cladding and the fuel. See also Reference [4] and Figure 3.2 in Chapter 3.2.3. This cell model comprises a standard isotope set for materials contained by the single zones. Further isotopes can be added to the three-zone standard set by completing 'ADDF' and 'ADDM', see also Pos.5 and Pos.6.

//**Pos. 4** The 'MINP' card defines different parameters which are in turn: fuel temperature, cladding temperature, moderator temperature, moderator to fuelrod volumetric

ratio (V_m/V_s), initial fissile enrichment, rod volume, moderator volume, outer cladding diameter, cladding thickness, fuel density and moderator density.

//**Pos. 5** 'ADDF' defines the extra isotopes involved in criticality analysis after burn-up calculations, which are not included in the standard set.

//**Pos. 6** The 'ADDM' card defines the soluble B_{10} concentration in the moderator. Unit of the values is numberdensity¹ [particles/cm³] $\cdot 10^{-24}$.

//**Pos. 7** The GRUCAL module calculates the macroscopic multi-group cross-section data, needed for the burn-up calculations. Therefore, this module applies microscopic cross-section group data from the GRUBA module, which calculates microscopic cross-sections using the libraries denoted in the following: G69P5E65B, G69P5J30B and G69P1V03. See also Reference [25]. For calculations, formula datasets corresponding to the libraries are used by the GRUBA module and are also denoted within the GRUCAL data block: F69UD06 and F69UD04. Further description of the databases applied for the calculations is given in Chapter 3.3.

//**Pos. 8** This position shows a standard input preparation for the GRUCAL module for cross-sections involved in burn-up calculations.

//**Pos. 9** The following six input data blocks are a standard input for cell-calculations.

//**Pos.10** The 'AMIX' keyword in the input block INPUT GRUMIXCELL defines the variable moderator conditions during burn-up. E.g. this could be done for voiding or the adjustment of soluble boron concentration in the moderator. Calculations done within this investigations only use the boron modeling. In every macro time-step the boron concentration is calculated by one INPUT_GRUMIX VOID block. The input blocks are ascending numbered for each time-step. Starting from the initial concentration, see Pos.6, the concentration for the current time-step is calculated by multiplying the preceding concentration with the multiplication factor denoted in the last line of each input block.

//**Pos.11** The 'BUTB' initializes the extra isotopes shown in 'ADDF' within the module BURNUP for criticality analysis.

//**Pos.12** The first GO^* -command initializes the archive file by the module ARCHIVE - see also Pos.1 - the second GO^* -command starts the burn-up calculations.

¹The scaling factor of numberdensities is derived from the unit of cross-sections [barn] which is of the order 10^{-24} .

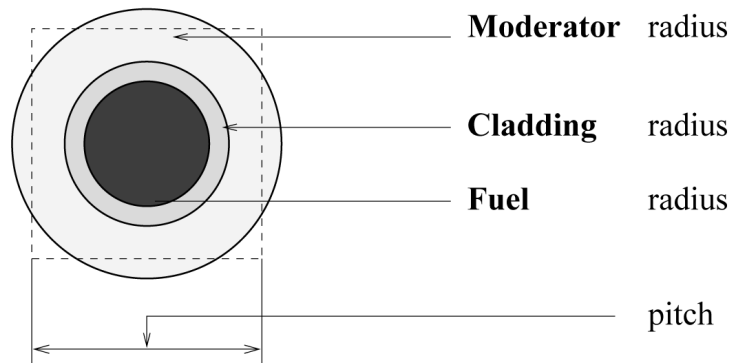


Figure 3.2: Fuel Cell

3.2.3 The Burn-up Model

This section deals with the basic KARBUS model applied for the burn-up investigations comprising a brief description of the geometric irradiation environment and the mathematical solutions applied for neutron flux calculations. Furthermore, an explanation for the constant power-rating, which was applied in the investigations, is given within this chapter. Information is mainly based on References [3] and [4].

The geometrical model applied by KARBUS is comparable with an irradiation experiment of a moderator-fuel cell which is lengthwise extended to infinity, leading to a one-dimensional model. This moderator-fuel cell is assumed to be part of an infinite quadratic lattice of identical cells, neglecting leakage by periodic boundary conditions. Since no leakage is taken into account the solution for neutron flux leads to the infinite multiplication factor k_{∞} ². A sketch of the moderator-fuel cell is shown in Figure 3.2 which was taken from Reference [4]. The illustration shows the applied three-zone model, which is commonly referred to as the three-zone Wigner-Seitz cell using averaged data for each zone such as for material properties and neutron flux.

Geometrical cell parameters concerning the moderator are set by the specific moderator volume. The overlay core structure is build up of quadratic cells which is one possibility for an infinite lattice structure, as applied in this case³. For cell flux-calculations, the quadratic cells are approximated by the one-dimensional, cylindrical Wigner-Seitz

²As a rule of thumb, depending on the Geometric Buckling, for 1GWe LWR cores the value of k_{eff} can be determined by lowering k_{∞} by about 3%. See Reference [33]

³For infinite lattice structures two configurations are common: quadratic or hexagonal cell cross-sections.

model. The geometric parameters for the moderator region, pitch and moderator radius are calculated, so that moderator volumes for both grids become equal.

Solving the neutron flux for the cell regions, a mean cell-flux is calculated from the infinite core flux solution. Starting from this average cell value, mean values for the moderator region and the fuel region are determined. The multi group-transport equation is hereby solved for the eigenvalues of the cell. The mean flux for the fuel region is also used to determine the fuel burn-up. See Reference [3], Chapter A.1.4.2.

The power-rating is set in this case around 200 W/cm, and has a major influence on thermo-hydraulics but a minor on neutron flux and burn-up. Since in this KARBUS job, temperatures are assumed to be constant during irradiation, no temperature dependent feedback influences the flux, e.g. doppler-feedback or moderator density. As can be seen in Chapter 4, the specific power-rating has significant influence on core design and reactor operation. Reference [4] p.15 shows for MOX-fuel, that power-rating varying in a wide range has a negligible influence on k_{∞} . Power rating depends on the comparatively long decay constants of the major isotope groups. Considering these calculations, variation of power-rating only influences the burn-up process in the time-scale. This effect cancels out when plotting versus burn-up. For alternative fuels like thorium based fuels, the effect of power-rating might be rather enhanced.

3.3 Validation Work Accomplishment

3.3.1 Validation settings

In this section the general proceeding of the validation work is described. The iterative process of preliminary adjustments and debugging in the KARBUS module, as well as the data post-processing will not be described in detail. Only the final validation calculations, the basic settings and parameters for the KWO validation project are listed, comprising the cross-section databases, the lattice parameters and others.

Starting point of the validation work was a modified version of the KAPROS module KARBUS, which was to be tested in a current computational environment. As reference data for the calculated results, experimental data was taken from the ICE project [18]. For evaluation purposes,[3] a former validation project accomplished on the basis of the same ICE project data was used as a reference. The validation work furthermore comprises a comparison of three different cross-section databases used within the modified KARBUS environment. Two current databases and one which was already used in [3] have been applied. A description of the databases is given below.

The general proceeding was the following: First of all, calculations for the three different databases were performed. Afterwards, the ICE data and the calculated results have been worked out for graphical evaluations and plotted into charts. Finally, evaluation was accomplished by comparison of the graphical data. Characteristic data and settings for the KWO-ICE calculations are listed in the following.

Cross-section Databases: All mentioned cross-section databases contain microscopic cross-section data points. This data is processed by the GRUBA module into multi-group macroscopic data by means of appropriate formula libraries. The formula libraries contain the calculation specifications for interpolation of the point data into continuous curves, see also Reference [25]. All libraries are 69-group libraries.

The first library which was already used in the KfK 5072 technical report [3], was the G69P1V03 cross-section library with the corresponding formula library F69UD04. For both recent databases namely G69P5J30B and G69P5E65B the formula library F69UD06 has been applied. The G69P5J30B cross-section library contains data from the western European JEFF3.0 database in the ENDF format; **JEFF** abbreviates **J**oint **E**valuation **F**ission and **F**usion Library. The G69P5E65B library contains the US American **ENDF/B-VI** database which is the abbreviation for **E**valuated **N**uclear **D**ata **F**ile, version **B-VI**.

KAPROS and KARBUS basic settings: This paragraph summarizes the basic settings concerning the computational environment, the KAPROS program-system and the KARBUS module. Settings are shown in Table 3.1.

Parameter	Setting	Reference
Operating Software	SuSE Linux9.2	
KAPROS Kernel	LNX2.16	OUTPUT.archiv
Burn-up libraries	KORFI3.NDLITE KORFI3.NDACT KORFI3.NDFPS	run.karbus
Cross-section- / Formula- Databases	G69P1V03 / F69UD04 G69P5J30B / F69UD06 G69P5E65B / F69UD06	input.karbus

Table 3.1: Basic Settings for the ICE/KWO-project.

ICE-Calculations Input Data: In this paragraph, the characteristic input data that is set in the *input.karbus* file is summarized in tables as an overview. The data already given in the text is only mentioned by references. Main input settings are shown by Tables 3.2 to 3.5 below.

Geometric Parameter	Value	Reference / Keyword
Fuel Pin Radius	4.65 [mm]	<i>input.karbus</i> , 'MINP'
Canning Thickness	0.7 [mm]	<i>input.karbus</i> , 'MINP'
Vm / Vs	1.4942	<i>input.karbus</i> , 'MINP'

Table 3.2: Geometric Settings and lattice parameters for the ICE/KWO-project

Pitch and moderator radius, shown in Figure 3.2, can be derived from the values given in Table 3.2, this is shown in Reference [3] p.212 et sqq. The irradiation-power history is plotted in Figure 3.1 and also itemized in detail in Table 3.5. The power history is also available as input sequence in the *input.karbus* file in the Appendix A.2, denoted by the keyword 'BU1D'. The additional isotope set contains the same isotopes as those used for the investigations in Chapter 5, shown in Table 5.1. Table 3.4 shows the variable boron concentration used during the KWO-ICE burn-up. Unlike the calculations accomplished in [3] only 28 time-steps are shown. This is due to the interruption of evaluations at the end of irradiation. The 29th time-step of 365 days zero power was neglected. The power history is listed in detail in Table 3.5 which was taken from Reference [3].

Parameter	Value	Keyword
Moderator Density	0.717944 [g/cm ³]	'MINP'
Fuel Density	0.927411 [g/cm ³]	'MINP'
Temperature of Fuel	1028 [K]	'MINP'
Temperature of Canning	605 [K]	'MINP'
Temperature of Moderator	572 [K]	'MINP'
Initial Enrichment U^{235}	3.1 [%]	'MINP'
Initial Enrichment Pu_{tot}	0.0 [%]	'MINP'
Initial B^{10} Concentration in the Moderator	318 [ppm]	'MINP'

Table 3.3: Further lattice and thermohydraulic settings for the ICE/KWO-project taken from *input.karbus*.

Time-step	B^{10} -Conc. [10^{-6}]	B^{10} -Conc. [ppm]	Time-step	B^{10} -Conc. [10^{-6}]	B^{10} -Conc. [ppm]
1	7,738E-06	322,1	15	4,686E-06	195,1
2	7,567E-06	315,0	16	4,249E-06	176,9
3	6,836E-06	284,5	17	3,414E-06	142,1
4	5,831E-06	242,7	18	2,891E-06	120,3
5	5,395E-06	224,6	19	2,651E-06	110,4
6	5,031E-06	209,4	20	2,338E-06	97,3
7	4,495E-06	187,1	21	1,711E-06	71,2
8	3,726E-06	155,1	22	1,404E-06	58,4
9	2,027E-06	84,4	23	6,705E-06	279,1
10	7,605E-07	31,7	24	5,733E-06	238,7
11	2,558E-07	10,6	25	3,978E-06	165,6
12	7,494E-06	312,0	26	3,000E-06	124,9
13	6,663E-06	277,3	27	2,248E-06	93,6
14	5,447E-06	226,7	28	6,976E-07	29,0

Table 3.4: Soluble B^{10} concentration during the ICE-KWO experiment, concentrations are given for each calculation time-step in numberdensities [10^{-6}] as well as in [ppm].

3.3.2 Validation results

This section contains the fundamental validation results of the KARBUS procedure. As mentioned in the previous section, validation analysis is based on a comparison of three different cross-section libraries and the measurement results of the KWO ICE-project in Reference [18]. Additionally, a former KARBUS validation [3], which was accomplished on the basis of the same KWO experimental data was used for as a reference for data evaluation. Therefore, most of the charts which are discussed in this section are also included in [3]. Few more charts have been added for informational purposes. Deviations and trends in the calculations are discussed.

Miscellaneous: The following issues are remarks on the evaluation. The charts show the results in numberdensities versus burn-up. Therefore, the abscissa's unit for burn-up is gigawatt days per ton of initial heavy metal (GWd/tHM). The ordinate's unit is atoms per initial metal atoms (Atoms/IMA). Numberdensity's unit used during validation is thus different from today's common unit of numberdensities (particles

per volume) used in Chapter 5. The unit of IMA was chosen for the purpose of comparability with the ICE data. It is obvious that for isotope ratios the units cancel out.

Evaluation in the charts is interrupted at the end of irradiation time. Thus, the decay of short living isotopes during the period of decay-heat cooling and storage is neglected. For the ratio of Cs^{134} to Cs^{137} no experimental data was available, since ICE only provided activity ratios for this isotope ratio. Activity ratios have not been calculated for validation.

The diagrams are separated into two different sets depending on their content:

- The first set comprises charts which compare isotope data from ICE and calculated results comprising Figures A.1 to A.31 shown in Appendix A.3. Only these charts have been used for code validation.
- The second set comprises charts that only compare the calculated results of the different databases in case ICE did not provide any data for evaluation. This set of charts is shown in the Appendix A.4 Figures A.32 to A.39. These charts were not used for validation but provided as additional information.

All the charts have been arranged alphabetically depending on the isotope they show. The charts containing ICE experimental data show the measuring points, denoted by crosses, as well as the measurement inaccuracy by using error bars. The error bars are given for inaccuracy of burn-up measurements in x-direction and, if available, for numberdensities in y-direction. The validation results are summarized in the Tables 3.6, 3.7 and 3.8. Validation was accomplished by the following:

For every isotope, the library giving the best approximation to the ICE data points was used to calculate deviations. The relative deviation of the data points to this curve is listed in the last column of the tables. For a conservative estimation, always the strongest outlier was taken for calculation, such giving the maximum relative deviation. The last but one column lists whether the best approximating curve under or overestimates the data points. To estimate the relative location of the remaining curves, in the third column the relative deviation of these curves to the best approximation is given. The corresponding sign denotes the location of the curve relative to the best curve. Further information is also given in the third column. If datapoints lie in between two curves, the relative deviation is calculated for both curves as done before. If datapoints are spread around one curve the estimation column shows a hyphen. The three different libraries compared, are denoted in column two. DB stands for database

or library, the last three letters are V03 for the G69P1V03 library, 30B for G69P5J30B and 65B for the G69P5E65B library. The first column denotes the Isotope to which the data corresponds.

Time-Step	Micro Time-Steps							
	1		2		3		4	
	days	W/cm	days	W/cm	days	W/cm	days	W/cm
1	5.8	219.6	1.0	0.0	-	-	-	-
2	4.6	219.6	-	-	-	-	-	-
3	25.0	219.6	25.0	219.6	-	-	-	-
4	25.0	219.6	2.0	0.0	-	-	-	-
5	3.5	219.6	-	-	-	-	-	-
6	30.0	219.6	41.5	0.0	-	-	-	-
7	6.5	219.6	-	-	-	-	-	-
8	25.0	219.6	25.0	219.6	-	-	-	-
9	25.0	219.6	25.0	219.6	25.0	219.0	5.8	0.0
10	5.9	219.6	-	-	-	-	-	-
11	31.0	219.6	28.0	0.0	-	-	-	-
12	6.9	219.6	-	-	-	-	-	-
13	30.0	219.6	30.0	211.0	-	-	-	-
14	30.0	219.6	30.0	219.6	3.5	0.0	-	-
15	4.7	219.6	-	-	-	-	-	-
16	20.0	219.6	20.0	219.6	-	-	-	-
17	20.0	219.6	20.0	219.6	3.5	0.0	-	-
18	3.0	219.6	-	-	-	-	-	-
19	20.0	219.6	3.0	0.0	-	-	-	-
20	4.0	219.6	-	-	-	-	-	-
21	28.0	219.6	28.0	219.6	-	-	-	-
22	13.8	219.6	380.0	0.0	-	-	-	-
23	5.3	219.6	-	-	-	-	-	-
24	30.0	219.6	35.0	219.6	-	-	-	-
25	30.0	219.6	30.0	219.6	3.0	0.0	-	-
26	3.4	219.6	-	-	-	-	-	-
27	25.0	219.6	25.0	219.6	-	-	-	-
28	20.0	219.6	29.0	219.6	-	-	-	-
29	1.0	219.6	365.0	0.0	-	-	-	-

Table 3.5: Irradiation power history of KWO-ICE, the table shows the macro and micro time-steps and the corresponding irradiation power for the whole experiment. Information was taken from the *input.karbus* input file.

1st Evaluation Table				
Isotope	DB	Comment	Estimate	Relative deviation
<i>Am</i> 241	DBV03 DBJ30 DB65B	best approximation worst curve, -5 % -4 %	under	100 %
<i>Am</i> 243	DBV03 DBJ30 DB65B	+30 % best approximation identical DBJ30 +30 %	over	23 %
<i>Cm</i> 242	DBV03 DBJ30 DB65B	best approximation -7 % worst curve, -10 %	under	25 %
<i>Cm</i> 244	DBV03 DBJ30 DB65B	best approximation -16 % identical DBJ30 -16 %	under	16 %
<i>Kr</i> 83/86	DBV03 DBJ30 DB65B	all curves identical all curves identical all curves identical	under	≫100 %
<i>Kr</i> 84/83	DBV03 DBJ30 DB65B	all curves identical all curves identical all curves identical	under	20 %
<i>Kr</i> 84/86	DBV03 DBJ30 DB65B	all curves identical all curves identical all curves identical	under	23 %
<i>Nd</i> 143/148	DBV03 DBJ30 DB65B	all curves identical all curves identical all curves identical	over	5 %
<i>Nd</i> 144/148	DBV03 DBJ30 DB65B	all curves identical all curves identical all curves identical	under	24 %
<i>Nd</i> 145/148	DBV03 DBJ30 DB65B	all curves identical all curves identical all curves identical	over	8 %

Table 3.6: First Evaluation table of the ICE validation. For each isotope the table denotes the database (DBs) producing the best curve and evaluates the relative deviation of measuring points from the best curve.

2nd Evaluation Table				
Isotope	DB	Comment	Estimate	Relative deviation
<i>Nd</i> 146/145	DBV03	all curves identical	under	39 %
	DBJ30	all curves identical		
	DB65B	all curves identical		
<i>Nd</i> 146/148	DBV03	all curves identical	under	31 %
	DBJ30	all curves identical		
	DB65B	all curves identical		
<i>Pu</i> 238	DBV03	best approximation	under	53 %
	DBJ30	worst curve, -10 %		
	DB65B	-6 %		
<i>Pu</i> 239	DBV03	worst curve +3 %	over	7 %
	DBJ30	best approximation		
	DB65B	identical DBJ30 ± 0 %		
<i>Pu</i> 240	DBV03	best approximation	over	6 %
	DBJ30	+4 %		
	DB65B	+4 %		
<i>Pu</i> 241	DBV03	good approximation +8 %	over	7 %
	DBJ30	best approximation	under	5 %
	DB65B	identical DBJ30 ± 0 %		
<i>Pu</i> 242	DBV03	best approximation	under	8 %
	DBJ30	-14 %		
	DB65B	identical DBJ30 -14 %		
<i>Pu</i> 240/239	DBV30	good approximation -7 %	under	7 %
	DBJ30	best approximation	over	3 %
	DB65B	identical DBJ30 ± 0 %		
<i>Pu</i> 241/240	DBV03	best approximation	over	2 %
	DBJ30	-11 %		
	DB65B	identical DBJ30 -11 %		
<i>Pu</i> 242/240	DBV03	best approximation	under	8 %
	DBJ30	-17 %		
	DB65B	identical DBJ30 -17 %		

Table 3.7: Second Evaluation table of the ICE validation. For each isotope the table denotes the database (DBs) producing the best curve and evaluates the relative deviation of measuring points from the best curve.

3rd Evaluation Table				
Isotope	DB	Comment	Estimate	Relative deviation
<i>Pu</i> 242/241	DBV03	best approximation	under	10 %
	DBJ30	−7 %		
	DB65B	identical DBJ30−7 %		
<i>Pu/U</i>	DBV03	−2 %	over	6 %
	DBJ30	best approximation		
	DB65B	identical DBJ30±0 %		
<i>U</i> 235	DBV03	all curves identical	under	5 %
	DBJ30	all curves identical		
	DB65B	all curves identical		
<i>U</i> 236	DBV03	best approximation	under	±1.5 %
	DBJ30	−6 %		
	DB65B	−2 %		
<i>U</i> 238	DBV03	good approximation −1 %	-	±1.7 %
	DBJ30	best approximation	-	±1.4 %
	DB65B	identical DBJ30		
<i>U</i> 235/ <i>U</i> 238	DBV03	all curves identical	under	7 %
	DBJ30	all curves identical		
	DB65B	all curves identical		
<i>Xe</i> 131/134	DBV03	all curves identical	under	55 %
	DBJ30	all curves identical		
	DB65B	all curves identical		
<i>Xe</i> 132/131	DBV03	all curves identical	over	35 %
	DBJ30	all curves identical		
	DB65B	all curves identical		
<i>Xe</i> 132/134	DBV03	all curves identical	under	25 %
	DBJ30	all curves identical		
	DB65B	all curves identical		
<i>Xe</i> 136/134	DBV03	all curves identical	-	3 %
	DBJ30	all curves identical		
	DB65B	all curves identical		

Table 3.8: Third Evaluation table of the ICE validation. For each isotope the table denotes the database (DBs) producing the best curve and evaluates the relative deviation of measuring points from the best curve.

3.4 Summary

This section summarizes the results of the validation work. Discussing trends and outliers, this leads to major suggestions for succeeding investigations. Generally speaking, there is no major difference between the curves of the three investigated libraries. It is obvious that in most cases the two more recent unadjusted databases G69P5J30B and G69P5E65B produce nearly identical plot-curves. However, for most of the investigated isotopes it is shown that the older GP69V03 library represents the best approximation to the ICE datapoints. This might be due to the fact that this library was “custom made” by merging best estimate data for single isotopes from different libraries on the basis of experiences. Validation proves the quality of the GP69V03 library. It should be pointed out that for the isotope groups of major importance, such as uranium and plutonium, the differences between the databases turns out to be very small, as expected.

Considering the relative deviation of datapoints from the curves, it is striking that the relative deviations found are small. However, the relative deviation values of some isotopes seem to be very high. This has to be discussed further by considering the specific isotopes as well as the calculation model which was applied.

Starting with the latter, the model contributes to increased relative deviations, since the applied three-zone model is very simple compared to the rather involved boundary conditions during irradiation of a core in praxis. This leads to a standard inaccuracy referred to as a bias. However, for burn-up investigations in a wide range, this model has herein proven to be very useful.

The high deviations associated with isotopes result from the fact that only relative deviations are calculated. Measuring methods for small absolute isotope concentrations, that means small numberdensities, mostly offer only low absolute measuring accuracy. Since low measurement accuracies are related to very small concentration, relative deviations may strongly vary. It has to be taken into account, that for this validation, the maximum burn-up did not exceed the 30 GWd/tHM which is quite low for todays burn-ups. The mentioned effect therefore mainly contributes to higher isotope fractions of plutonium⁴ as well as minor actinides like americium and curium showing low absolute concentrations. For increased burn-ups as well as for MOX fuels, the inaccuracy for the mentioned isotopes is expected to be lower.

It can be concluded that for burn-up investigations the KARBUS module gives a good representation of the buildup of different isotope groups, especially for high burn-ups

⁴Also Plutonium 238!

and MOX fuel. Yet, particularities for some isotopes should be taken into account. Accounting for the best approximation curve, the suggestion might be to take the GP69V03 library for investigations. However there are strong arguments to apply the more recent libraries. The GP69V03 library is not commonly used or maintained nowadays and furthermore partly customized. In particular for the purpose of comparability with other applications e.g. Monte Carlo Simulations, one of the more recent databases, containing standardized main dataset should be preferred for current investigations.

Chapter 4

Basic Requirements of High Burn-up fuels in LWRs

Various aspects of nuclear energy production suggest an increase of fuel burn-up. Economic standpoints as well as the open issue of the nuclear fuel cycles' back end are the driving force for investigations upon this topic. High burn-ups correspond to longer cycle times in plants and less refueling outage time per year. This contributes to reduce generation costs and result in better fuel utilization due to lower fissile tails, leading to higher plant efficiencies. Furthermore, the increase of burn-up reduces the volume of spent fuel and fuel throughput, thereby lowering the back end costs for storage, reprocessing and deposition.

This chapter will give a brief introduction to the broad topic of high burn-ups in light water reactors and the multiple challenges in its further extension. The following Chapter 5 is addressed to the implications of going to high burn-ups considering the buildup of isotope fractions. Two parameters are investigated for high irradiated uranium fuel: The impact of soluble boron in the coolant of pressurized water reactors (PWRs) and as design parameter, the moderator to fuel ratio. Average burn-ups around 50 GWd/tHM are reached in modern pressurized water reactors, slightly less for boiling water types. Extending the burn-up to higher values demands further enrichment, however many more details have to be thoroughly investigated in order to assure safe operation. The physical consequences on neutronics or the impact of high irradiation doses on cladding materials and fuels during high burn-ups rise the need for further developments. In the following the added value, interactions and implications of high burn-ups in nuclear power reactors will be pointed out.

4.1 Economic Benefits of High Burn-ups

All efforts extending the burn-up in light water reactors are subject to be accomplished in the present working power plants with the least modification possible. Due to the enormous fixed costs of nuclear plants, the complexity of their systems and the difficulties of licensing a balance between the need of optimization during long lifetime and the expenses for modifications has to be found [5]. Hence, amortization considerations try to avoid redesign to keep outage and costs as small as possible. The currently discussed modifications are thus limited to the inner design of fuel assemblies and control rods.

Total production costs of electric power can be separated into fixed costs comprising the investment costs and variable costs depending on the hours of operation. Characteristic for nuclear power plants are comparatively high shares of fixed costs and lower shares of variable costs per net power output. Variable costs include costs for fuel, fuel cycle and manufacturing resources, among others. Optimization of fuel assemblies for high burn-ups concern the variable costs for fuel and fuel cycle and effect on production costs by a higher operational availability. Modern nuclear power plants can produce electricity worth up to one million Euro a day [11]; fewer days outage and higher capacity factors thus promise fair savings. Design goal for high burn-ups in current LWRs is the extend of cycle times at given maintenance interval frequencies. At present, the maximum burn-up of a core¹ limits the cycle time in LWRs; maintenance work is done during refueling outage.

The following information is mainly based on [14]. Assumed the modifications for burn-up concern only the assemblies, the direct fuel costs should be a good way to estimate the costs of increasing the burn-up. The direct fuel costs are sub-divided into costs for mining and purification, enrichment, fabrication, spent fuel storage, reprocessing, waste disposal and transport. Discussing the impact of burn-up on direct fuel costs, it is important to note that the latter represent only 20% of the generating costs [14]. An increase in direct fuel costs could therefore be tolerated if there are larger benefits from increased generation earnings. Higher fuel costs are also acceptable if other costly restraints are avoided. E.g. plants with limited spent fuel storage capacities could be forced to close down before reaching their engineering lifetime when available storage capacity is exhausted.

Front-end fuel costs will rise for higher burn-ups. Higher enrichments rise the expenses for conversion and enrichment. As fabrication costs for assemblies have a fixed rate

¹The end of cycle (EOC) burn-up is reached when the value of k_{eff} falls below one.

per kilogram they should decrease with higher burn-up. Nevertheless, this approach neglects two influences:

1. Fuel vendors may recover their development costs for more complex assemblies and advanced materials.
2. Up to now the criticality safety limit for enrichment is 5 wt.% [11], [14]. For enrichments exceeding that limit, which will be reached soon, difficult and expensive licensing for new fabrication plants has to be passed². This will provoke a kind of step change in the fuel cycle, in techniques but also in costs, and thus rise the all over front-end costs.

The breakdown of back-end costs is counterbalanced. A smaller fuel throughput will reduce costs for transport and storage due to reduced fuel volume. High burn-ups are accompanied by increased decay-heat and higher neutron output. Both will complicate waste management during interim storage, transport, reprocessing, conditioning and disposal, raising the back-end costs. The crucial factor for the future back-end fuel costs will be the development of waste treatment techniques and storage capacity.

The breakdown of the overall direct fuel costs leads to a rough estimate of their dependence upon burn-up. Taking into account the above mentioned assumptions Reference [14] observed a minimum of the fuel costs per MWh electric power to be around 55 GWd/tHM. All costs are weighted with a monetary discount factor for the period of time when expenditure occurs. Discounting reduces the relative contribution of back-end costs occurring later in time. Figure 4.1, taken from Reference [14], displays the results for two different discount rates. However an extend of burn-up to higher values than 55 MWd/tHM is still to be considered. Reference [32] investigates the optimum discharge burn-up and cycle length in PWRs for maximum discharge burn-ups of 70 GWd/tHM. Considering different enrichments and cycle lengths a decline of fuel costs for higher burn-ups was found for all configurations. The consequential costs for excess enrichments above 5 wt.% U^{235} were estimated but not included in the calculations. Differences in the findings of the two studies are due to different assumptions and difficulties in predicting parameters. In Reference [10] it was recently reported that leveled fuel costs decrease with burn-ups however, no fuel cycle benefits for burn-ups higher than 75 MWd/tHM can be found. Increased unit costs for high enrichments have not been taken into account. Therefore, considering all fuel cycle costs in the development of the overall fuel costs, the model given by Reference [14] seems preferable.

²Today's enrichments are 4.5 wt.% U^{235} for average burn-ups of 50 GWd/tHM.

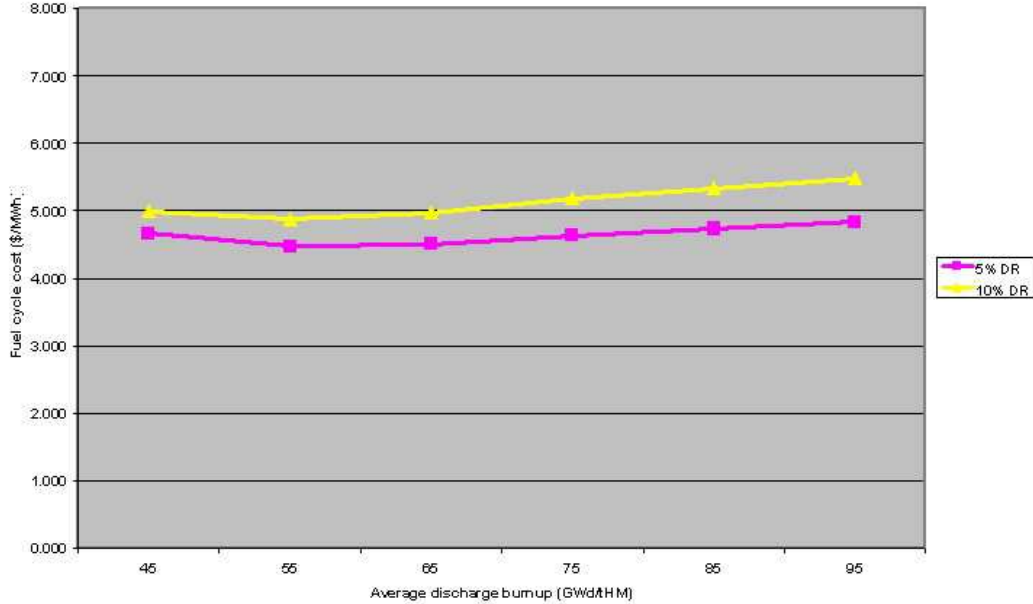


Figure 4.1: Fuel cycle levelized costs (\$/MWh) electric power versus burn-up and discount rate (DR) taken from [14].

4.2 Implications on the Core System [10] [14]

Rising the enrichment of fissile components in assemblies implies changes of various nuclear design parameters in the whole core. Hence accomplishing ambitions of high burn-ups are rather involved. Enrichment influences all major incore processes, such as neutron flux, reactivity, power peaking, feedback coefficients, control rod reactivity and safety margins. This section briefly discusses the influence of high burn-ups on major core design parameters.

High enrichments result in high multiplication factors at the begin of cycle (BOC). According to Equation (2.4), the excess reactivity ρ_{BOC} is also very high. To compensate excess reactivity at BOC, a combination of different neutron poisons is applied, solid burnable poisons and soluble boron in the coolant of PWRs. Characteristic advantages and drawbacks in the use of the mentioned poison types are shown in the subsequent section. However, Reference [13] indicates no design limits to realize burnable poisons in PWRs up to 100 MWd/tHM. Investigations should focus on the impact of poisons the neutronic system.

The use of burnable poisons influence on the neutron energy distribution. The higher the content of thermal absorber is, the harder the spectrum becomes which in turn influences important system parameters such as power peaking factors, control rod reactivity and reactivity feedback coefficients.

Discussing thermal reactors, control mechanisms are usually based on thermal flux Φ_{TH} . The definition of the thermal reaction rate³ R_{TH} [39] makes it obvious that the thermal flux scales with $1/\Sigma_F$. The macroscopic thermal fission cross-section is proportional to the number density of the fission atoms. This corresponds to the fuel enrichment, which is also valid for MOX. The result is, that higher enrichments needed for high burn-ups lower the thermal flux and in turn lead to a hardening of the neutron spectrum. This has certain consequences on control parameters: Thermal neutron absorbers will loose efficiencies with decreasing thermal flux. The spectral change will be noticeable in lower control rod reactivity worths and shutdown margins, requiring more control rods, as well as higher contents of burnable and soluble neutron poisons. Due to higher absorber contents and such enhanced thermal capture, this effect additionally contributes to the spectral hardening. Especially soluble boron rises another limit to enrichment, for a certain concentration in the moderator, the moderator temperature coefficient could become positive.

Only a slight influence on the Doppler coefficient is to be seen by higher enrichments. It becomes less negative. The moderator feedback will become more negative by increasing the enrichment due to reduced thermal flux which lowers the relative influence of thermal capture in the moderator and in turn makes the moderation process more dominant. Various feedback parameters have been investigated in Reference [10] within a parametric study depending on the enrichments and for different cycle patterns.

Important for efficient power generation in a nuclear reactor core is a power peaking factor close to one. A value nearby one describes a flat flux profile producing a homogeneous burn-up profile. This in turn is a prerequisite to maximize the average burn-up and reach maximum earnings from power production. Due to the reshuffling in a high burn-up multi batch cycle, high burned assemblies are arranged next to fresh ones. This variation in burn-up and local reactivity values increases the power peaking factor especially in radial direction. The impact aggravates for higher burn-ups. To assure fuel integrity and heat transport, various power limits are defined: Critical Power Ratio (CPR) in LWRs, Departure from Nucleate Boiling (DNB) in PWRs, fuel melting criteria, Pellet Cladding Interaction (PCI) and corrosion limits. All criteria

³The impacts per unit volume.

describe damaging effects with a strong temperature dependence. The local and global core temperature profiles are proportional to the power distribution. This makes it obvious that the highest local power or temperature peak limits the core power. Thus, a high power peaking factor could penalize the core power and lead to lower efficiencies for high burn-ups.

4.3 High Burn-up Fuels [2] [14]

Fuel behavior, particularly for long irradiation time, is a very complex system of interactions and up to now not very well understood. This section will outline the reasons for the complex behavior during burn-up and show some of the major challenges arising from its increase.

Fuel design includes not only the fuel pellets and pins but the cladding and their interactions. The cladding plays a decisive role in the safety management of a plant and the effort to prevent dissemination of radionuclides from the reactor. Three barriers fulfill this function whereas the cladding is the first one, followed by the pressure vessel in combination with the primary loops and the containment. The main task is to assure the demanded power rating up to maximum burn-up as well as the fuelrod integrity and safety criteria at the same time. This is particularly challenging for high burn-ups, long irradiation times and during disturbed operation, e.g. reactor scrams.

During irradiation the fuel is modified by radiation as well as by chemical, thermal and mechanical interactions. A burn-up of 10 GWd/tHM corresponds to the fission of 1% heavy atoms. Each fission produces two fission products. The comparably large mass and diameter of the fission products lead to a small range in the surrounding fuel matrix. With the fission products carrying the major part of fission energy, all energy is distributed in a very small area. The high energy impact on the matrix causes a large number of displacements of initial matrix atoms. This effect and the doubling of atoms during fission increases lattice imperfections, changing the fuel properties and initiating the solid swelling of the fuel. The interaction of many effects impose high uncertainties to predictions, with increasing difficulties for higher burn-ups. A desirable way to investigate long term fuel behaviour are experiments. However, they are time consuming - four to six years of irradiation of normal fuel in a reactor - or require special high flux facilities, making them rather expensive. Today one is already working close to the material limits to cover the enormous burden during irradiation. In the following, a few high burn-up effects on fuel and fuelrods are described.

As mentioned above, burn-ups strongly effects the fuel properties. Main reasons are increasing lattice imperfections, fuel cracking and growing porosity of the fuel due to weakening of the grain boundaries by fission gas agglomeration. A major consequence is a strong dependence of heat conductivity and heat transfer on burn-up. Heat transport is crucial for systems of very high power density such as nuclear reactors. Less heat transport results in temperature increase, enhancing damage due to corrosion effects, cladding fatigue or fuel melting. Fission gas release during burn-up rises the inner pressure of the fuel rod which leads to a cladding lift-off with feedback to heat transfer. Thermal fuel swelling in combination with solid swelling could cause contact forces between fuel an cladding, leading to mechanical interaction. This effect is called pellet-cladding mechanical interaction (PCMI). Consequences are cladding attenuation by deformation or enhanced stress crack corrosion (SCC).

4.4 Soluble and Solid Burnable Poisons [11] [26]

The consequence of higher enrichments is an increased excess reactivity. To compensate for the surplus of reactivity at begin of cycle, different neutron poisons are being used. According to Reference [11], the most common ones are boron B^{10} and gadolinium Gd^{157} compounds. erbium Er^{167} , samarium Sm^{149} , hafnium Hf^{177} and europium Eu^{151} are less frequently applied since not all of them are sole thermal neutron absorbers. Neutron poisons can be separated in two groups: Soluble and solid poisons. As for the former, in PWRs only boric acid is used as soluble poison. Solid poisons, known as burnable absorbers (BAs), can be further classified. Depending on their usage, BAs are called Integral Burnable Absorbers (IBAs) if non-removable from the core and Burnable Poison Rods (BPRs) if inserted in assembly guide tubes. BPRs can be removed during refueling outage. It is not common to use BAs for more than one cycle thus all absorbers are designed to operate during the first cycle of fresh, unirradiated assemblies. All BAs contribute to a small reactivity penalty at the end of life of an assembly, due to incomplete consumption of the absorber. This reduces the maximum burn-up, particularly for the use of IBAs. No parasitic absorption rises from soluble boron because it is completely removable from the coolant. A further advantage arising from the solubility is the possibility to change the concentration of the absorber during operation of the reactor which is used for reactivity fine-tuning during burn-up. The general impact of absorbers is a reduction of thermal flux caused by thermal neutron capture. Absorbers should therefore be dispersed as homogeneous as possible.

Apart from the homogeneous dissolution of soluble boron, dispersion could be reached by a large number of symmetrically arranged BA-rods. One possibility to manufacture IBAs is to homogeneously mix the BAs into the fuel pellets, another to coat the pellets. This is commonly used in both LWR types. Due to the neutron poison enrichment in BA-rods, a strong thermal flux suppression takes place in the vicinity of the rod. A result of this can be unwanted power peaking and non-uniform burn-up. But this effect can also lead to an advantage compared to soluble boron: Unwanted power peaking can be diminished locally. A further disadvantage of solid Boron compounds used within the fuel rods rises from its contribution to inner rod pressure. Helium is produced from the (n, α) reaction of the B^{10} . The impact of soluble Boron will be discussed extensively in the next chapter. Modern pressurized water reactors are commonly operated with a combination of soluble and burnable absorbers to optimize power distribution and burn-up.

Higher excess reactivity that occurs with higher enrichments will require additional absorbers. The maximum absorber volume however is restricted by the core design. For example the number of unused assembly guidetubes limits the number of BPRs. Two restricting parameters limit the soluble boron content: The maximum solubility of boric acid in water of the cold injection tanks to prevent precipitation and the Moderator Density Coefficient (MDC) that has to remain negative in all conditions.

As mentioned above, the presence of neutron poisons during depletion hardens the neutron spectrum [31], [36]. This leads simultaneously to an increase of the plutonium production and to a decrease of U^{235} fission. Both may increase reactivity of the spent nuclear fuel. Therefore, for a given burn-up, an assembly exposed to absorbers might have higher reactivity than assemblies that have not been exposed to BAs. Discharged spent fuel reactivity limits the possibility of cask loading and justification for dry cask storage.

Burn-up credit [36], is a concept that takes credit of the reactivity attenuation during fuel burn-up due to the depletion of fissile nuclide and the production of actinides and neutron absorbing fission products. The reactivity reduction depends on the depletion environment, operating conditions and presence of BAs. American Nuclear Regulatory Commission's Spent Fuel Project Office recommends licensing that restricts the use of burn-up credit to assemblies not using burnable absorbers. This excludes a major part of the spent fuel assemblies from cask loading and limits the practical use of burn-up credit. Reference [36] expects the typical increase of reactivity to be less than 1% of Δk , for a one-cycle BPR exposure in PWRs.

4.5 Isotope Fraction Buildup

The characteristics of high burn-up fuels lie in their long incore irradiation times. This leads to an augmented buildup of actinides due to a breeding process, especially in the isotope fractions of plutonium and minor actinides. Both isotope groups are highly active, long living components of spent nuclear fuel with costly impact on the back end of the fuel cycle.

The change in the neutron energy distribution for high enrichments directly enhances the buildup of actinides. According to Reference [3], the spectral hardening shifts the mean neutron energy in the thermal range closer to the first resonance of U^{238} at 6.68 eV. The probability of resonance capture rises strongly, ending up in an enhanced buildup of Pu^{239} . Succeeding capture and decays in the subsequent isotope groups of Pu^{239} effect the buildup of transurania, favored by resonances in all plutonium isotopes below 6.68 eV. An important fact is, that the buildup process can be controlled by the influence of design parameters via the neutron spectrum. In particular plutonium is a contentious issue. In LWRs plutonium and its buildup via self-breeding contributes fairly to the energy yield of the fuel. Dedicated LWR-designs could enhance breeding and thus extend criticality to higher burn-ups. In other words, one and the same burn-up requires less initial enrichment for higher breeding ratios. Assumed the neutron spectrum enhances the fission of Pu^{239} and Pu^{241} , a large part of plutonium is burned in-situ, influencing not only the neutron energy spectrum but also producing less delayed neutrons. As shown in [3], higher plutonium contents lead to increased neutron yields enhancing fission as well as influencing the reactivity feedback coefficients. This is crucial for reactivity control and the inherent safety parameters of the core. Generally speaking, an increase of fissile plutonium downgrades the reactivity safety coefficients⁴ in LWRs, the Moderator Density Coefficient as well as the Doppler Coefficient of the fuel. Both is leading to a limitation of fissile plutonium shares in fuels to values smaller than $\sim 6 - 7$ wt.%, see Reference [4].

A major problem given by an increased plutonium production is the risk of misuse for weapon production -the proliferation aspect- and the consequences on the back-end processing. Two reasons lower the threat of proliferation by extending the burn-up: Hardening of the neutron spectrum and increased irradiation time not only enhances plutonium buildup but also the in-situ burning of Pu^{239} and Pu^{241} . This leads to a

⁴The unit of the feedback coefficients of reactivity is given by a reactivity change per change of the according variable. E.g. $d\rho/dT$ for the temperature coefficient. The common unit is [pcm/K^o, ρ_{H_2O} , ppm...]. **pcm** means **percent milli ρ** .

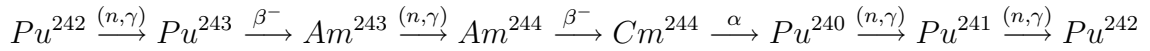
decrease of the specific plutonium production. Higher burn-up leads to an augmented buildup of higher numbered isotopes which deteriorate the quality of plutonium for weapon use and lowers the shares of fissile plutonium. E.g. Pu^{238} and Pu^{240} are not wanted for the use in nuclear weapons, the latter produces high neutron output due to spontaneous fission, Pu^{238} emits high decay heat. Pu^{238} is mainly build up due to $(n, 2n)$ reactions in Pu^{239} as well as by β -decay of Np^{238} and α -decay of Cm^{242} . Also few $(n, 3n)$ reaction in Pu^{240} contribute to the buildup. The strong decay heat of Pu^{238} , as well as the spontaneous fission of Pu^{240} limits the fraction of this Isotope for reprocessing and accounts for the proliferation resistance, which will be discussed later in Chapter 5.3.

4.6 Spent Nuclear Fuel: Treatment and Reprocessing

Many isotope fractions of the transuranics increase with higher burn-ups. This section is dedicated to its impact on the back-end processing, i.e. handling, reprocessing and deposition. Corresponding to their impact on the conditioning process, transuranics have to be divided into two groups: One containing all isotopes with relatively short half-lives up to a few ten years, another covering the remaining ones with long half-lives of several hundred or thousand years.

According to Reference [4], short half-lives imply high irradiation intensity, noticeable as high decay heat production due to α and β activity and may require continuous cooling. γ -radiation and neutron emission from spontaneous fission necessitate remote handling techniques and strong shielding due to the range of radiation. In practice the cooling time is dominated by short-living isotopes; an increase in burn-up will extend cooling time to keep radiation limits for interim storage and transport flasks. The most important shares are rising from Pu^{238} , Cm^{242} , Cm^{243} , Cm^{244} and Am^{241} with strong α - and Pu^{241} with strong β -decay heat. All these isotopes can undergo spontaneous fission and thus contribute to neutron output.

Isotopes with long half-life, such as Np^{237} , Pu^{242} and Am^{234} , emit radiation with less intensity, however it will take a very long period of time until radiation dose will have decreased to harmless values. Thermal fission cross-sections for isotopes of the second group are usually very small. Therefore, a kind of isotope circulation takes place, wherein breeding and β -decay rises the atomic number while α -decay turns it back to its initial value.



One possibility to brake through these circles of predominantly minor actinides is incineration by a very hard neutron spectrum, enhancing fission. Such neutron spectra can be found in fast reactors. Since a working solution for waste⁵ incineration is not available, nuclear waste has to be deposited. Waste is immobilized and enclosed by glass or concrete in special inert casks to assure safe storage over long periods of time. A common problem of deposition is not only the radio toxicity of the isotopes but also the fact that many of the actinides themselves are very toxic to organisms. Therefore they should be excluded from the biogeochemical cycle forever.

The impact of increasing the burn-up on the fuel cycle is the following: The required cooling time rises with the time of fuel irradiation. It takes several years after reactor shutdown reducing the heat and radiation level to fulfill the licensing limit of radiation for transport and reprocessing. The extend of cooling time could balance the surplus of storage capacity gained by higher burn-up. Increased radiation intensity of spent fuel could require more or improved transport flasks which will rise expenditures.

The fuel fabrication time could be influenced as well. Increased residual decay heat and radiation during the fabrication process will extend the time of fabrication. Dissolutions of fuels during the recovery process of plutonium possibly have to be diluted due to criticality problems. Important for MOX fuel is to keep the time between plutonium separation and restart of the reactor as short as possible. Pu^{241} is a fissile isotope with short half-life of 14.35 years [17] and its decay penalizes the burn-up as its successor Am^{241} does with reactivity.

Higher contents of actinides in spent fuel will at least prolong the excore time during reprocessing which counteracts with some of the benefits of high burn-ups. Increased radiation in spent fuel will probably limit the conditioning process and increase costs.

4.7 Summary:

This chapter briefly describes the basic issues and motivations related to an increase of burn-up. It was shown that higher burn-ups in common LWRs could be a way to gain further margins of earnings from electric power production. A certain minimum of fuel cost is to be expected around 55 GWd/tHM [14] which will soon be realized

⁵SNF components that are, commonly in thermal neutron reactors, not fissionable.

without extra efforts. For an 18-month cycle length, [32] found decreasing fuel costs up to 70 GWd/tHM. However, many uncertainties exist within the predictions, e.g. in few months in 2005, costs for uranium ore have more than doubled. Burn-up increase beyond 55 GWd /tHM will require extensive research and development with a distinct increase in very high burn-ups of 70 GWd/tHM and more. However, there are different aspects encouraging a moderate rise of burn-up beyond 55 MWd/tHM despite rising fuel costs, compensated by a reduction of the all over generation costs. The technical and physical impacts as well as the interactions with increased burn-ups making fast realization of very high burn-ups unlikely, have been discussed. Furthermore, parameters and methods influencing burn-up have been pointed out.

In a physical manner, one of the most important parameters is the energy distribution of the neutrons. Therefore two technical design parameters effecting the neutron spectrum and thus the burn-up process are investigated in the next chapter, namely the soluble boron concentration in PWRs and the moderator to fuel ratio as a principle design option.

Chapter 5

Parametric Investigations on High Burn-ups in LWRs

This chapter is dedicated to investigations on high and very high burn-ups in light water reactors (LWRs). Within a parametric study, the influences of large burn-up extends on isotope fraction buildup are in special focus. Two parameters with a strong influence on the neutron spectrum are investigated in depth. Namely, the design option of the moderator to fuelrod volumetric ratio (V_m/V_s) and the soluble boron concentration of PWR coolants. One comprehensive section's focus is, in the face of proliferation resistant fuels, on plutonium and especially on Pu^{238} .

The purpose of this chapter is to provide a guideline for fuel optimization of modern high burn-up fuels in LWRs with regard to the basic depletion mechanisms in isotope fractions. Depending on the application, this should help to selectively customize fuels as well as boundary conditions of the depletion environment. Application areas are the alignment of reactor processes and the back-end of the fuel cycle to high burn-ups or the refinement of irradiation experiments.

The included burn-up calculations were accomplished as described for the validation in Chapter 3 with the KAPROS module KARBUS. Few adjustments which are described in this Chapter have been accomplished. This chapter evaluates burn-ups up to 140 GWd/tHM which is, generally speaking, unrealistically high for today's applications. The previous chapter estimates mean burn-ups for LWRs of 70 GWd/tHM to be feasible within a few years. Beyond this, the extend of burn-up will be very demanding. However, the calculated results for the mid-range of burn-up scale are not expected to be less significant. Information about parametric influences on very high burn-ups might be of particular interest for feasibility evaluations for future nuclear

systems and techniques. E.g. the idea of long term fuel reprocessing like the concept of a pool of reactors as described in Reference [4], following the design goal of a closed nuclear fuel cycle.

5.1 Impact of Boric Acid Concentration on High Burn-ups

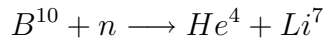
Pressurized water reactors are the most prevalent reactor types for commercial nuclear energy production. This basic design principle prevents coolant from phase change during heating-up and thereby causes a homogeneous¹ density distribution in the core. This offers the possibility to solve neutron poisons in the moderator. A major advantage thereby is a smooth flux depression all over the core. The only poison which is used in this manner is the B^{10} isotope that provides a high thermal capture cross-section $\sigma_{n,\alpha}$. Soluble boron is a very important issue for PWRs as combined with burnable poisons it compensates for excess reactivity and manages criticality fine-tuning during burn-up. The first section of this chapter makes some introductory remarks on the use of boric acid in the core system of PWRs. Aspects of the water chemistry and basic interaction as well as feedback processes arising from the use of boric acid are shown. The second part of the chapter analyses via parametric study the influences of different constant and variable soluble boron concentrations on burn-up.

5.1.1 Introductory Remarks on Boric Acid

Boron as soluble boron in PWRs is always used in form of diluted boric acid. The following information is mainly based on References [19], [20]. Boric acid is also called ortho boric acid. Solving B_2O_3 in water produces the boric acid which is a weak acid with the empirical formula H_3BO_3 . According to Reference [17], natural boron consists of two stable nuclides with a share of 19.9 at.% in B^{10} and 80.1 at.% in B^{11} . Given that the isotope fractions are fixed and chemical detection methods evaluate the total boron content in a solution, the amount of boron is commonly related to the total number or mass of boron atoms. If values are related to pure B^{10} or isotope enriched boron, it is usually denoted. The B^{10} content of a solution can be evaluated e.g. by mass-spectroscopy or by neutron beam attenuation.

¹Homogeneous density in this case means that coolant density changes are only smooth during heating-up, compared to e.g. boiling.

Boric acid in PWRs has to fulfill a major task by the thermal neutron absorption in B^{10} working as a chemical shim for reactivity control. Beyond this, B^{11} is an excellent reflector and contributes to the reduction of the thermal leakage [34]. Both can be seen by the cross-sections of the boron isotopes. A small (n, γ) cross-section $\sigma_{(n,\gamma)}$ of 0.005 barn in combination with a high scattering cross-section σ_s marking good reflectors as B^{11} . The B^{10} isotope also has a relatively small (n, γ) cross-section $\sigma_{(n,\gamma)}$ of 0.5 barn but a very high $(n, \alpha)^2$ cross-section of 3840 barn [17]. Advantageous of the high $\sigma_{(n,\alpha)}$ is, that it prevents transmutation of B^{10} to highly absorbing isotopes which otherwise gives rise to activation. The absorbing reaction in the soluble boron is the following:



Since neutron absorption due to boron mainly occurs in the thermal range of neutron energies, it leads to a spectral hardening. In consequence, transmutation of U^{238} and the buildup of plutonium is enhanced by the use of thermal neutron poisons. Especially for the actinides this happens with cumulative shares going to high burn-ups, contributing to the fuel in different manners. Principle feedbacks during burn-up and on the fuel cycle have been shown in the former chapter. In the following, the impact of soluble boron is quantified by the change in isotope fraction buildup.

Increasing burn-up requires augmented initial enrichment in fissile isotopes which leads to higher excess reactivity. In principle, a surplus of reactivity is compensated by adding negative reactivity, namely increasing the soluble boron concentration. As excess reactivity decreases with burn-up the boron concentration is reduced, referred to as the boron letdown [37]. A major advantage in the use of boric acid is the fact that it can be smoothly increased and selectively recovered from the coolant nearly in the entire range of solubility. The reactor system gives upper limit values for the use of boric acid in PWR coolants: e.g. the maximum solubility of boric acid in the coolant, chemical effects of corrosion, precipitation and others, depending on feedback coefficients and safety margins.

According to Reference [35], the solubility of boron shows a strong temperature dependence and as expected for weak acids, it is particularly small for low temperatures. Thus, the limiting value of solubility does not arise from maximum solubility during normal hot operation but from the required shutdown-concentrations³ in cold condi-

²Normally the most probable capture reaction is the (n, γ) -capture which is the typical breeding reaction leading to transmutation.

³Note that moderation in H_2O is more effective at low temperatures and therefore, higher shutdown-concentrations are required.

tions. Depletion of boric acid due to precipitation and crystallization of B_2O_3 , shifting temperatures to lower solubility equilibriums has to be excluded. The highest soluble boron concentrations can be found in the storage tanks of the emergency injection system with slightly varying concentrations depending on the design. Common concentrations are somewhat above 2200 ppm [8]. According to suppliers, the solubility for boric acid at room temperature is about 50 g/l at 20°C which corresponds to 14000 ppm. Subsumed, maximum solubility does not rise a physical limit to enrichments or reactor operation. Since orthoboric acid is only weakly dissociating, in practice, precipitation might occur far below the solubility limit.

A limiting boundary condition are safety margins due to reactivity coefficients. This problem is connected with the light-water which at the same time occupies several operational tasks in the system: cooling, moderating and in case of PWRs, carrying the neutron absorber boron. Less coolant density -due to higher temperatures or lower pressure- is accompanied by less moderation, such reducing the power production. This effect leads to self-stabilization and self-controlling of the reactor, often referred to as inherent system security. For high enrichments and thus high soluble boron concentrations, a strong neutron absorbing effect in the coolant is necessary. A negative reactivity effect or less moderation due to decreasing coolant density could be overcome by a strong positive reactivity effect due to less absorption in the diluted boron. The impact on reactivity coming from a density change is denoted as the Moderator Density Coefficient (MDC)⁴. During normal operation the density gradients are relatively small, rising only from the axial temperature profile of the core. (Rise and drop of the global system temperature are done at subcritical level after core shutdown.) The criterion for normal operation in PWRs influenced by the boron concentration is a negative MDC. According to Reference [11], the boron concentration in PWRs at full power must not exceed 1300 ppm during fuel cycle to keep the MVC (MDC) negative⁵. An important difference between the Doppler feedback and the reactivity coefficient of moderator density are their feedback timescales. The Doppler Coefficient has a very fast response in the range of milliseconds compared to the MDC which counteracts in the range of seconds. Therefore, a negative Doppler Coefficient is always considered to

⁴According to [29], the (MDC) in BWRs is expressed as the Moderator Void Coefficient (MVC). In case of coolant boiling the MVC describes the volumetric fraction of steam voids in the coolant. High density gradients, boiling as well as void fractions in PWRs correspond to disturbed operation. It might be that the given definition for MDC and MVC is not commonly used in science.

⁵Negative in this case means, a negative impact on reactivity caused by decreasing density. Commonly a negative sign denotes counteracting impact when the relevant parameter increases.

be more important which vice versa allows boric acid concentrations exceeding the 1300 ppm security margin. This was done during reactor upgrade studies e.g. in Reference [32]. In practice, to not only sustain the MDC negative but also for water chemical aspects the amount of soluble boron is kept as low as possible. This is accomplished by combining soluble boron with burnable poisons.

The water chemistry due to corrosion effects, rises a second boundary condition depending on the current concentration of boric acid. Information in this subsection is mainly based on References [16], [24], [34]. Enhanced acidity increases corrosion and thus the amount of activated corrosion products in the primary coolant system which should be prevented in the first place. To minimize corrosion especially of the Zircaloy cladding and in the steam generators tubes, it is desirable to have a slightly alkaline pH-value around pH 7.4. Reference [24] suggests a pH-value of $\text{pH } 7.2 \pm 0.2$ to minimize corrosion. As alkalizing agent neutralizing the boric acid commonly lithium hydroxide is used, less prevalent is the use of potassium hydroxide. Concerning the Lithium⁶, concentrations should not exceed 2.2 ppm to avoid Zircaloy-cladding oxidation. Higher lithium contents may lead to non negligible concentrations and precipitation conditions, especially for sub-cooled nucleate boiling. The Axial Offset Anomaly [9], is a possible failure of a core due to deposition of corrosion products as a result of nucleate boiling. Generally speaking, to prevent precipitation effects it is favorable to have as few chemical loads and impurities in the coolant as possible.

A possible remedy to reduce chemical loads could be the use of enriched boric acid (EBA). However B^{11} has a negligible contribution to the cross-section but a fair one to the total acidity while using natural boric acid. Since only the total cross-section of the boric acid is important for absorption, the use of B^{10} -EBA lowers the acidity of the coolant and such the concentration of additives needed. Beyond this, EBA helps to assure operational safety margins such as contributing to power upgrades by facilitating higher enrichments and increased MOX shares.

The total amount⁷ of soluble boron in the PWR not only depends on the initial enrichment and burn-up state, but on many more influencing variables. To only mention a few, e.g. the lattice parameters as the volumetric moderator to fuel ratio or the amount of the used burnable poisons. Especially MOX cores require a greater concentration of

⁶As mentioned above, Li^7 is in situ produced by the $B^{10}(n, \alpha)Li^7$ reaction due to the soluble boron. High Li^7 enriched (99 at.%) is used as alkalizing agent to prevent high transmutation of Li^6 into unwanted tritium.

⁷Today's required total boron content at begin of cycle starts according to Reference [24] inside the range of 1000 - 2000 ppm.

the neutron absorbing B^{10} in the coolant [4], due to the discussed influences of spectral hardening. The benefits of using enriched boron may be penalized by its price, which is according to Reference [21] around two hundred times the price of natural boron. Therefore, systems to recover soluble boron and lithium from the coolant are needed when introducing enriched chemicals.

5.1.2 Input Adjustments for Calculations

This section specifies the adjustments which have been made in the input of the KAPROS module KARBUS for the burn-up investigations depending on soluble boron. Starting from the input configuration of KARBUS as being used for the validation of the KWO experiment in Chapter 3. The main adjustments have been to extend the burn-up range, to enlarge the set of isotopes calculated and to include a variable B^{10} concentration in the moderator cell during burn-up.

Adjustments in Detail:

- **Increase of Burn-up Range**

The maximum burn-up range for the investigations was roughly estimated by preliminary calculations. Therefore, for a three-batch cycle with no boron, the fuel was irradiated in the conditions of the KWO experiment. To estimate a possible end of cycle (EOC) burn-up, k_{∞} at EOC was assumed to become equal to 1.03 which corresponds to the 3% rule of thumb [33] for $k_{eff} = 1$, see also Chapter 3.2.3. To estimate very conservatively, it was supposed that maximum EOL burn-up could be as high as the batch number times the single EOC burn-up. The calculations did not consider an equilibrium core with different burnup stages in the assemblies as in practice. The calculation setup can be compared to an irradiation experiment of a single fresh fuel rod. However, for estimations purpose, variations in fuel rod burn-ups and burn-up extend due to strongly enhanced breeding effects have been taken into account. Since at this early point, it was planned to accomplish investigations for different fuels and respectively higher enrichments, the burn-up range was extended to approximately 140 GWd/tHM. The exact value of maximum burnup influenced by the increment of the timesteps was 142.51 GWd/tHM. Adjustments were confined to the *input.karbus* and *input.mixima* data files. Also the auxiliary *pelist2* program for data postprocessing was slightly modified. This program writes the unformatted *ft35* output data into ASCII-text data files for plotting. The adjustments

done in KARBUS applications are the following: The *input.karbus* file was modified by adding for burn-up increase an equivalent number of time steps to the 'BU1D' card. The increment of time step has also been adjusted. Modifications in *input.mixima* were carried out in the same manner as done before by adding one extra card for each further time step.

Using a fixed fuel rod power rating of 200 W/cm and equal time steps, the maximum burn-up was reached throughout 71 steps, each with a 47.48 days irradiation period. Calculations end up with the last irradiation time step. No cooling time or refueling outage time has been considered during and beyond irradiation period. Actually, in normal reactor operation patterns, this fairly contributes to the isotope fraction buildup due to decay.

Investigations on the increment of the time steps do not show significant influence on the calculations. The influence of a diminished increment is negligible for investigations of high burn-ups with constant irradiation power and was found to be $\ll 1\%$. For transient power operation this is supposed to be much more influencing due to e.g. the Xenon effect and should be further investigated. Therefore, time steps at the beginning of irradiation have been reduced in their increment. This effect is also important for the boron content in the coolant, compensating for the excess reactivity, see also next item. Figure 5.1 displays the graph of variable boron letdown which also reveals the increment of the time steps.

- **Enlargement of the Isotope-Set**

To optimize investigation analysis, the dataset of isotopes was extended in the isotopes monitored for criticality and output data. Basis of the applied dataset was, due to comparability, the dataset used during the validation work of the ICE-experiment at KWO, see also Chapter 3. KARBUS uses a basic isotope dataset which only contains isotopes of fuel, cladding and moderator defined by the input. However, further isotopes to be accounted for criticality can be added in a special card called 'ADDF' within the *input.karbus* file. For the burn-up calculation a database containing around 3000 isotopes is used and embedded in the KARBUS module BURNUP. As investigations were mainly focused on high burn-ups, the following isotope groups (listed in Table 5.1 in detail) are particularly monitored for burn-up issues: These are isotopes of fuel, structure materials, moderator, neutron poisons, plutonium isotopes, minor actinides, absorbing fission products, fission gases as well as precursors and successors of these mentioned groups.

Ag^{109}	Ce^{144}	Gd^{156}	Lu^{176}	Np^{237}	Pm^{149}	Ru^{101}	Sm^{151}	Xe^{134}
Am^{241}	Cm^{242}	Gd^{157}	Mo^{95}	Np^{239}	Pm^{150}	Ru^{102}	Sm^{152}	Xe^{135}
Am^{242}	Cm^{244}	Gd^{158}	Mo^{97}	O	Pm^{148M}	Ru^{103}	Tb^{159}	Xe^{136}
Am^{243}	Cs^{133}	Gd^{160}	Mo^{98}	Pp^{105}	Pr^{141}	Ru^{104}	Tc^{99}	Zr
Am^{242M}	Cs^{134}	H	Mo^{100}	Pp^{106}	Pr^{143}	Ru^{106}	U^{234}	Zr^{91}
B^{10}	Cs^{135}	I^{127}	Nd^{143}	Pd^{107}	Pu^{238}	Sm^{144}	U^{235}	Zr^{93}
Cd^{111}	Dy^{164}	I^{129}	Nd^{144}	Pd^{108}	Pu^{239}	Sm^{145}	U^{236}	Zr^{96}
Cd^{113}	Eu^{153}	In^{115}	Nd^{145}	Pm^{144}	Pu^{240}	Sm^{146}	U^{237}	
Ce^{140}	Eu^{154}	Kr^{83}	Nd^{146}	Pm^{145}	Pu^{241}	Sm^{147}	U^{238}	
Ce^{141}	Eu^{155}	Kr^{84}	Nd^{147}	Pm^{146}	Pu^{242}	Sm^{148}	Xe^{131}	
Ce^{142}	Gd^{154}	Kr^{86}	Nd^{148}	Pm^{147}	Rh^{103}	Sm^{149}	Xe^{132}	
Ce^{143}	Gd^{155}	La^{183}	Nd^{150}	Pm^{148}	Rh^{105}	Sm^{150}	Xe^{133}	

Table 5.1: Dataset of the 103 isotopes used for criticality analysis during burn-up, taken from *OUTPUT.mixima*.

Isotopes which are not itemized in Table 5.1 however have not been involved in the criticality calculation procedure. Especially for the investigations concerning Pu^{238} one more precursor, Np^{237} , was added to the 'ADDF' dataset.

The calculated output data for the isotope fractions are unlike the KWO experiment given in the unit of numberdensities which is [Atoms/cm³] and commonly scaled with a factor of 10⁻²⁴. In other words, given values of numberdensities have to be multiplied by a factor of 10²⁴ to get the correct value.

• Including variable Boron Concentrations

The investigations on boron have been separated into two sections: In the first part only a constant B^{10} concentration in the moderator was investigated. Thus getting an overview on basic influences changing the boron concentration. In the second part, a variable boron concentration was applied, corresponding to the conditions in operating PWRs.

Setting the variable B^{10} concentration, no change in the KARBUS modules was necessary. This feature was already included and also used during the validation of the KWO experiment. Therefore, only the selected value of the boron concentration has to be inserted in the *input.karbus* datafile within the 'MINP' keyword. The increment of the time steps was adjusted in the 'AMIX' keywords. Soluble boron concentrations within the KARBUS module are always given in numberdensities of B^{10} denoted as $Nd_{B^{10}}$. Since the boron concentrations are

usually given in ppm natural boron, concentrations have to be recalculated as shown in the following Equation (5.1); Table 5.2 denotes the symbols:

$$Nd_{B10} = [C_{Btot} \frac{\chi_{B10}}{100} \cdot \frac{\rho_{cool}}{u_{cool}} \cdot \frac{Av}{10^6}] \cdot 10^{-24} \quad (5.1)$$

In the following the adjustments related to soluble boron are described. The

Symbol	Denotation	Unit
Nd_{B10}	numberdensity of B_{10}	[particles· 10^{-24} /cm ³]
C_{Btot}	total boron concentration	[ppm]
χ_{B10}	enrichment in B_{10}	[at.%]
Av	Avogadro constant: $6.023 \cdot 10^{23}$	[atoms/Mol]
ρ_{cool}	coolant density	[g/cm ³]
u_{cool}	atomic mass of coolant	[g/Mol]

Table 5.2: Symbol legend of Equation (5.1)

boron letdown was expected to be linearly depending on burn-up, but constant for each time step. Thus, the boron concentration was reduced throughout a step function from the maximum at begin of cycle (BOC) to approximately 0 ppm at EOC. For most calculations using a variable boron concentration, a maximum value of 376 ppm B^{10} was used. The latter corresponds to approximately 1900 ppm B_{nat} . Investigating on a three-batch cycle, the boron-curve was run through three times until end of life (EOL) and fuel was irradiated to a maximum burn-up of 142 MWd/tHM. To account for the xenon-jump at the beginning of irradiation, boron concentration was adjusted according to the smaller time steps at begin of first cycle in minor steps. Figure (5.1) shows the graph of an applied boron letdown function. Furthermore three representative, constant boron concentrations are plotted.

Modifications to adjust calculations to variable boron contents were only necessary in the *input.karbus* file. New keyword options 'AMIX', to model the boron concentration, were inserted in the *input.karbus* data file, one for each time step. These cards include a multiplying factor to calculate the boron concentration for the current time step. The former concentration multiplied by the factor gives the new value. The boron letdown is scaled by the BOC maximum concentration which is taken from the entry of the constant boron modeling 'MINP'.

The letdown factors were calculated such, that increments become equidistant.

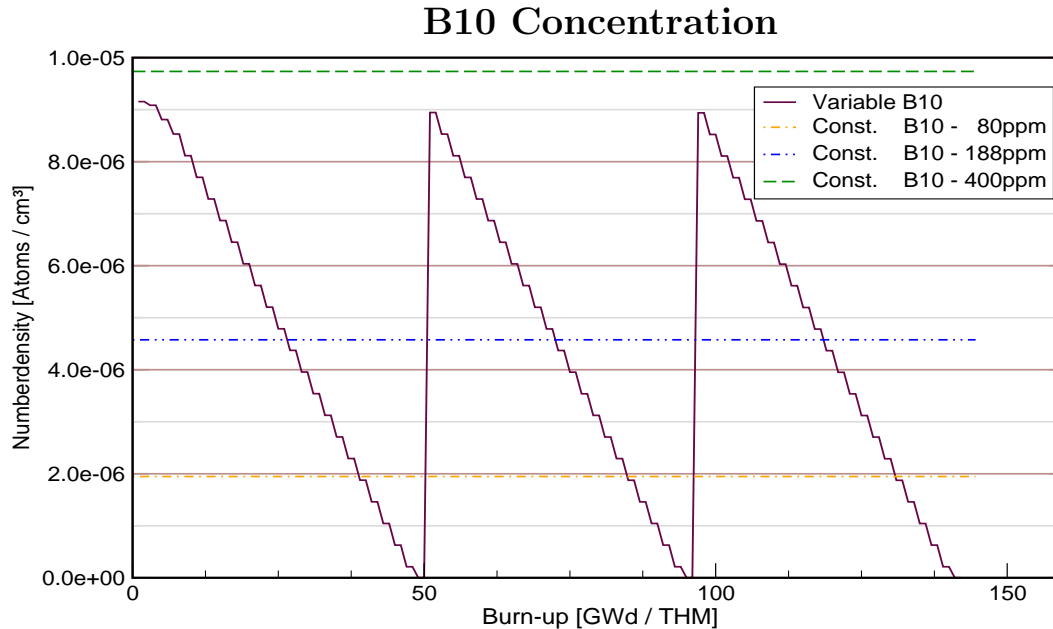


Figure 5.1: Variable letdown and constant B^{10} -concentrations plotted against burn-up.

For boron modeling, the first steps were adjusted in the same manner as has been done for the time increments. Naturally, Equation (5.1) was also used to calculate variable soluble boron concentrations.

5.1.3 Calculations on Soluble Boron Concentrations

The maximum soluble boron concentration applied in most cases during calculation seemed to be slightly overestimated for practical cores. Mainly two reasons suggested the selected concentrations⁸: The model itself does not correspond to the equilibrium condition for a core operated in praxis. Excess reactivity at the beginning of a fuel cycle would therefore be lower and consequently, the boron concentration will be, too. Contrary to this, at the beginning of irradiation the excess reactivity in the model is much higher, corresponding to a full core of fresh 5% enriched uranium fuel. The surplus of reactivity at the begin of cycle is compensated by more boron in the model. A second reason for higher boron concentrations in the model was already discussed in Chapter 4.4. High enriched LWR fuels are always applied in combination with burnable

⁸Typical maximum concentrations calculated lye around 400 ppm B^{10} which corresponds to approximately 2000 ppm B_{tot} .

absorbers to compensate for excess reactivity. As the model fuel does not contain any burnable absorbers, more boron was added instead. Prevalent maximum concentrations in PWRs lay around 1300 ppm boron at BOC, which is reduced to approximately 0 ppm at EOC.

The first part of this chapter explains the basic impact of soluble boron modeling during burn-up. The focus is turned on the qualitative effects that can be observed considering single isotopes. Buildup of isotopes was analyzed in detail using two basic settings:

- The first set investigated the influence of the total amount of soluble boron present during burn-up. A constant boron modeling was applied to estimate general trends for the buildup of different isotopes.
- The second part evaluates the influence of variable soluble boron concentrations. The buildup of isotopes during variable boron modeling is compared to constant concentrations. A suggestion is made to approximate variable concentrations in a model with constant concentrations.

Calculations for variable boron concentrations are computationally more expensive. The idea was to develop a guideline for constant approximations, to accelerate calculations and make modeling more precise. A further field of application for the results are fuel irradiation experiments. Within these experiments, realization of variable boron modeling is often complicated. Results are discussed on the basis of Reference [37], investigating the *Impact of Soluble Boron Modeling for PWR burn-up Credit Criticality Safety Analyses*.

Basic Settings

In the following, the basic settings of the *input.carbus* file used for the calculations on variable boron are shown by Tables 5.3 and 5.4. Further explanations for the settings have already been given in Chapter 3. The power history was not plotted in detail, as it is of a very simple structure. At the BOC the power history starts with three shorter full power macro time steps: one step of 2.0 days, one of 21.74 days, and a third step of 23.74 days. These steps are followed by 68 equal full power steps of 47.48 days duration, no micro time steps have been used. The rod irradiation power was constantly set to 200 W/cm. Table 5.5 shows a typical boron modeling for one cycle, for an initial concentration of 400 ppm B^{10} . This boron curve was run through three times for three cycles until reaching the EOL burn-up. All calculations in this chapter

Geometric Parameter	Value	Reference / Keyword
Fuel Pin Radius	4.11 [mm]	<i>input.karbus</i> , 'MINP'
Canning Thickness	0.64 [mm]	<i>input.karbus</i> , 'MINP'
Vm/Vs	1.28264	<i>input.karbus</i> , 'MINP'

Table 5.3: Geometric Settings and lattice parameters for PWR soluble boron investigations

Parameter	Value	Keyword
Moderator Density	0.74730 [g/cm ³]	'MINP'
Fuel Density	0.89683 [g/cm ³]	'MINP'
Temperature of Fuel	773 [K]	'MINP'
Temperature of Canning	605.8 [K]	'MINP'
Temperature of Moderator	583 [K]	'MINP'
Initial Enrichment U^{235}	5.0 [%]	'MINP'
Initial Enrichment Pu_{tot}	0.0 [%]	'MINP'
Initial B^{10} Concentrations in the Moderator	80 - 400 [ppm]	'MINP'

Table 5.4: Further lattice and thermohydraulic settings for PWR soluble boron investigations taken from *input.karbus*.

have been executed with the G69P5E65B cross-section library using the corresponding F69UD06 formula database.

5.1.4 Results and Discussion

In the investigations on soluble boron, some isotope groups have been in special focus, depending on their impact. Among these were the fresh fuel isotopes such as U^{235} and U^{238} as well as fuel components with special impact related to burn-up and recycling. These are generally all fissile⁹ isotopes, strong neutron absorbers and minor actinides. Representatives of the absorber group are isotopes of samarium, europium and gadolinium, minor actinides are the elements neptunium, americium and curium. Isotopes that are related to the mentioned groups in terms of being a precursor, have also been involved. As the infinite multiplication factor k_{∞} is a characteristic parameter for the fission reaction, it has also been in special focus.

⁹Under conditions of LWRs.

Time-step	B^{10} -Conc. [10^{-6}]	B^{10} -Conc. [ppm]	Time-step	B^{10} -Conc. [10^{-6}]	B^{10} -Conc. [ppm]
1	9,734E-06	400,0	14	4,648E-06	191,0
2	9,658E-06	396,9	15	4,206E-06	172,8
3	9,366E-06	384,9	16	3,764E-06	154,7
4	9,070E-06	372,7	17	3,321E-06	136,5
5	8,628E-06	354,5	18	2,879E-06	118,3
6	8,186E-06	336,4	19	2,437E-06	100,1
7	7,744E-06	318,2	20	1,995E-06	82,0
8	7,301E-06	300,0	21	1,553E-06	63,8
9	6,859E-06	281,8	22	1,110E-06	45,6
10	6,417E-06	263,7	23	6,681E-07	27,5
11	5,975E-06	245,5	24	2,259E-07	9,3
12	5,532E-06	227,3	25	2,409E-09	0,1
13	5,090E-06	209,2			

Table 5.5: Soluble B^{10} concentration during PWR boron evaluations, concentrations are given for each calculation time-step in numberdensities [10^{-6}] as well as in [ppm]. Initial cycle concentration: 400 ppm.

The following section estimates the general consequences of constant boron concentrations present during burn-up. Three different concentrations have been used. All values of soluble boron are in concentrations of B^{10} , exceptions are denoted otherwise.

General Influence of Soluble Boron

Table 5.6 shows the three different concentrations which have been used to evaluate the effects raised by the soluble boron. For evaluation of these basic influences, a minimum, a maximum and an average concentration was set. The fourth concentration denoted in the table will be referred to later on. Figures 5.2 to 5.5 show the general results of the preliminary investigations and give a representative overview on the mechanisms of soluble boron.

Figure 5.2 shows the impact of different boron concentrations on the infinite multiplication factor. As expected, increased soluble boron concentrations lower the value of the multiplication factor. This is due to the additional absorption effect in the neutron balance. It can be observed, that the influence of boron concentrations on k_{∞} is

	Initial B^{10} Concentration:	
	ppm	numberdensities
Minimum Concentration	0	0.0
Mean Concentration	188	4.5752E-6
Maximum Concentration	400	9.7345E-6
Best Approximation	80	1.9469E-6

Table 5.6: Soluble boron concentrations in B^{10} applied for investigations of global trends.

linear. To emphasize the impact of boron on EOL burn-up, an assumed $k_{eff} = 1$ was highlighted in the chart.

Chart 5.3 shows the impact of boron for the isotope group of plutonium with two different concentrations. It is shown that for all isotopes except Pu^{242} , higher boron concentrations lead to a distinct increase in the buildup. The strongest effect is observed for the isotope of Pu^{239} . This is of particular interest for the coupled buildup process of transuranics by the transmutation chain. As described in detail in Chapter 4.5, the buildup process is started by neutron absorption in the U^{238} and enhanced by spectral hardening. It is obvious that Pu^{239} , being the initial isotope for others, shows the strongest impact of boron variation. This influence decreases for isotopes of higher orders due to further transmutation reactions, reducing the isotope concentrations. The effects on the plutonium isotope Pu^{238} is discussed in detail in Chapter 5.3. As a consequence of the effects observed, Figures 5.3 and 5.4 show the increase of the total plutonium fraction related to uranium. The share of plutonium is distinctly increased by higher boron concentrations. These results are confirmed by Figure 5.5 showing the enhanced buildup of Am^{241} for increased boron concentrations. Further results showing the influences of soluble boron for different isotopes in detail, are presented in the Appendix B.1 by Figures B.1 to B.6.

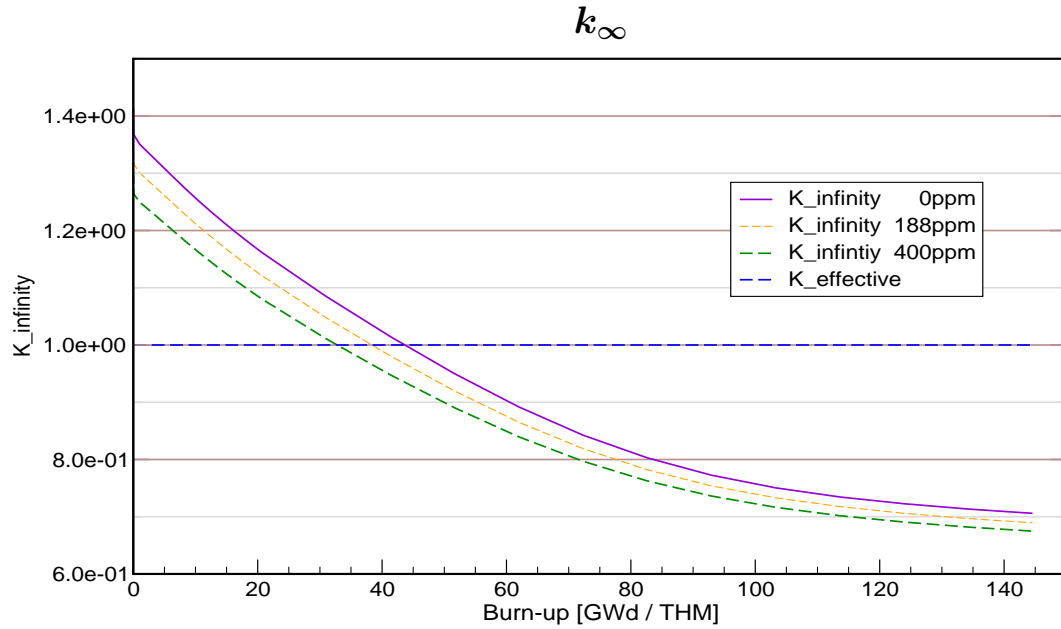


Figure 5.2: Influence of constant soluble boron concentrations on k_{∞} , curves for k_{eff} and three different concentrations plotted.

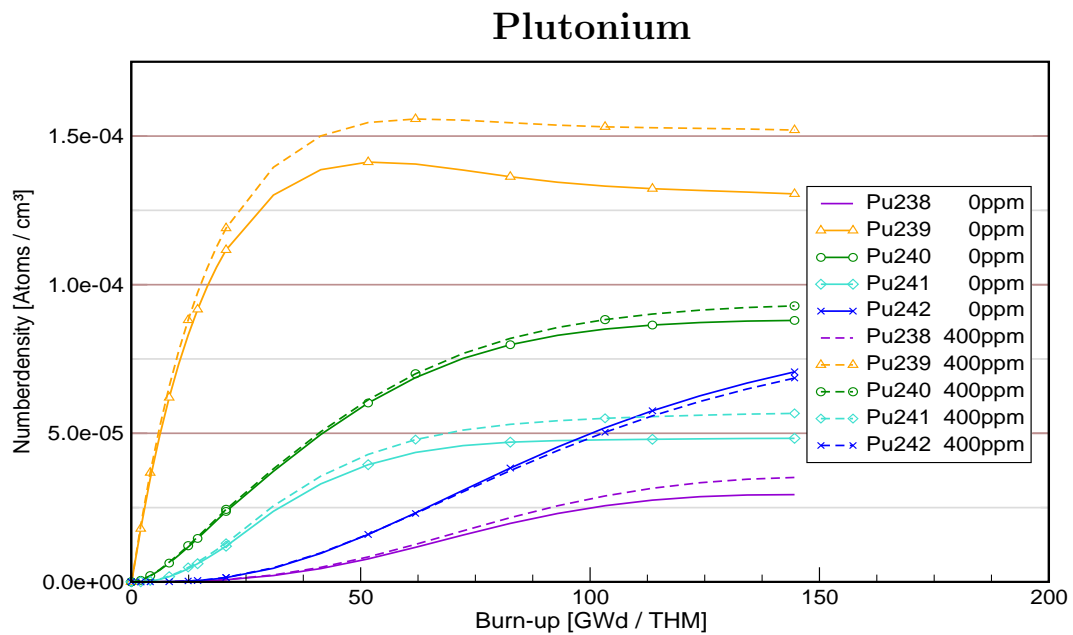


Figure 5.3: Influence of constant soluble boron concentrations on the isotope group of plutonium, minimum and maximum concentration curves plotted for every isotope.

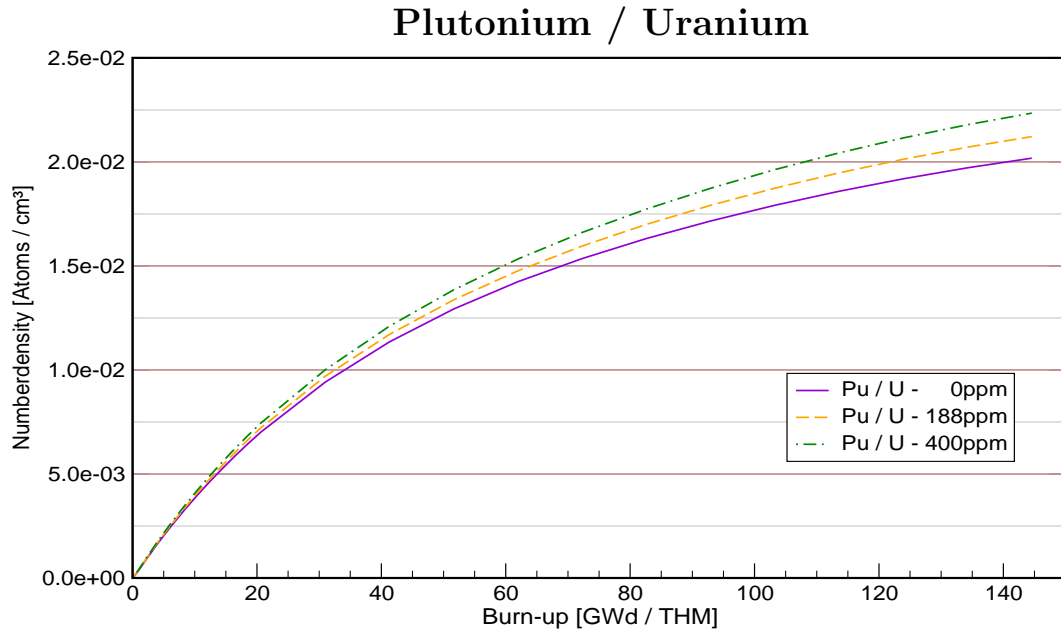


Figure 5.4: Influence of constant soluble boron concentrations on the plutonium-uranium ratio, ratio plotted for three different concentrations.

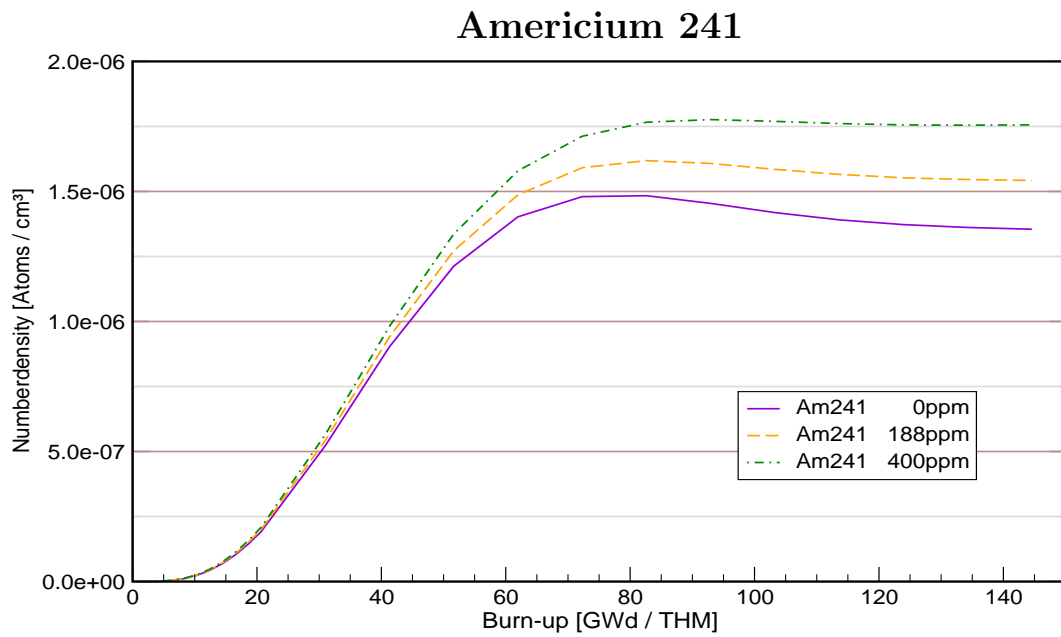


Figure 5.5: Influence of constant soluble boron concentrations on Am^{241} , curves plotted for three different concentrations.

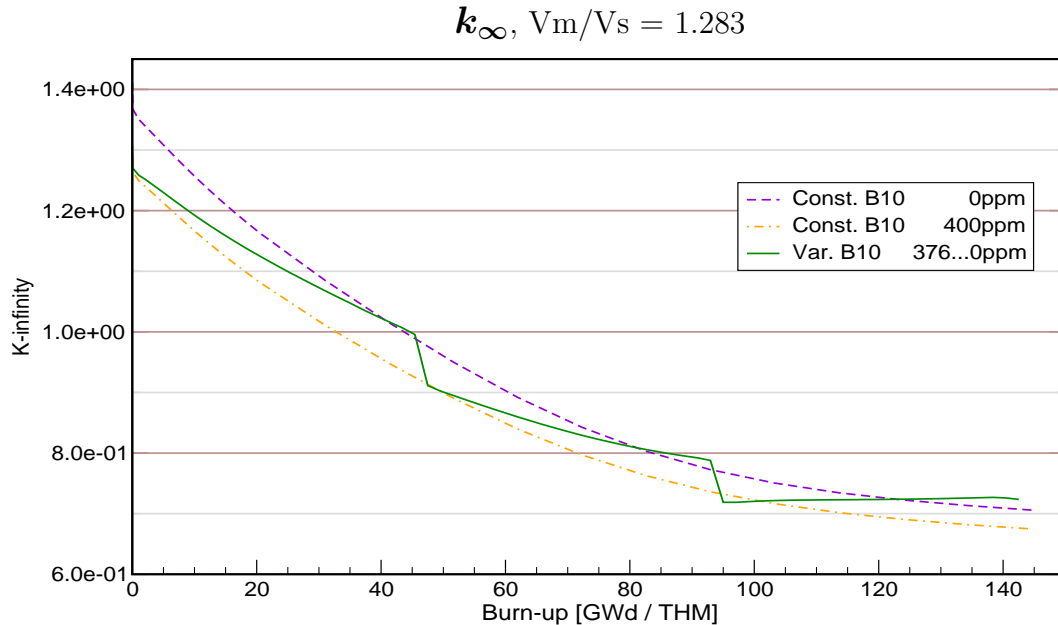


Figure 5.6: Chart shows k_{∞} for the marginal constant concentrations and the adjusted curve for variable boron concentration, V_m/V_s : 1,283.

The following paragraph deals with the influence of variable boron concentrations during burn-up. As a first estimate, the k_{∞} curves in Figure 5.2 were used to adjust a variable concentration to the maximum range covered by the constant concentrations. The intention was to fit the variable k_{∞} curve to the constant's, especially in the low burn-up range. Therefore, the maximum value of B^{10} for the variable modeling was slightly reduced from 400 to 376 ppm initial soluble boron. The results are shown in Figure 5.6. However, this was the reason to repeat calculations for an average constant boron concentration with the value of 188 ppm applied in the charts. Further comparisons for different isotopes confirmed the adjusted proceeding.

Variable Boron Concentrations:

This section investigates the impact of variable boron concentrations on the buildup of isotopes, which is a problem close to praxis. As discussed in detail in Chapter 4.4, the buildup of transuranics contributes a lot to many problems of SNF treatment, such as complication of transporting due to criticality increase, extended interim storage time or increased decay heat, to only mention a few. Being able to perform good estimations not only for the transuranic buildup is therefore of particular interest. The intention

of this chapter is to provide a constant boron concentration for burn-up calculations, which is deduced from an initial variable concentration, so that the constant boron value approximates the variable boron modeling as good as possible during isotope build-up.

A current issue in this field which is akin to this problem is discussed in Reference [37]. The problem is referred to as *burn-up credit*, which was explained in Chapter 4.4. This reference found, that calculating with a mean constant boron concentration¹⁰ estimates the buildup of transuranic isotopes rather conservatively. This means, calculations using an average boron concentration during burn-up will overestimate the variable modeling. To evaluate the criticality caused by transuranics, this overestimation is very helpful. An exact approximation for the build-up of isotopes will be derived in this chapter. This approximation only evaluates deviations but does not account for whether it under or overestimates.

Apart from any approximation derived for isotopes, Figure 5.6 shows that the best approximation for the infinite multiplication factor will be an average concentration. For all variable concentrations denoted *Var.B10* in the charts, a variable boron concentration between 376 and 0 ppm B^{10} was applied. The variable modeling was already shown in Figure 5.1. The moderator to fuelrod volumetric ratio was abbreviated (V_m/V_s) and is of the value 1.283.

The curves for variable boron modeling in comparison with the average 188 ppm concentration curve are shown in the Appendices B.2 and B.3. These charts include an additional curve for 80 ppm constant modeling, which will be discussed in the following. Charts B.7 to B.19 in Appendix B.2 are selected isotopes showing good correlations between the 80 ppm approximation and the variable boron concentration. Charts showing qualitatively only minor differences between the two constant approximations, e.g. if isotopes are independent of boron modeling, are presented in Appendix B.3. The latter appendix also contains charts for isotopes which do not fit the 80ppm-approximation. These discrepancies will be discussed in the following. See Figures B.20 to B.37.

Results can be summarized by the following: The findings proposed by [37] have been verified. Using an average concentration for constant boron modeling leads to a rather conservative overestimation of isotope buildup. Concerning the idea of a constant boron modeling to provide best estimate values for variable modeling, it was found that the use of an average soluble boron approximation does not give accurate results, especially for increased burn-ups.

¹⁰Which is the half of an initial (maximum) variable concentration.

An approximation which estimates many of the major isotopes very accurately, is to use 20-25% of the initial variable concentration for the constant modeling. It is important to point out, that no parametric studies have been accomplished to proof the 20-25% rule of thumb for further initial concentrations of variable modelings. As shown in Figure B.37, the rule is not valid for k_∞ modeling.

Considering isotopes contributing to burn-up effects and problems of SNF treatment, the described concentration of 80 ppm constant boron modeling provides a good approximation to the buildup of many isotopes. However, the quality of results strongly depends on the isotope considered. There is a group of isotopes for which both approximations give similar results. That means, the build-up of these isotopes is largely independent of the boron concentration. For a small group of isotopes, the rule of thumb should not be applied. These are also shown in the Appendix B.3. Tables 5.7 and 5.8 discuss most of the isotopes with regard to the 80 ppm/188 ppm approximation. The abbreviation *BU* in the tables stands for burn-up, *appr.* for approximation. The first column denotes the isotope, the second column comments on the results, column three denotes a classification point for the burn-up range where a change in approximation takes place, if can be identified. The last four columns evaluate the quality of estimation for two boron concentrations, below and above the classification point.

As a result of the evaluations, three general conclusions can be made:

- The evaluation confirms the major trend stated above, that increased boron concentrations lead to an enhanced buildup of the most isotopes due to spectral hardening.
- It is obvious that for higher burn-ups, the deviations increase, since most of the error causes contribute cumulative to high burn-ups.
- Depending on the application, approximations should be selected with regard to the burn-up range. Some isotopes show a different approximative behavior for high and low burn-ups. A recommended classification is below and above 50 GWd /tHM, which does not mean that this separation is commonly necessary.

Tables 5.7 and 5.8 give an overview on the effect for different isotopes. If neglecting isotopes that do not show a dependence on soluble boron during burn-up, the 80 ppm approximation leads to a distinct improvement in approximating the isotope buildup.

Variation of Time Step Increment:

Concerning the increment of time steps for constant boron concentration, it was found that this parameter is of minor influence. Reducing the increment by a factor of four, only a very slight influence on the buildup of isotopes could be found which should be negligible. The effect might increase for different settings of the irradiation history and should therefore be evaluated for every setup.

Isotope	Comment	Classific. Point [GWd/tHM]	Quality of estimate:			
			188 ppm		80 ppm	
			≥	≤	≥	≤
Am^{241}	80 ppm very good appr. in the full BU range	40	+	±	++	++
Am^{242}	188 ppm good appr. for low BU range	100	++	+	±	+
Am^{243}	both curves nearly identical, good appr. in the full BU range		+	+	+	+
Am^{243M}	80 ppm good appr. for the full BU range	50	+	-	++	+
Cm^{242}	80 ppm good appr. for the high BU range,	80	++	±	+	+
Cm^{244}	curves nearly identical, very good appr.		++	++	++	++
Eu^{153}	both appr. nearly identical, overestimation		-	-	-	-
Eu^{155}	80 ppm good appr. in the full Bu range	70	-	-	+	±
Gd^{155}	80 ppm better appr.	25	±	-	+	±
Gd^{157}	both appr. identical, bad appr.	30	+	-	+	-
Np^{237}	both appr. nearly identical, bad appr.		-	-	-	-
Pm^{239}	both appr. identical, very good appr. in the low BU range	50	++	±	++	±
Pm^{147}	curves nearly identical, very good appr. in the full BU range		++	++	++	++
Pu^{238}	both appr. nearly identical, bad appr.		-	-	-	-
Pu^{239}	80 ppm very good appr. in the full BU range	40	+	±	++	++

Table 5.7: The table evaluates the quality of two constant boron approximations, 188 ppm and 80 ppm, to the variable modeling, (376...0 ppm).

Isotope	Comment	Classific. Point [GWd/tHM]	Quality of estimate:			
			188 ppm		80 ppm	
			\geq	\leq	\geq	\leq
Pu^{240}	both appr. identical, very good appr. for the high BUs	40	-	++	-	++
Pu^{241}	80 ppm very good appr. in the full range	50	++	-	++	++
Pu^{242}	curves identical very good appr. in the full BU range		++	++	++	++
Pu/U	80 ppm very good appr. in the full BU range	60	++	\pm	++	++
Rh^{103}	80 ppm very good appr. in the full BU range	50	++	-	++	++
Sm^{147}	both appr. nearly identical, very good appr. in the low BU range	50	++	-	++	-
Sm^{148}	80 ppm very good appr. in the full BU range	100	+	+	++	+
Sm^{149}	80 ppm very good appr. in the full BU range	30	+	-	+	++
Sm^{150}	both appr. identical, good appr. for low BU range	30	+	-	+	-
Sm^{151}	80 ppm very good appr. in the full BU range	30	+	-	++	++
Tc^{99}	both appr. identical, bad appr.		-	-	-	-
U^{234}	both appr. identical, bad appr.	40	+	-	+	-
U^{235}	curves identical, very good appr.		++	++	++	++
U^{236}	curves identical, very good appr.		++	++	++	++
U^{238}	curves identical, very good appr.		++	++	++	++

Table 5.8: The table evaluates the quality of two constant boron approximations, 188 ppm and 80 ppm, to the variable modeling, (376...0 ppm).

5.2 Impact of wider Lattices

This chapter discusses the impact of wider lattices on isotope buildup in the presence of soluble boron. The moderator to fuelrod volumetric ratio, denoted V_m/V_s , is characteristic for the width of lattices. It represents a major design parameter for core construction, since the volumetric ratio in LWRs predominantly influences the neutron energy spectrum.

The consequences have been discussed in detail in Chapter 4. Two of the major effects of lattice variation are caused by the shift of the neutron spectrum. Changes in the spectrum always lead to the altered isotope build-up processes, analyzed in the previous section. The second major consequence of varying the ratio of thermal to fast neutrons is the effect of changing the state of moderation. The ratio of thermal to fast neutrons defines whether a core is under or over-moderated. This is of major importance for the reactor feedback parameters. Over-moderation contributes to unwanted positive moderator-temperature and void coefficients¹¹.

5.2.1 Input Adjustments for Calculations of Wider Lattices

Input adjustments to investigate the impact of lattice variation have been very simple. Only the moderator to fuelrod volumetric ratio had to be reset in the 'MINP' card of the *input.karbus* file. This was shown in Chapter 3.2.1. Further settings could be transformed from the previous investigations and are listed in the Tables 5.3, 5.4 and 5.5 of the previous section. Table 5.9 shows the three different V_m/V_s ratios which have been investigated. The first case represents a tight lattice as it is used in common LWRs, the second is a so called wider MOX lattice, which is needed to moderate the harder MOX spectrum. Compared to the $V_m/V_s=1.283$ case, the moderator volume for the wider MOX lattice was increased by 40% resulting in a V_m/V_s ratio of 1.796. The last case represents a fictive lattice with an assumed V_m/V_s ratio of 2.565, to evaluate the trends. Compared to the initial case, the moderator volume was doubled.

5.2.2 Lattice Effects on Soluble Boron

To gain comparable results for the burn-up process, the intention was to adjust the boron concentrations to the new lattices. Values of k_∞ should therefore be approx-

¹¹LWRs should therefore be slightly undermoderated.

Volumetric ratio	Value
Tight lattice	1.28264
Wider MOX Lattice	1.79570
Wide Lattice	2.56528

Table 5.9: The table specifies the three different moderator to fuelrod volumetric ratios applied for the investigations.

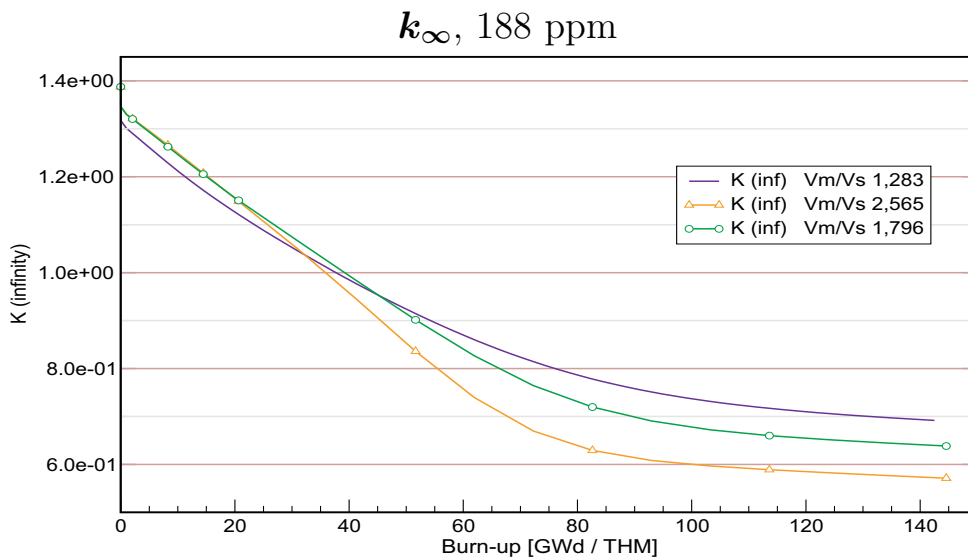


Figure 5.7: The chart shows k_{∞} curves for a mean boron concentration of 188 ppm, for three different V_m/V_s ratios.

imately the same, especially for the BOC. However, investigations show that the progress of the infinite multiplication factor is rather different for each lattice. The necessary adjustment via soluble boron would result in neutron spectra too different for comparison. This can be seen in Figures 5.7 and 5.8. As the initial k_{∞} values are similar for any of these cases, investigations have been accomplished with the former constant values of soluble boron shown in Table 5.6 and the variable modeling of 376...0ppm. The results for k_{∞} are shown for the three lattices in Figures 5.9 to 5.11. It can be seen that for all cases the variable boron curve fits the marginal curves very well. Generally speaking, a higher moderator fraction will increase the absorption efficiency of the boron by softening the neutron spectrum.

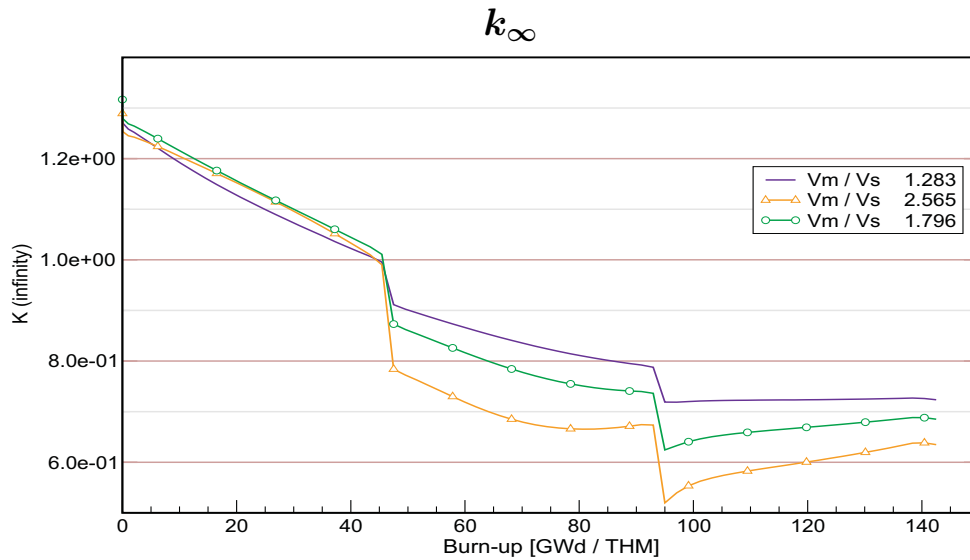


Figure 5.8: The chart shows k_{∞} curves for a variable boron modeling (376...0 ppm), for three different V_m/V_s ratios.

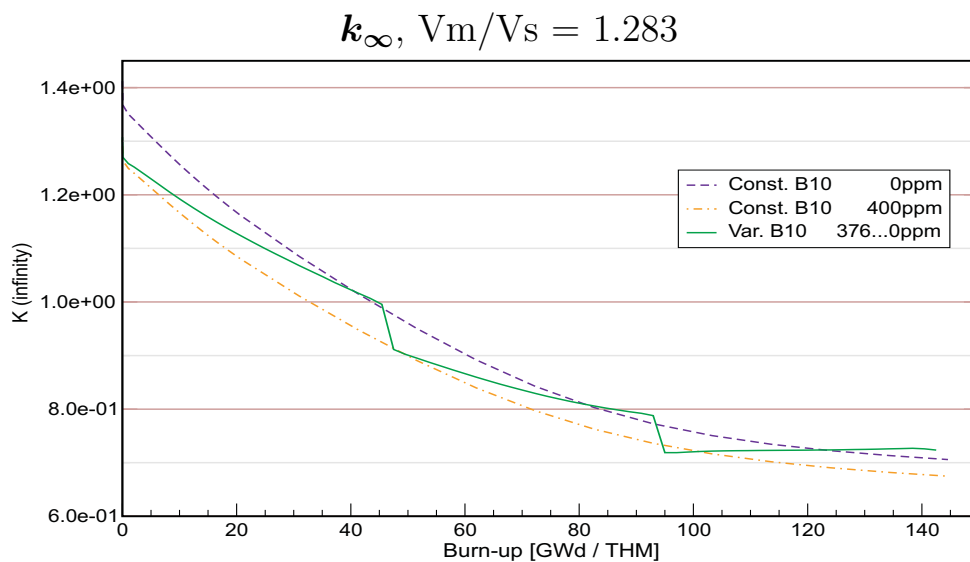


Figure 5.9: The chart shows k_{∞} for the marginal constant concentrations and for the variable boron modeling (376...0 ppm), V_m/V_s : 1.283 .

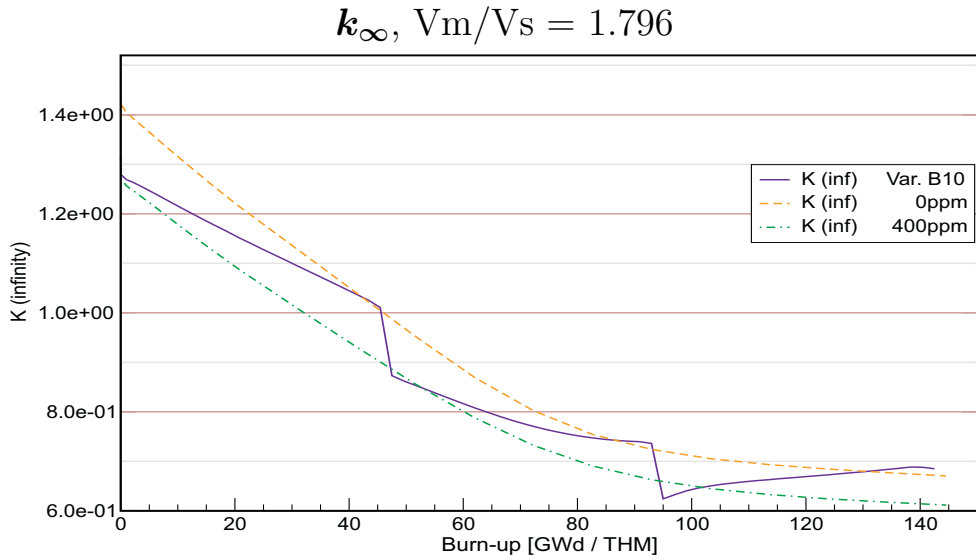


Figure 5.10: The chart shows k_{∞} for the marginal constant concentrations and for the variable boron modeling (376...0 ppm), V_m/V_s : 1.796 .

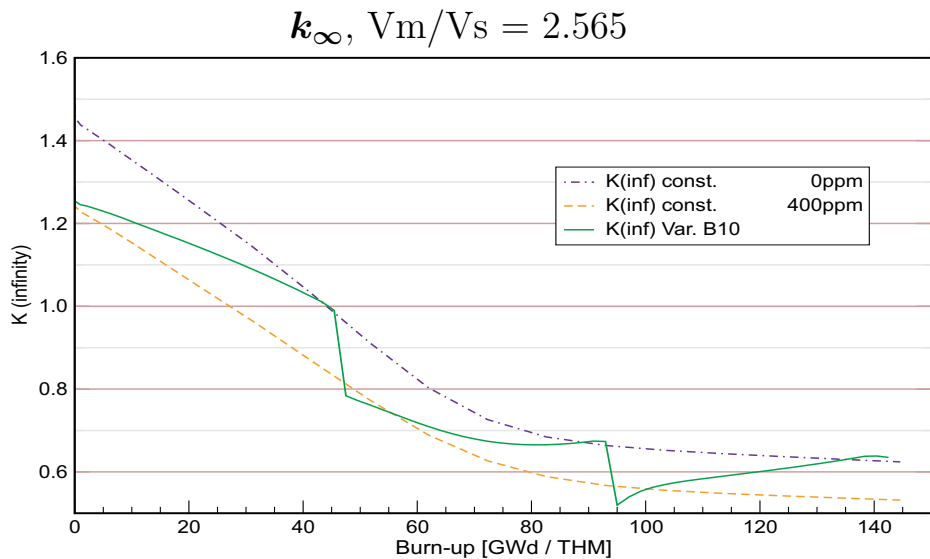


Figure 5.11: The chart shows k_{∞} for the marginal constant concentrations and for the variable boron modeling (376...0 ppm), V_m/V_s : 2.565 .

5.2.3 Results for Lattice Variation

Considering the infinite multiplication factor for different lattices, two points are striking. In the first third of the burn-up range, all k_∞ -values are approximately identical for the three lattices; for constant boron concentration as well as for variable boron modeling. Going to the range of high burn-ups, the lattice effects become clearly noticeable. This can be seen in Figure 5.7 and 5.8. For increased burn-ups, the lowest volumetric ratio corresponds to the highest k_∞ values and vice versa. However, all calculations used the same fuel.

This effect can be attributed to the plutonium buildup caused by enhanced breeding for harder neutron spectra. The fissile components of plutonium contribute to the multiplication factor, especially in the last two thirds of the burn-up range. This effect might be of particular interest for the increase of burn-up, since thereby fuel-utilization can be raised. The soft neutron spectrum of the wide lattice predominantly burns the U^{235} , whereas the tight lattice benefits of the additional plutonium fissiles.

This effect of varying plutonium build-up is shown for the three different lattices in Figures B.38 to B.40 in the Appendix B.4. It can be observed, that lattice effects as well as the influence of boron concentrations, depend on the isotope. The evaluation of the single plutonium isotopes is also presented in the Appendix B.4 by Figures B.41 to B.45. Except for Pu^{242} , a wider lattice decreases the buildup of isotopes.

Since the effect of spectral hardening with regard to the plutonium buildup and its successor isotopes has already been discussed for soluble boron, evaluations do not go into detail at this point.

5.3 Buildup of Pu^{238}

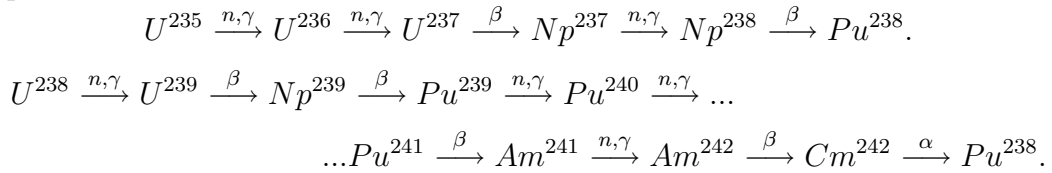
Plutonium 238 has been an ongoing issue of discussion in the last twenty years. However this isotope is, concerning the atomic share, none of those which is primarily build up during burn-up in LWRs. Its properties make it very interesting for aspects of plutonium generation and proliferation in LWRs in the context of “unsafe” countries. Pu^{238} but also the other even numbered isotopes of plutonium contribute to the deterioration of plutonium for nuclear weapon production. This topic became important again, when Russia and the USA agreed upon the Strategic Arms Reduction Talks (START) contract in the 1990th, to dismantle some ten thousands of nuclear warheads. Thus 260 tons of weapon grade plutonium and about 1000 tons of high enriched uranium became available for the civil fuel cycle [15]. To assure peaceful application of this fuel in civil reactors, these fissiles have to be deteriorated.

The aim of proliferation resistance can be realized by two isotope effects. The production of weapon grade plutonium necessitates the handling of huge feed material amounts for enrichment. Handling can be complicated and possibly prevented by increased decay heat of the initial materials as it is the case e.g. for long-term irradiated fuels. Particularly Pu^{238} has a very high α -decay heat and also emits strong γ -radiation. The second effect which can be used to complicate the recovery of weapon grade plutonium from LWR fuel is the effect of spontaneous fission (SNF). Spontaneous fission neutrons have to be avoided since these uncontrolled initial neutrons prevent the precise triggering of the critical mass of a bomb. SNF can be observed for all plutonium isotopes, however the even ones, 240 and 242, show remarkably strong SNF. To produce weapon grade plutonium, these isotopes have to be removed via involved isotope separation processes.

To realize proliferation resistance through Pu^{238} , two general concepts are discussed: the first was proposed and recently revised by Kessler. His results show that 12% Pu^{238} in a critical plutonium sphere can melt the explosive lenses altogether [30]. The other concept recently proposed by Saito et al. was the idea of Protected Plutonium Production (PPP). The idea is to dope fresh uranium and MOX fuel with minor actinides (MAs) which are a source for Pu^{238} as precursors in the transmutation chain. During irradiation of fresh fuel the buildup of Pu^{239} from U^{238} will immediately be accompanied by the buildup of Pu^{238} .

Since Pu^{238} is not a natural isotope, it has to be generated artificially. Its two “quasi-

stable”¹² precursors are two isotopes of MAs, namely Np^{237} and Am^{241} . Both are artificial isotope components of SNF, turning their role from unwanted long-living components of nuclear waste into useful isotopes. The advantage of using Np^{237} and Am^{241} for PPP is, that transmutation into Pu^{238} also works for LWR neutron spectra. The two corresponding buildup chains for Pu^{238} are shown below, starting from natural isotopes.



The production of the amounts of Pu^{238} needed for Kessler’s proposal is demanding. In Reference [27] an enhanced buildup of Pu^{238} in Np^{237} samples was proved to be up to 24 at.% using a fast reactor. This might be a good basis to realize Kessler’s idea. Information in this section is mainly based on References [15], [27] and [30].

The following charts show the influences of the investigated parameters on the buildup of Pu^{238} . Precursors are not mentioned in particular, this was already shown in the previous sections.

Results of Investigations on Pu^{238}

Figure 5.12 shows the general influence of boron on the buildup of Pu^{238} , with increased concentrations of soluble boron generating more Pu^{238} . This effect is again caused by the spectral hardening, which increases the buildup of Pu^{238} precursors.

The latter assumption is validated by Figure 5.14, comparing three different lattices. The chart shows a distinct decrease of Pu^{238} buildup for an increased moderator volume, corresponding to a softer neutron spectrum. Figure 5.13 compares two different variable boron concentrations and the constant 80 ppm approximation. For Pu^{238} , the chart shows a strong overestimation of the variable boron modeling by the constant 80 ppm approximation. Thus, using a constant boron modeling would be a bad approximation for the buildup.

¹²This means long-living.

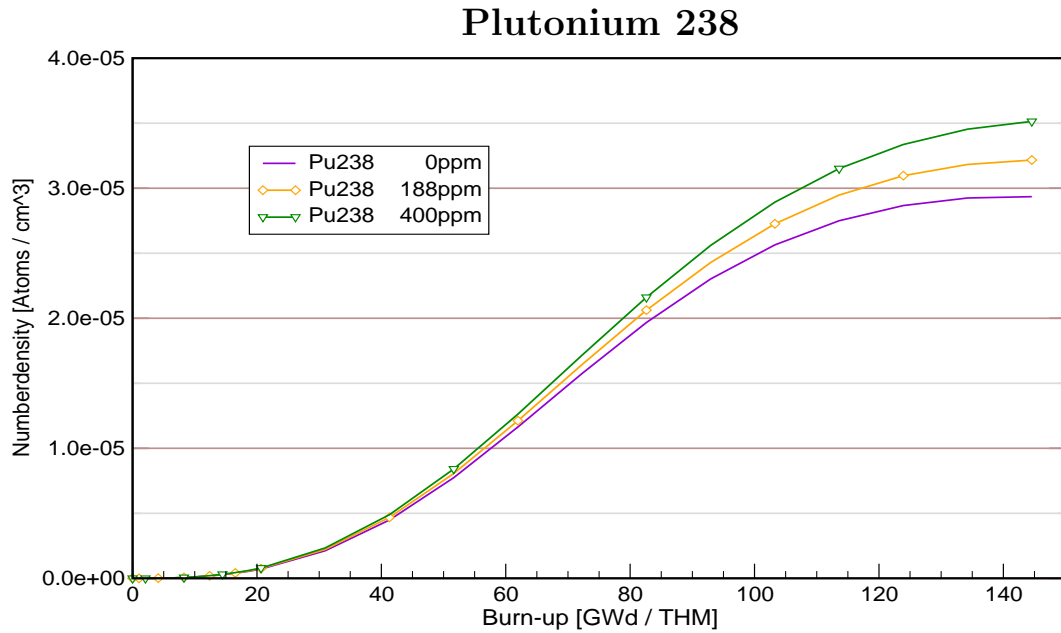


Figure 5.12: Pu^{238} : the chart shows curves for constant boron modeling for three different concentrations.

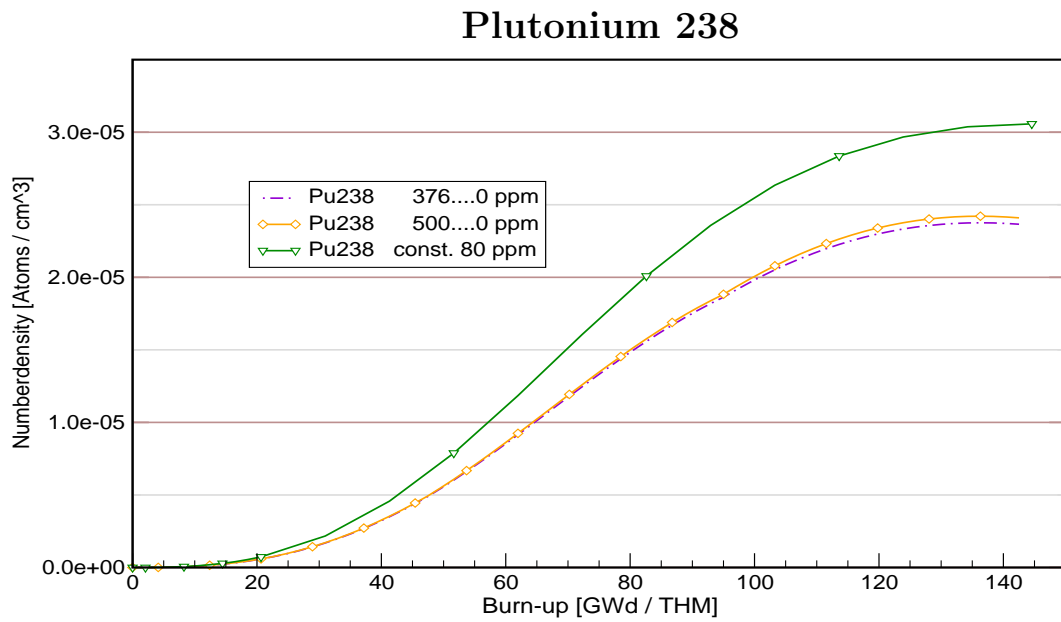


Figure 5.13: Pu^{238} : the chart shows curves for constant 80 ppm and variable boron modeling (376...0 ppm) and (500...0 ppm).

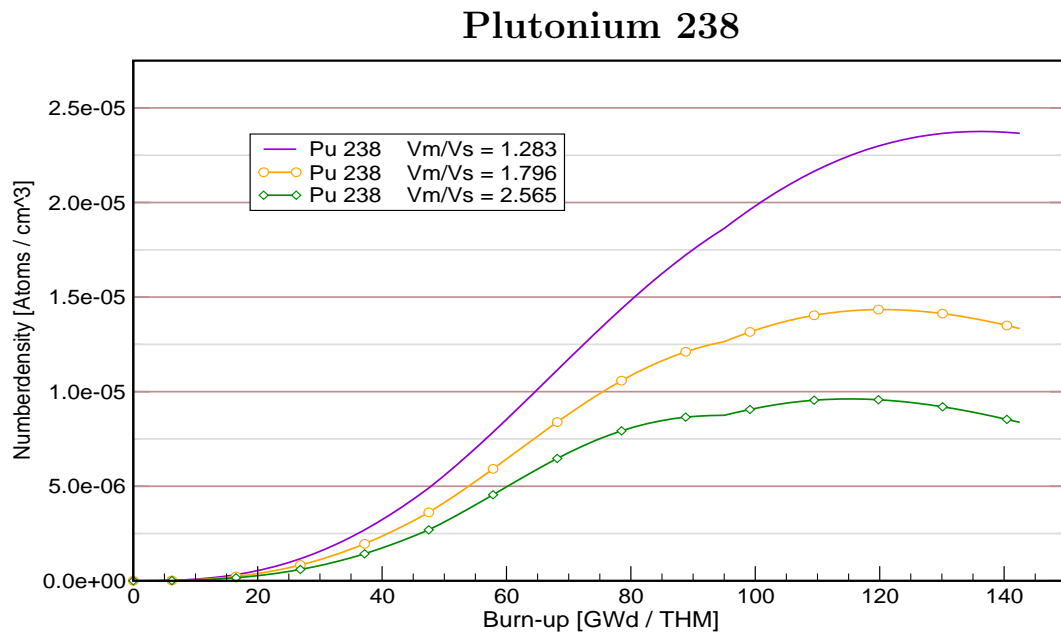


Figure 5.14: Pu^{238} : the chart compares curves for variable boron modeling (376...0 ppm) for three different V_m/V_s ratios.

5.4 Summary

The calculations accomplished within this chapter have been dedicated to high burn-ups in uranium fuel. For a final evaluation, one has to account for the conditions of the calculations. According to the model, these are far from practical depletion environments. However, Chapter 3 showed that the calculation tool KARBUS is very powerful for burn-up calculations, investigating global trends and influences. Despite some exceptions for single isotopes, reliability was proven and the calculated results seem to be very satisfying. To improve calculations, a variable boron modeling was introduced to the calculation model. Comparing results of variable modeling to results of constant modeling has revealed major differences. Depending on the isotope, variable and constant modeling differ strongly. Thus, a new rule of thumb for approximating variable boron modeling was proposed. For most isotopes whose buildup depends upon boron modeling, using 20...25% of the initial variable boron concentration gives good results.

Summarizing the investigations, it can be pointed out that these results could be a good basis for further developments in the sense of benchmark investigations. However, the characteristics of the basic model have to be considered when applying them in real systems.

Chapter 6

Conclusion and Prospects

Increasing the burn-up in LWRs is a current issue. The driving force is mainly the reduction of electricity generation costs. However, further topics have recently attained more and more importance, for example, the open issue of the fuel cycles back-end. Chapter 4 focused on this topics in detail showing the requirement to develop new fuels and concepts in the field of nuclear power production.

Investigating the effects of high burn-ups in fuels is indispensable for further developments, since isotope build-up and the resulting fuel behavior acts mostly accumulative and becomes apparent especially for high burn-ups. The applied KAPROS module KARBUS could be a very helpful tool to investigate on high burn-ups and its effects in the context of a benchmark. This was shown in Chapter 3 during validation.

Chapter 5 accomplished investigations on the mentioned effects of high burn-ups in 5% enriched uranium fuel. Major trends for the buildup of isotope groups depending on the core system parameters have been pointed out. The investigations focused on soluble boron concentration in PWRs and the moderator to fuelrod volumetric ratio as a design option. Variable and constant boron modeling has been compared, leading to interesting results.

It is today's challenge of research to develop solutions for the following topics:

- Saving resources and safeguarding future energy supply while consumption increases, leading to increased plant efficiencies and new fuel cycle concepts beyond the common LWR. Among these are the introduction of the alternative thorium fuel-cycle, preventing the buildup of transuranics as well as reactor concepts with increased breeding ratio.

- Solving the open issue of fuel cycle's back-end to reach the design goal of a closed nuclear fuel cycle. Reactor operation accumulates spent nuclear fuel and storage capacities are running out. Concepts should be developed to reduce the radio toxicity and the amount of spent nuclear fuel. The resources of SNF, fissiles and breeding materials have to be recovered. The introduction of elaborated ADS systems for nuclear waste incineration might thereby be a milestone in spent fuel treatment techniques and the last fundamental piece to close the nuclear fuel cycle.

It is today's fundamental task to develop and combine both topics into a closed concept, comprising enrichment, composition of reactor types combined in a pool, reactor operation techniques, advanced spent fuel reprocessing and waste treatment techniques. This will be rather challenging.

Appendix A

Appendix of Chapter No.3

A.1 ksuxgo

ksuxgo input-dataset [SIZE[=] size] [PL[=] nisl] [NBLK[=] nblock] [SEP] [TEST]
(blanks after [=] sign are required!)

input-dataset Full name of the input-dataset in the current directory

SIZE= size Length of the Lifeline in bytes

PL= nisl Lifeline-distribution in per cent:
nisl% Pointer Lifeline and (100-nisl)% Internal Lifeline

NBLK= nblock Number of 1024-word blocks of the external lifeline
Required for locks greater than 4 mb words (default 4096)

SEP Output-dataset KSUX.user.FT07 with job-separator for printout

TEST Ordering of Modul-Libraries.
Without input TEST the library ordering is
/opt/KAPROS/KSLIB:/home/send/KSLIB
With input TEST the ordering is
current directory:/home/send/KSLIB:/opt/KAPROS/KSLIB

DEBUG Debugging output will be printed

A2

A.2 input.karbus

```
*KSIOX DBN=INPUT ARCHIV,TYP=CARD,PMN=PRDUM //Pos. 1
```

```
31 'SEQ ' 'GEN '
```

```
1024 'KSSKUX ARCHIVE LINUX '
```

```
8 'FUEL CYCLE BACKEND STUDY KWO '
```

```
*$*$
```

```
*KSIOX DBN=INPUT KARBUS,TYP=CARD,PMN=PRDUM
```

```
'CHIT' 2
```

```
'OBUC'
```

```
'GRMX'
```

```
'EFTB'
```

```
10 5.5
```

```
'U 234 ' 193. 2.45
```

```
'U 235 ' 193.5 2.418
```

```
'U 236 ' 193. 2.45
```

```
'U 238 ' 197.2 2.81
```

```
'NP237 ' 200. 2.5
```

```
'PU238 ' 200. 2.55
```

```
'PU239 ' 201.8 2.871
```

```
'PU240 ' 195. 2.9
```

```
'PU241 ' 202.1 2.972
```

```
'PU242 ' 200. 3.00
```

```
'BUCO' '0101'
```

```
'DUMM'
```

```
'NOPR'
```

```
'WN2N'
```

```
'POWI'
```

```
'BU1D' 29
```

```
//Pos. 2
```

```
2
```

```
5.8 1.
```

```
-219.609 0.
```

```
1
```

```
4.6
```

```
-219.609
```

2
25. 25.
-219.609 -219.609

2
25. 2.
-219.609 0.

1
3.5
-219.609

2
30. 41.5
-219.609 0.

1
6.5
-219.609

2
25. 25.
-219.609 -219.609

4
25. 25. 25. 5.8
-219.609 -219.609 -219.609 0.

1
5.9
-219.609

2
31. 28.
-219.609 0.

1
6.9
-219.609

2
30. 30.
-219.609 -210.979

3
30. 30. 9.2
-219.609 -219.609 0.

A4

1

4.7

-219.609

2

20. 20.

-219.609 -219.609

3

20. 20. 3.5

-219.609 -219.609 0.

1

3.

-219.609

2

20. 3.

-219.609 0.

1

4.

-219.609

2

28. 28.

-219.609 -219.609

2

13.8 380.

-183.68 0.

1

5.3

-219.609

2

30. 35.

-219.609 -219.609

3

30. 30. 3.

-219.609 -219.609 0.

1

3.4

-219.609

```

2
25.      25.
-219.609 -219.609
2
30.      29.
-219.609 -219.609
2
1.        365.
-219.609  0.0
*$$
*KSIOX DBN=INPUT NDCALC,TYP=CARD,PMN=PRDUM           //Pos. 3
'GEO ' 1
'UVEC'
4
'U 234 ' 19.0 234. 0
'U 235 ' 19.0 235. 1
'U 236 ' 19.0 236. 0
'U 238 ' 19.0 238. 0
'SVEC'
1
'ZR      ' 6.5485 91.22
'VOFR'
'MINP'
1
'          ' 'U 235 ' 'U 235 ' *$ KWO EINHEITSZELLE   //Pos. 4
1028. 605. 572. 1.49423 0.031000 0. 0.
0.46500 0.07000 0.927411 0.717944
1.0 0.0 0.0 0.0
0.0 0.031000 0.0 0.969000
1.
1.
'ADDF' 90                                           //Pos. 5
'GD154 ' 920. 1.E-20
'GD155 ' 920. 1.E-20
'GD156 ' 920. 1.E-20
'GD157 ' 920. 1.E-20

```

'GD158	'	920.	1.E-20
'GD160	'	920.	1.E-20
'NP237	'	920.	1.E-20
'NP239	'	920.	1.E-20
'PU238	'	920.	1.E-20
'AM241	'	920.	1.E-20
'AM242	'	920.	1.E-20
'AM42M	'	920.	1.E-20
'AM243	'	920.	1.E-20
'CM242	'	920.	1.E-20
'CM244	'	920.	1.E-20
'XE131	'	920.0	1.E-20
'XE132	'	920.0	1.E-20
'XE133	'	920.0	1.E-20
'XE134	'	920.0	1.E-20
'XE135	'	920.0	1.E-20
'XE136	'	920.0	1.E-20
'SM144	'	920.0	1.E-20
'SM145	'	920.0	1.E-20
'SM146	'	920.0	1.E-20
'SM147	'	920.0	1.E-20
'SM148	'	920.0	1.E-20
'SM149	'	920.0	1.E-20
'SM150	'	920.0	1.E-20
'SM151	'	920.0	1.E-20
'SM152	'	920.0	1.E-20
'RH103	'	920.0	1.E-20
'RH105	'	920.0	1.E-20
'PM144	'	920.0	1.E-20
'PM145	'	920.0	1.E-20
'PM146	'	920.0	1.E-20
'PM147	'	920.0	1.E-20
'PM148	'	920.0	1.E-20
'PM48M	'	920.0	1.E-20
'PM149	'	920.0	1.E-20
'PM150	'	920.0	1.E-20

'CS133	'	920.0	1.E-20
'CS134	'	920.0	1.E-20
'CS135	'	920.0	1.E-20
'TC 99	'	920.0	1.E-20
'AG109	'	920.0	1.E-20
'RU101	'	920.0	1.E-20
'RU102	'	920.0	1.E-20
'RU103	'	920.0	1.E-20
'RU104	'	920.0	1.E-20
'RU106	'	920.0	1.E-20
'PD105	'	920.0	1.E-20
'PD106	'	920.0	1.E-20
'PD107	'	920.0	1.E-20
'PD108	'	920.0	1.E-20
'ND143	'	920.0	1.E-20
'ND144	'	920.0	1.E-20
'ND145	'	920.0	1.E-20
'ND146	'	920.0	1.E-20
'ND147	'	920.0	1.E-20
'ND148	'	920.0	1.E-20
'ND150	'	920.0	1.E-20
'EU153	'	920.0	1.E-20
'EU154	'	920.0	1.E-20
'EU155	'	920.0	1.E-20
'CD111	'	920.0	1.E-20
'CD113	'	920.0	1.E-20
'MO 95	'	920.0	1.E-20
'MO 97	'	920.0	1.E-20
'MO 98	'	920.0	1.E-20
'MO100	'	920.0	1.E-20
'ZR 91	'	920.0	1.E-20
'ZR 93	'	920.0	1.E-20
'ZR 96	'	920.0	1.E-20
'PR141	'	920.0	1.E-20
'PR143	'	920.0	1.E-20
'I 127	'	920.0	1.E-20

A8

'I 129 ' 920.0 1.E-20
'IN115 ' 920.0 1.E-20
'LA139 ' 920.0 1.E-20
'KR 83 ' 920.0 1.E-20
'KR 84 ' 920.0 1.E-20
'KR 86 ' 920.0 1.E-20
'TB159 ' 920.0 1.E-20
'CE140 ' 920.0 1.E-20
'CE141 ' 920.0 1.E-20
'CE142 ' 920.0 1.E-20
'CE143 ' 920.0 1.E-20
'CE144 ' 920.0 1.E-20
'DY164 ' 920.0 1.E-20
'LU176 ' 920.0 1.E-20

'ADDM' 1

'B 10 ' 572. 7.738E-06

//Pos. 6

'FINV' 400. 45000 *\$ 3600 MWTH, 200 W/CM POWER RATING

\$\$

*KSIOX DBN=CELSPECIFICATION, TYP=CARD, PMN=PRDUM, IND=1

*\$ MODULE NAME FOR GROUPCONSTANT CALCULATIONS

'GRUCEL '

*\$ SN IACC ITMAX EPS NBUC BGHT BWDT

04 1 06 1.E-4 0 0. 0.

*\$ N(I), I=1, NM

12 3 8

*\$ NTEXT(I), I=1, MIN(0, 15)

'CORE EINHEITSZELLE '

\$\$

*KSIOX DBN=GRUCAL, TYP=CARD, PMN=PRDUM, IND=1

//Pos. 7

'ARBFELD ' 200000

'GRUBA '

*\$ '/opt/KAPROS/data/G69P5E65B '

*\$ '/opt/KAPROS/data/G69P5J30B '

'/opt/KAPROS/data/G69P1V03 '

```

'STEUER '
*$ '/opt/KAPROS/data/F69UD06 '
  '/opt/KAPROS/data/F69UD04 '
*$ 'TRACE '
*$ 'ERKLTYP '
*$ 'FORMELN ' 28 30
'GRUCAL '
  'WIMSLIB ' , , , ,
'MISCH '
*$ 'NOPRINT '
'NOTGRMAT'
'DATBLOCK'
*$ DEFINE EVALUATION TYPES
'TYP '
'ZUSATZ ' 2
  'SN2N '
  'STRTR '
*$ END OF ADDITIONAL EVALUATION TYPES

```

```

'AUSWERT '
'ZUSATZ ' 25
'SFISS ' , , ' 1 0
'SCAPT ' , , ' 1 0
*$ 'STOT ' , , ' 1 0
*$ 'STOT ' , , ' 0 0
'SN2N ' 'U 234 ' 1 1 'U 234 '
'SN2N ' 'U 235 ' 1 1 'U 235 '
'SN2N ' 'U 236 ' 1 1 'U 236 '
'SN2N ' 'U 238 ' 1 1 'U 238 '
'SN2N ' 'NP237 ' 1 1 'NP237 '
'SN2N ' 'PU238 ' 1 1 'PU238 '
'SN2N ' 'PU239 ' 1 1 'PU239 '
'SN2N ' 'PU240 ' 1 1 'PU240 '
'SN2N ' 'PU241 ' 1 1 'PU241 '
'SN2N ' 'PU242 ' 1 1 'PU242 '
'SFISS ' 'U 234 ' 0 1 'U 234 '

```

//Pos. 8

A10

```
'SFISS ' 'U 235 ' 0 1 'U 235 '  
'SFISS ' 'U 236 ' 0 1 'U 236 '  
'SFISS ' 'U 238 ' 0 1 'U 238 '  
'SFISS ' 'NP237 ' 0 1 'NP237 '  
'SFISS ' 'PU238 ' 0 1 'PU238 '  
'SFISS ' 'PU239 ' 0 1 'PU239 '  
'SFISS ' 'PU240 ' 0 1 'PU240 '  
'SFISS ' 'PU241 ' 0 1 'PU241 '  
'SFISS ' 'PU242 ' 0 1 'PU242 '  
'SCAPT ' 'FERTILE ' 0 2 'U 238 ' 'PU240 '  
'SCAPT ' 'FISSILE ' 0 3 'U 235 ' 'PU239 ' 'PU241 '  
'SFISS ' 'FISSILE ' 0 3 'U 235 ' 'PU239 ' 'PU241 '
```

*\$ SECUNDARY INPUT

*\$ 'SEKINPT '

*\$ 1 ' ,

*\$ 16

*\$ SEC INPUT END

'GRUCEND '

\$\$

*KSIOX DBN=INPUT REMCOR,TYP=CARD,PMN=PRDUM

//Pos. 9

*\$ 'CNTR'

'DUMM'

'NCOR' 1 69

*\$ 'NOPR'

\$\$

*KSIOX DBN=INPUT CHICOR,TYP=CARD,PMN=PRDUM

*\$ 'CNTR'

'DUMM'

'DAFI'

*\$ 'NOPR'

\$\$

*KSIOX DBN=INPUT WETHES,TYP=CARD,PMN=PRDUM

'BEGI'

\$\$

*KSIOX DBN=INPUT WEPERS,TYP=CARD,PMN=PRDUM

```

'BEGI'
*$ 'BUCI' 5 3.E-3
*$*$
*KSIOX DBN=INPUT WEKCPM,TYP=CARD,PMN=PRDUM
'NOPR'
'LDIM' 65000
*$*$
*KSIOX DBN=INPUT WEFILE,TYP=CARD,PMN=PRDUM
*$ 'CNTR'
'DUMM'
*$*$
*KSIOX DBN=INPUT GRDASQ,TYP=CARD,PMN=PRDUM
'TYPG'
'DUMM'
*$*$
*KSIOX DBN=INPUT DXBURN,TYP=CARD,PMN=PRDUM,IND=1
'GRC1' 4 14 27 42 69
'GRC2' 6 5 9 14 27 42 69
'BUCO' 'D101'
'EPFI' 208.
'GRST' 2
'GRNR' 2
'GRMX'
  'POWR' 10*5.41E-4
'GHET'
*$*$
*KSIOX DBN=INPUT GRUMIXCELL,TYP=CARD,PMN=PRDUM,IND=1 //Pos.10
'AMIX'
1
1
3
1
'B 10 ' 1.
*KSIOX DBN=INPUT GRUMIXCELL,TYP=CARD,PMN=PRDUM,IND=2
'AMIX'
1

```

A12

1

3

1

'B 10 ' 0.97792

*\$.

*\$.

*\$.

*\$.

*\$. //Cards for timesteps IND=3... IND=26 are cut.

*\$.

*\$.

*\$.

*\$.

*KSIOX DBN=INPUT GRUMIXCELL,TYP=CARD,PMN=PRDUM,IND=27

'AMIX'

1

1

3

1

'B 10 ' 0.74917

\$\$

*KSIOX DBN=INPUT GRUMIXCELL,TYP=CARD,PMN=PRDUM,IND=28

'AMIX'

1

1

3

1

'B 10 ' 0.31036

\$\$

*KSIOX DBN=INPUT GRUMIX,TYP=CARD,PMN=PRDUM,IND=1

'NDCA'

'NOPR'

'GHET'

\$\$

```

*KSIOX DBN=DXCONTRL,TYP=CARD,PMN=KETT,IND=1
'D' 'E'
*$$
*KSIOX DBN=DX LDIM,TYP=CARD,PMN=KETT,IND=1
'LDIM' 004 004 1
*$$
*KSIOX DBN=DXDIF,TYP=CARD,PMN=KETT,IND=1
'DIXY' 0 0
'NOTE' 1
' DIXY CALCULATION FOR FUNDAMENTAL MODE MEAN PWR ZONE
'KN' 16
 2 0 26 10 0 1 0 0 1 70 0 0 0 0 0 0
'CN' 6
0.0010 0.0010 1.E+10 01.E+10 1.E+10 1.E+10
'REGN' 0
01 001 004 001 004 *$ Z1
'HSTP' 0
 3 0. 003 2.
'VSTP' 0
 3 2. 003 0.
'DXNF' 0
*$$
*KSIOX DBN=DXEVA,TYP=CARD,PMN=PRDUM
'EVA' 0 0
'GLBL' 06
1
'NUSF 'SCAPT 'SFISS
'SCAPT FERTILE 'SCAPT FISSILE 'SFISS FISSILE
'EVAF' 0
*$$
*KSIOX DBN=INPUT DXPODA,TYP=CARD,PMN=PRDUM
*$ 'NSGM' 'SIGMNO
'NOPR'
'SPLP'
'GRPS' 1 1
'INDI' 1 01

```

A14

*\$ 'CNTR'

\$\$

*KSIOX DBN=INPUT BURNUP,TYP=CARD,PMN=PRDUM

//Pos.11

'BUTB'

90

'GD154 ' 'GD155 ' 'GD156 ' 'GD157 ' 'GD158 ' 'GD160 '
'NP237 ' 'NP239 ' 'PU238 ' 'AM241 ' 'AM242 ' 'AM42M '
'AM243 ' 'CM242 ' 'CM244 ' 'XE131 ' 'XE132 ' 'XE133 '
'XE134 ' 'XE135 ' 'XE136 '
'SM144 ' 'SM145 ' 'SM146 ' 'SM147 '
'SM148 ' 'SM149 ' 'SM150 ' 'SM151 ' 'SM152 ' 'RH103 '
'RH105 ' 'PM144 ' 'PM145 ' 'PM146 ' 'PM147 ' 'PM148 '
'PM48M ' 'PM149 ' 'PM150 ' 'CS133 ' 'CS134 ' 'CS135 '
'TC 99 ' 'AG109 ' 'RU101 ' 'RU102 ' 'RU103 ' 'RU104 '
'RU106 ' 'PD105 ' 'PD106 ' 'PD107 ' 'PD108 ' 'ND143 '
'ND144 ' 'ND145 ' 'ND146 ' 'ND147 ' 'ND148 ' 'ND150 '
'EU153 ' 'EU154 ' 'EU155 ' 'CD111 ' 'CD113 ' 'MO 95 '
'MO 97 ' 'MO 98 ' 'MO100 ' 'ZR 91 ' 'ZR 93 ' 'ZR 96 '
'PR141 ' 'PR143 ' 'I 127 ' 'I 129 ' 'IN115 ' 'LA139 '
'KR 83 ' 'KR 84 ' 'KR 86 '
'TB159 ' 'CE140 ' 'CE141 ' 'CE142 ' 'CE143 '
'CE144 ' 'DY164 ' 'LU176 '

'REAC' 2 0.06958 0.02126 0.3413

'NAMS' 'H ' 'FPP 9 '

'ORDT' 36

'CUTO' 1.E-05

'PRMT'

\$\$.

*GO SM=ARCHIV

//Pos.12

*GO SM=KARBUS,ML=0

A.3 ICE Charts, Comparison of Measuring Data and Calculations.

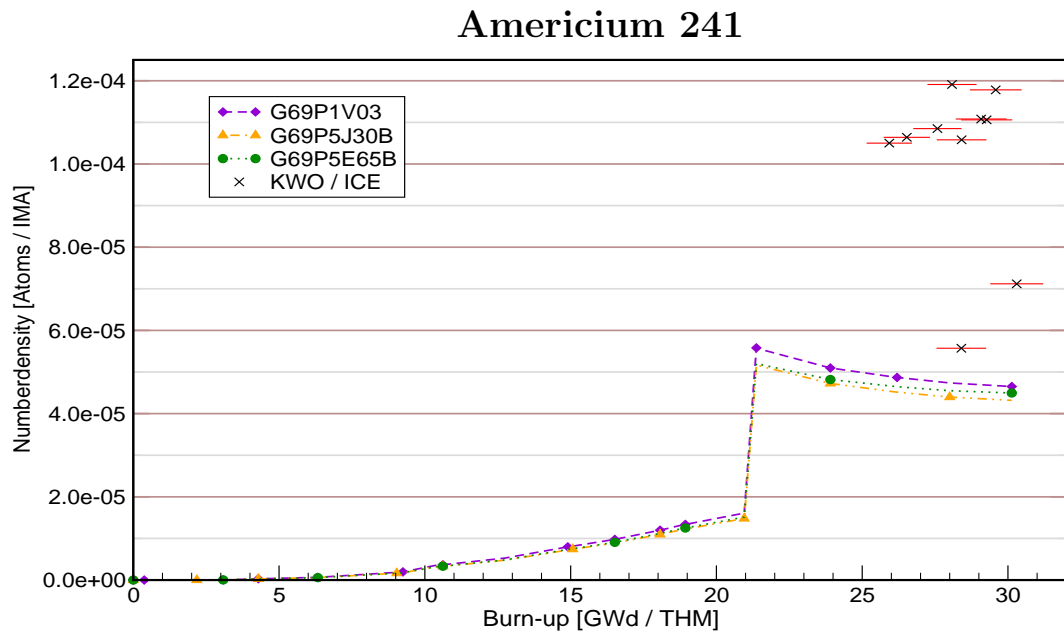


Figure A.1: Comparison of number densities plotted against burn-up, KARBUS-calculations and KWO/ICE-Experiment for Am^{241} .

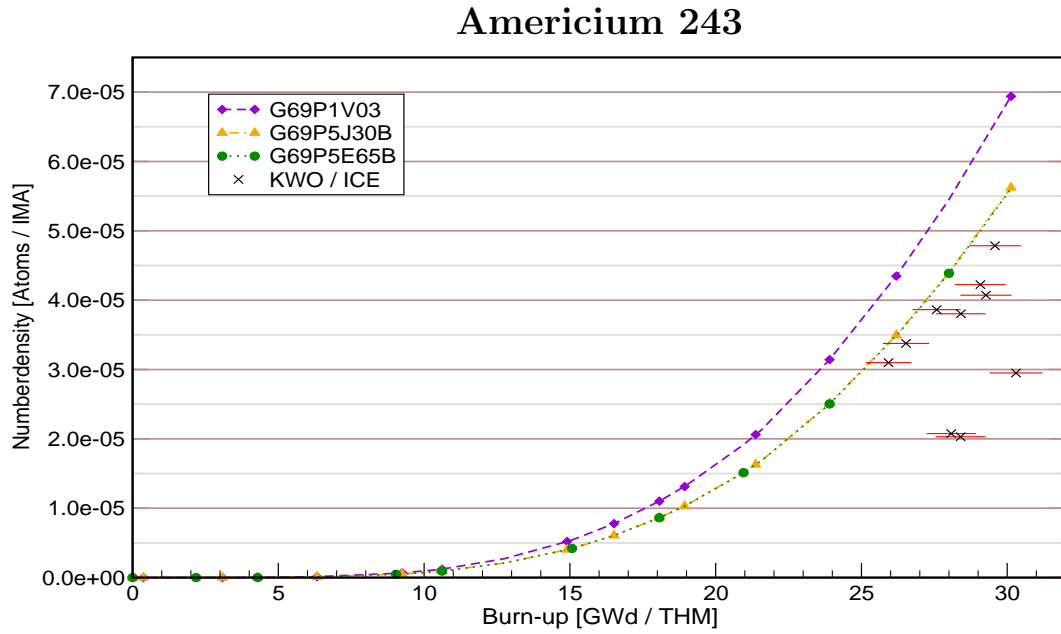


Figure A.2: Comparison of number densities plotted against burn-up, KARBUS-calculations and KWO/ICE-Experiment for Am^{243} .

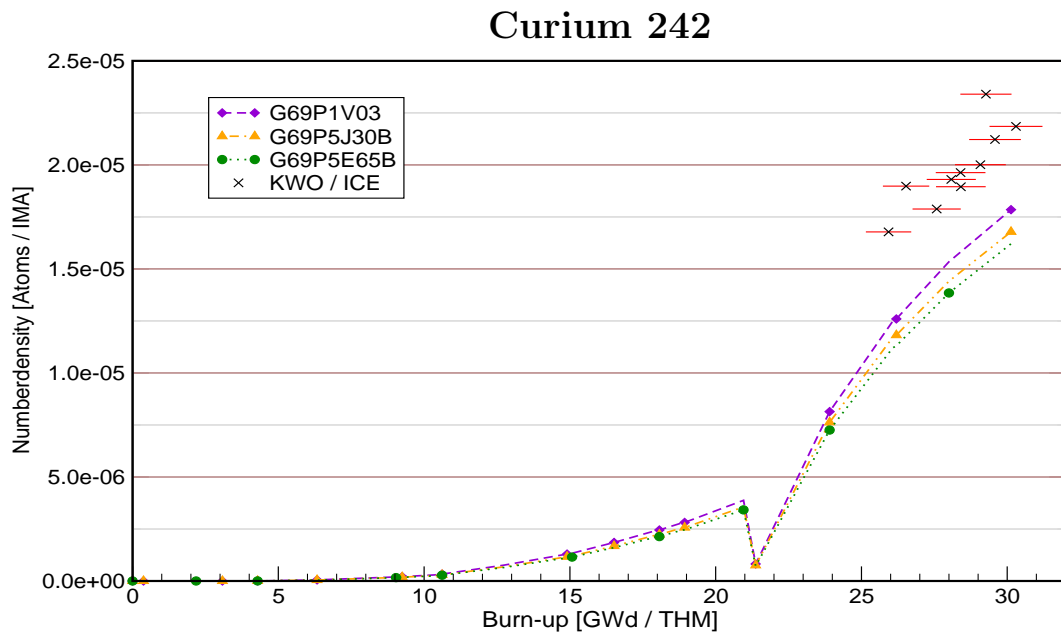


Figure A.3: Comparison of number densities plotted against burn-up, KARBUS-calculations and KWO/ICE-Experiment for Cm^{242} .

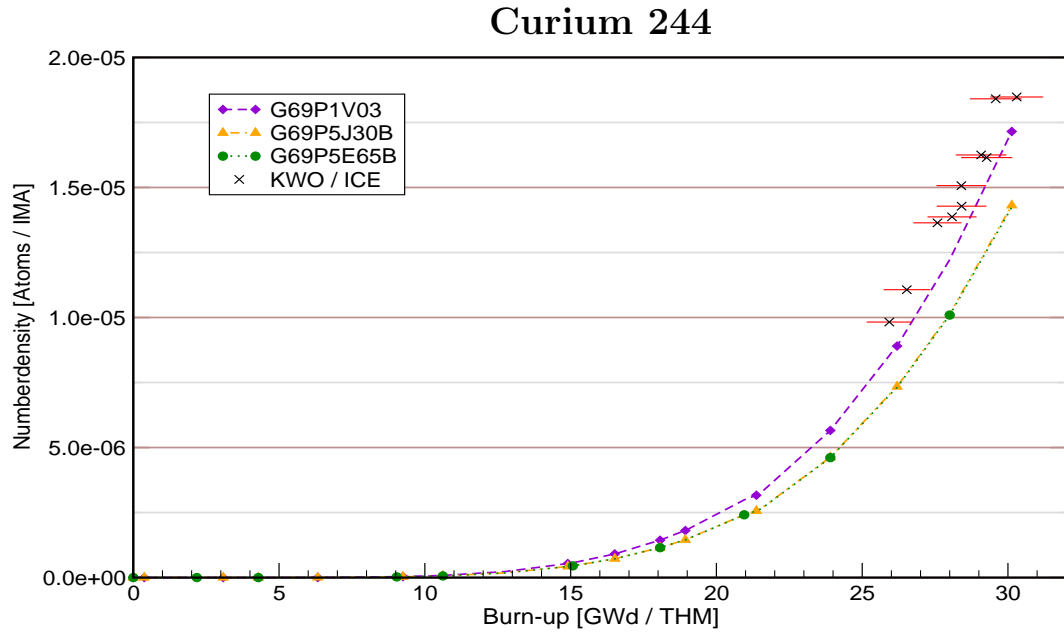


Figure A.4: Comparison of number densities plotted against burn-up, KARBUS-calculations and KWO/ICE-Experiment for Cm^{244} .

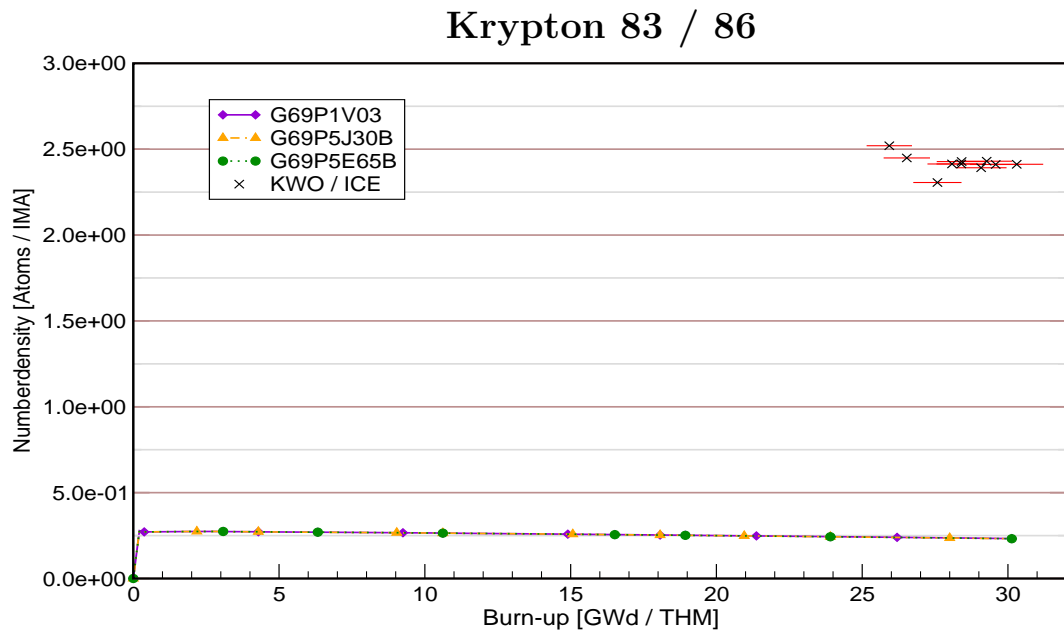


Figure A.5: Comparison of isotope ratio plotted against burn-up, KARBUS-calculations and KWO/ICE-Experiment for Kr^{83} to Kr^{86} ratio.

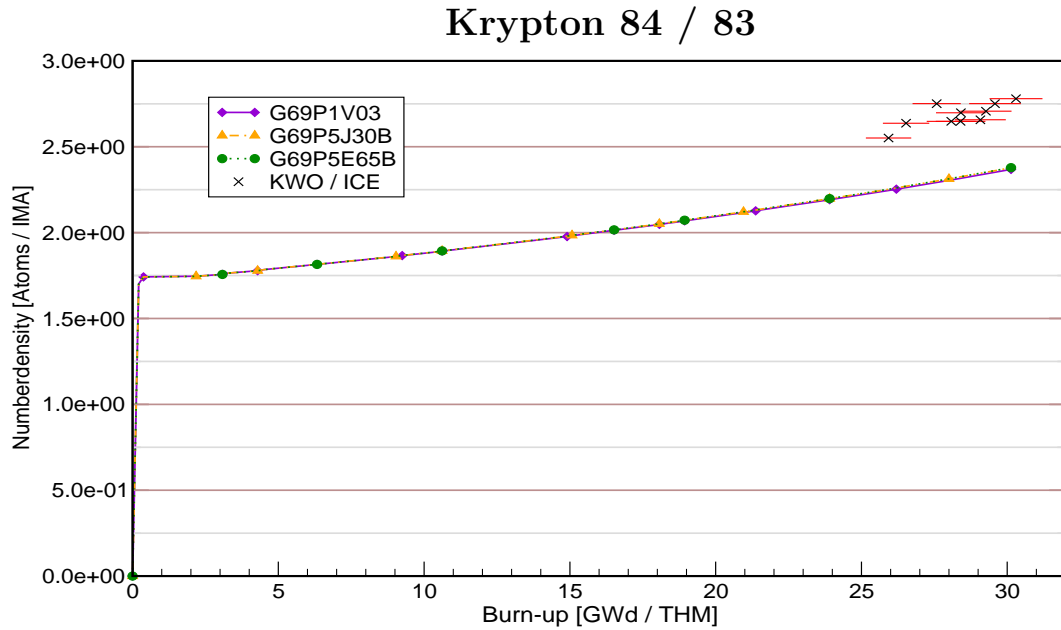


Figure A.6: Comparison of isotope ratio plotted against burn-up, KARBUS-calculations and KWO/ICE-Experiment for Kr^{84} to Kr^{83} ratio.

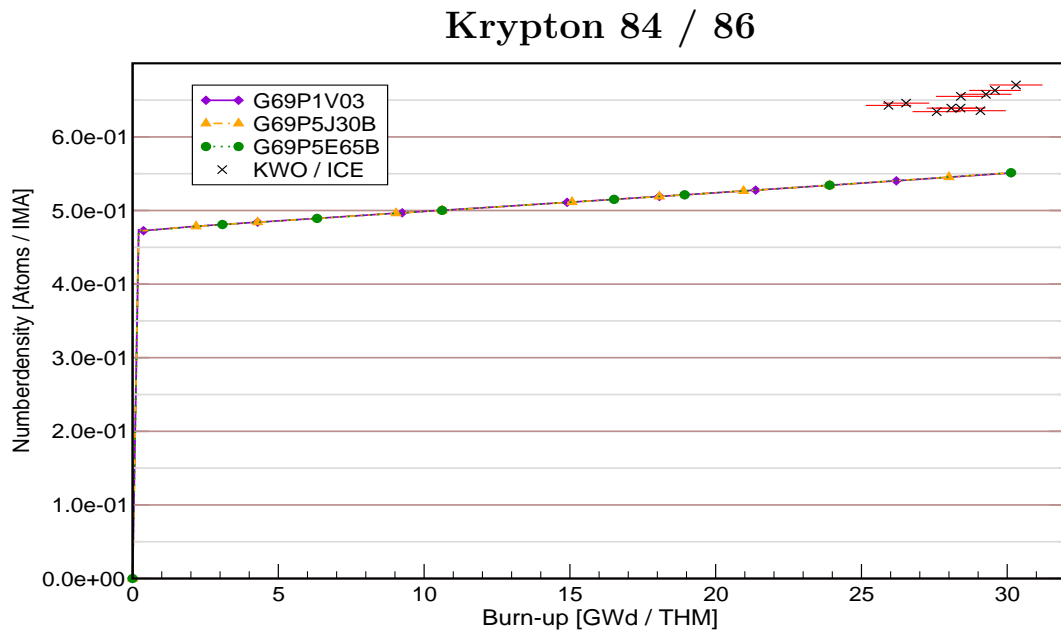


Figure A.7: Comparison of isotope ratio plotted against burn-up, KARBUS-calculations and KWO/ICE-Experiment for Kr^{84} to Kr^{86} ratio.

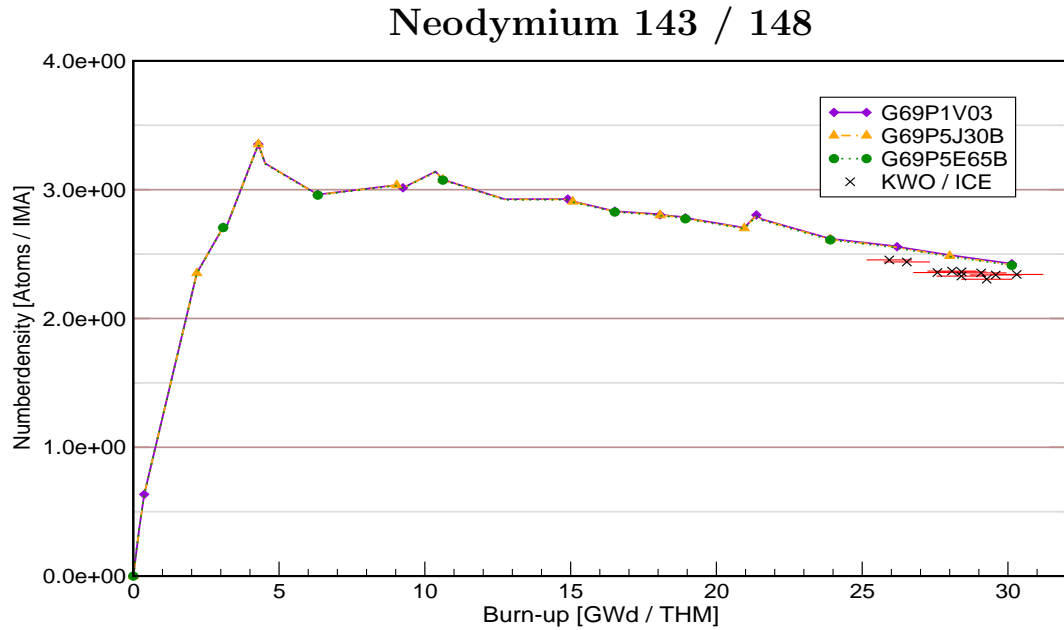


Figure A.8: Comparison of isotope ratio plotted against burn-up, KARBUS-calculations and KWO/ICE-Experiment for Nd^{143} to Nd^{148} ratio.

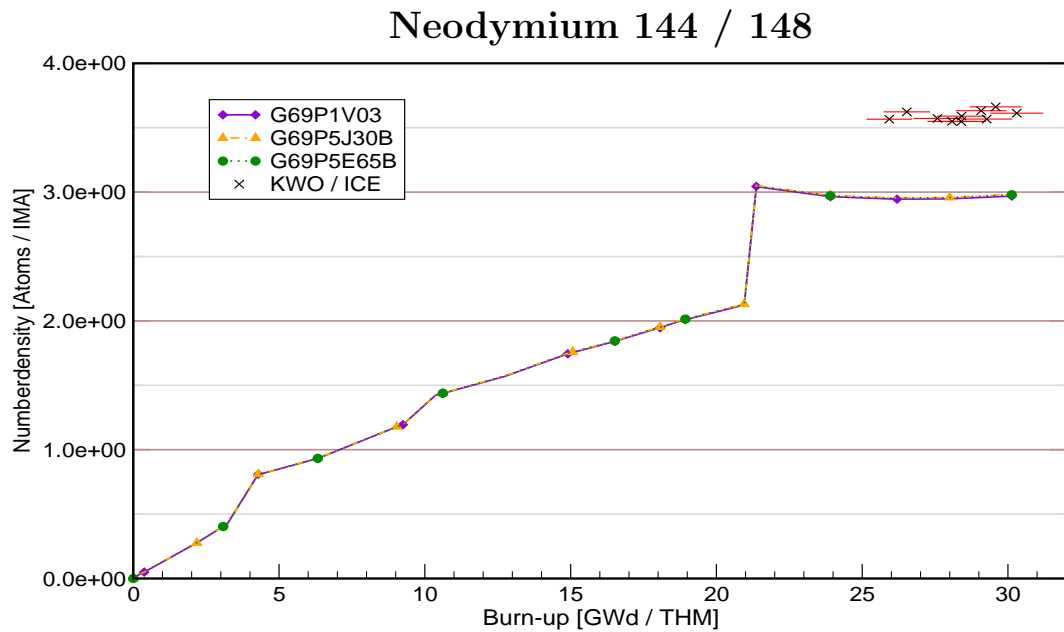


Figure A.9: Comparison of isotope ratio plotted against burn-up, KARBUS-calculations and KWO/ICE-Experiment for Nd^{144} to Nd^{148} ratio.

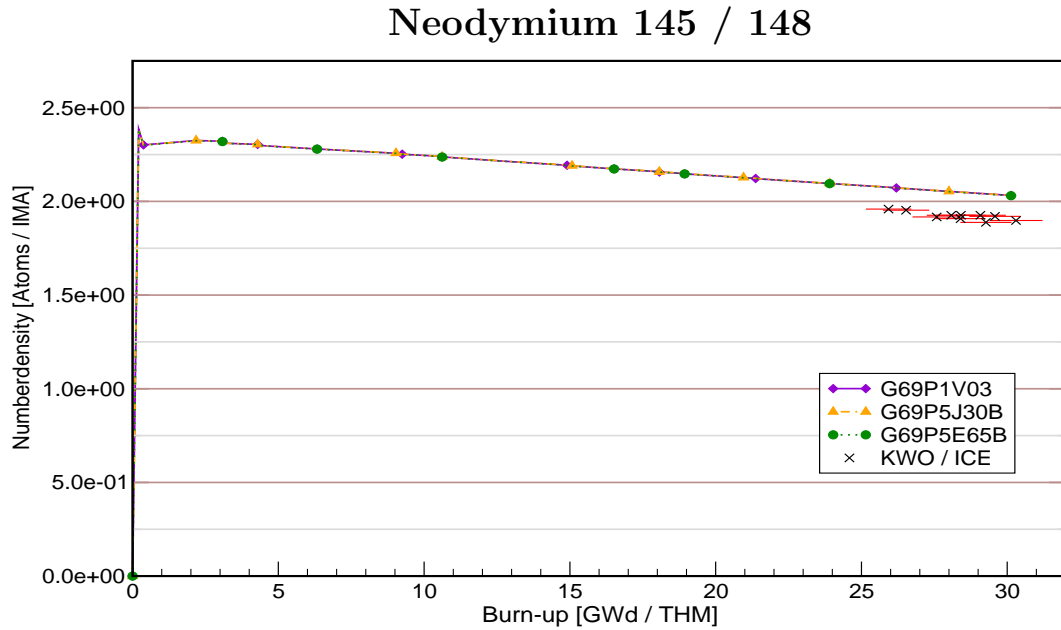


Figure A.10: Comparison of isotope ratio plotted against burn-up, KARBUS-calculations and KWO/ICE-Experiment for Nd^{145} to Nd^{148} ratio.

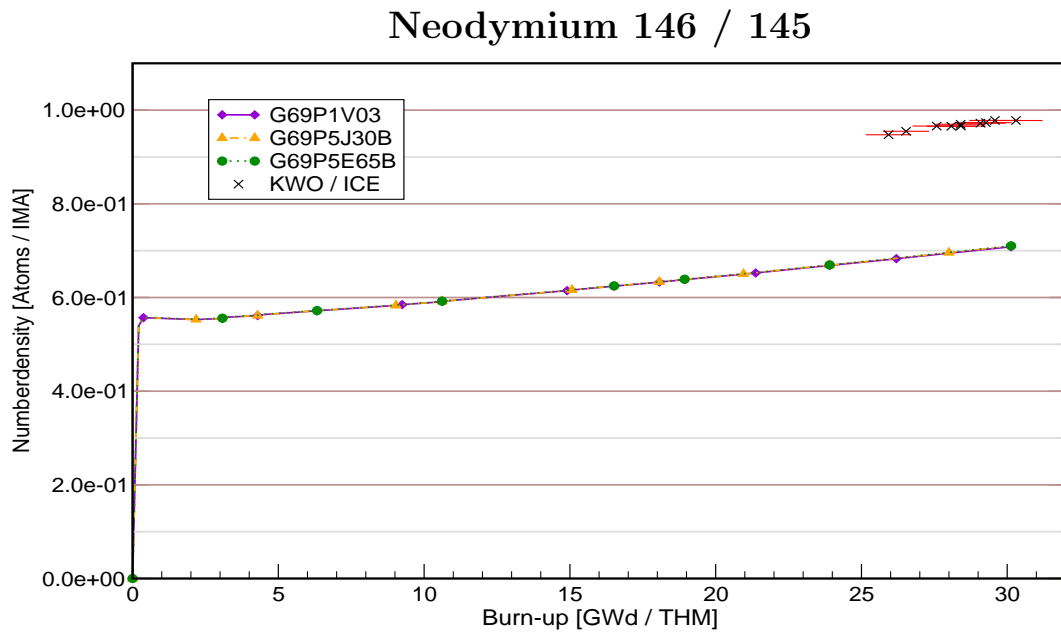


Figure A.11: Comparison of isotope ratio plotted against burn-up, KARBUS-calculations and KWO/ICE-Experiment for Nd^{146} to Nd^{145} ratio.

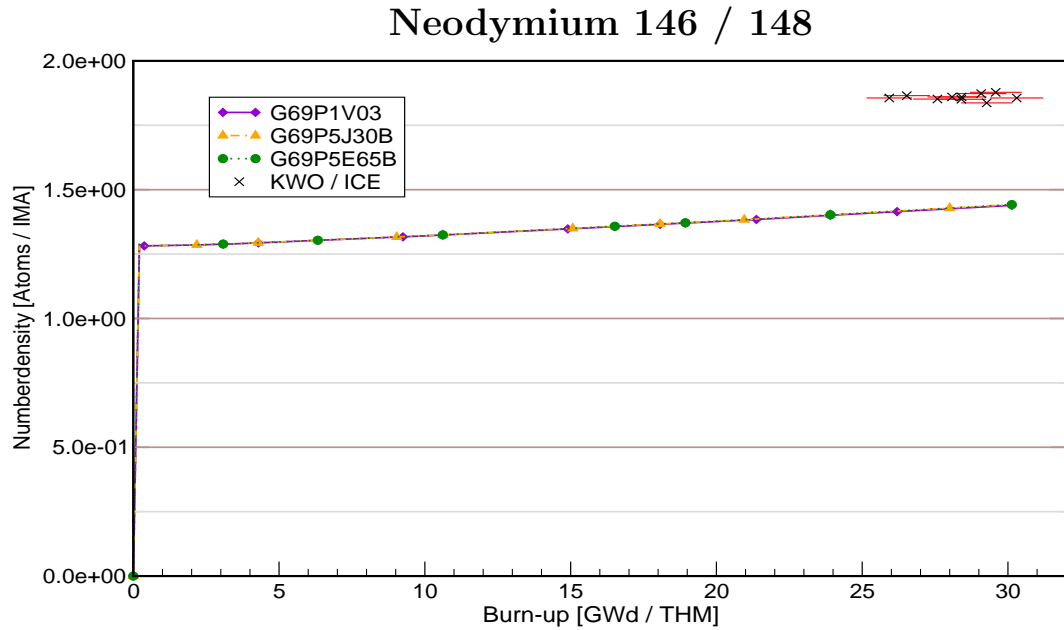


Figure A.12: Comparison of isotope ratio plotted against burn-up, KARBUS-calculations and KWO/ICE-Experiment for Nd^{146} to Nd^{148} ratio.

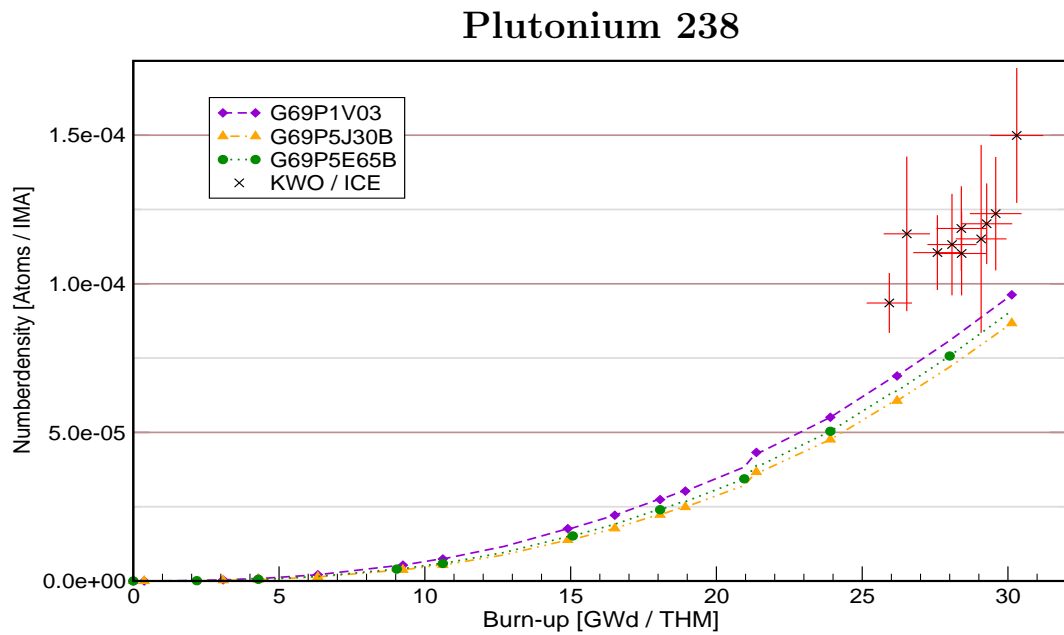


Figure A.13: Comparison of number densities plotted against burn-up, KARBUS-calculations and KWO/ICE-Experiment for Pu^{238} .

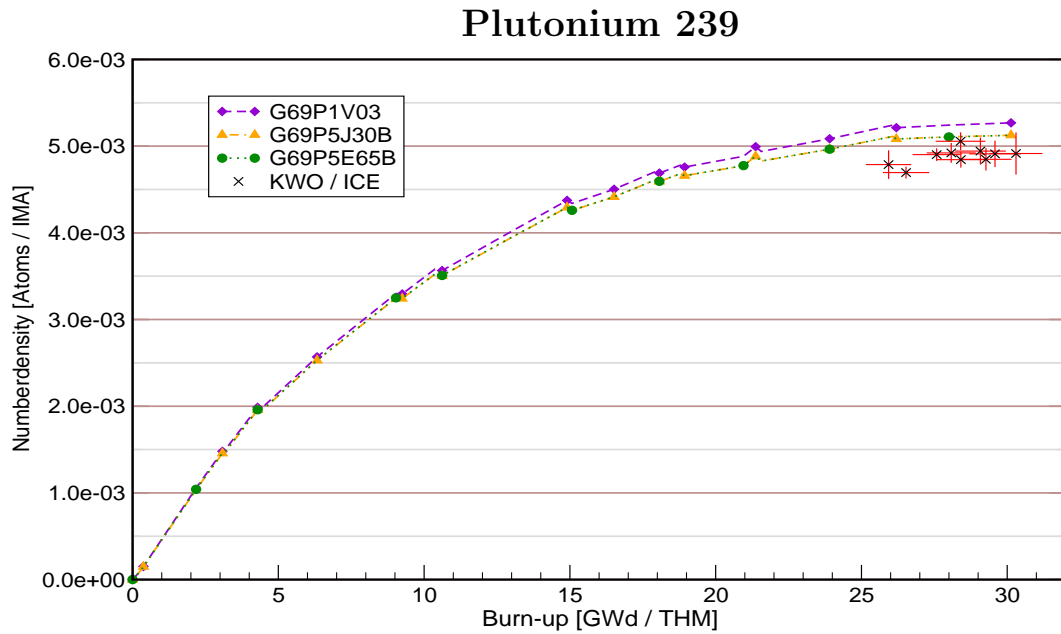


Figure A.14: Comparison of number densities plotted against burn-up, KARBUS-calculations and KWO/ICE-Experiment for Pu^{239} .

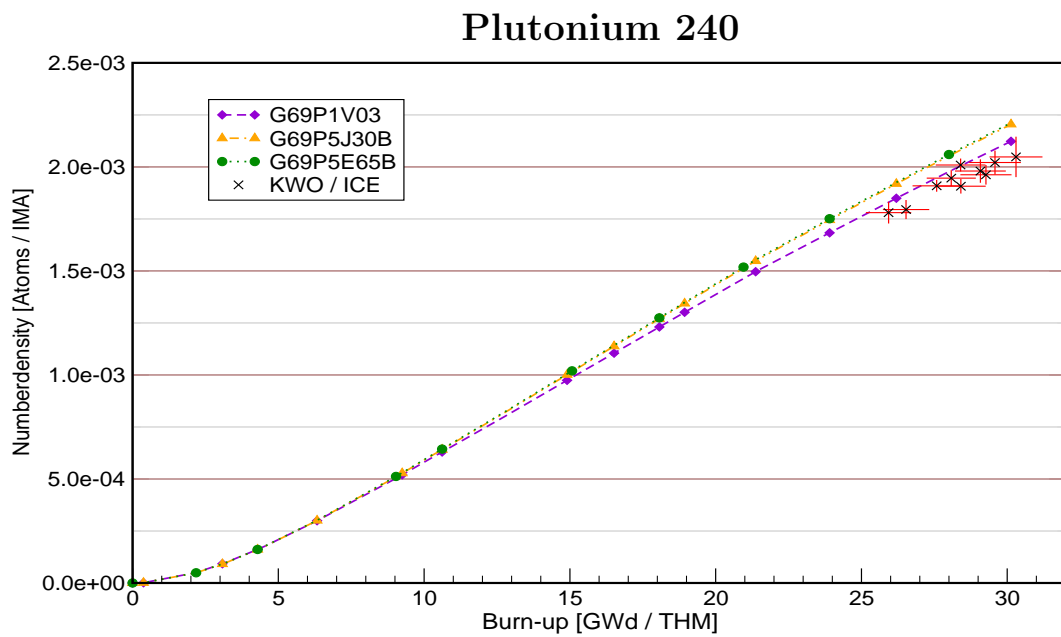


Figure A.15: Comparison of number densities plotted against burn-up, KARBUS-calculations and KWO/ICE-Experiment for Pu^{240} .

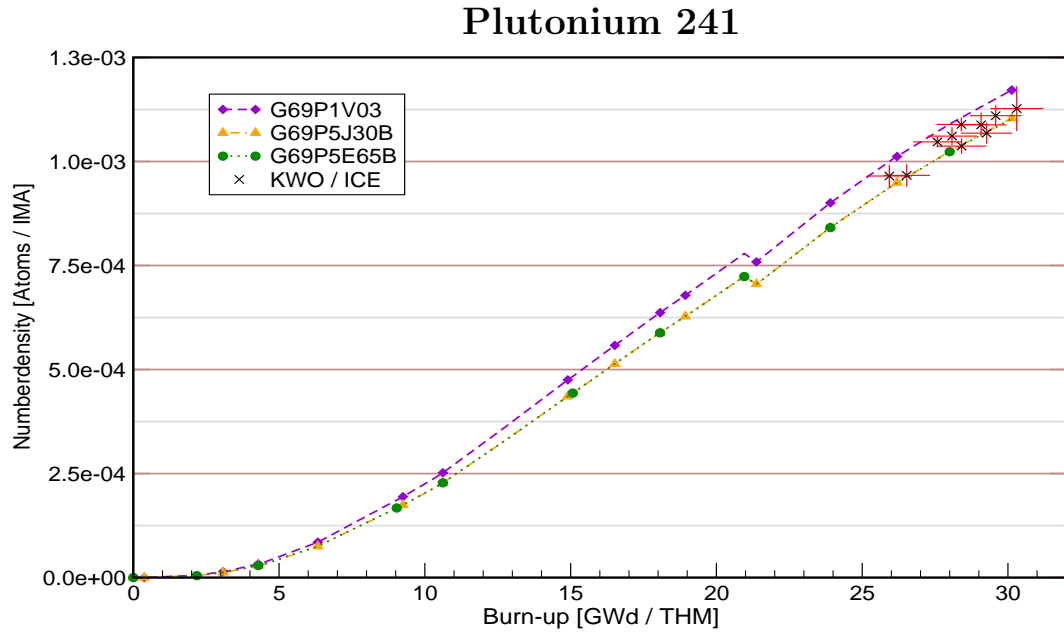


Figure A.16: Comparison of number densities plotted against burn-up, KARBUS-calculations and KWO/ICE-Experiment for Pu^{241} .

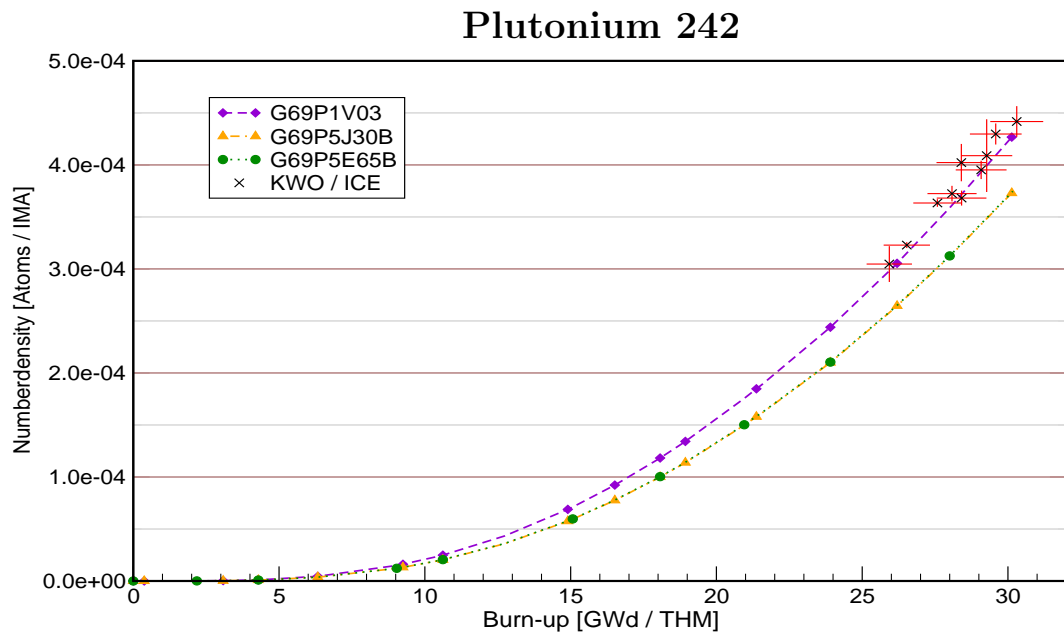


Figure A.17: Comparison of number densities plotted against burn-up, KARBUS-calculations and KWO/ICE-Experiment for Pu^{242} .

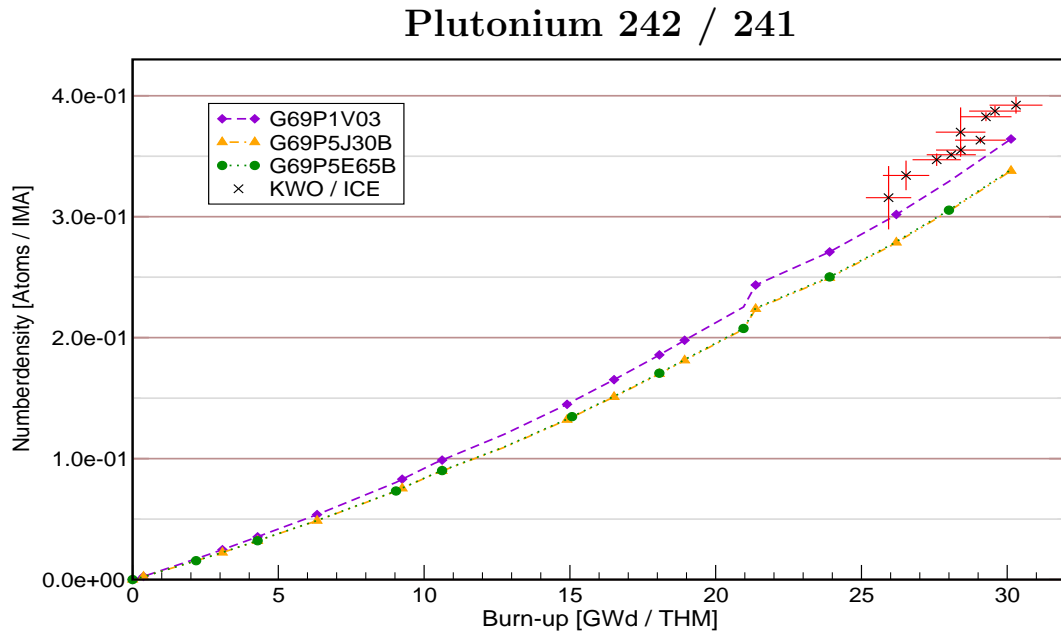


Figure A.18: Comparison of isotope ratio plotted against burn-up, KARBUS-calculations and KWO/ICE-Experiment for Pu^{242} to Pu^{241} ratio.

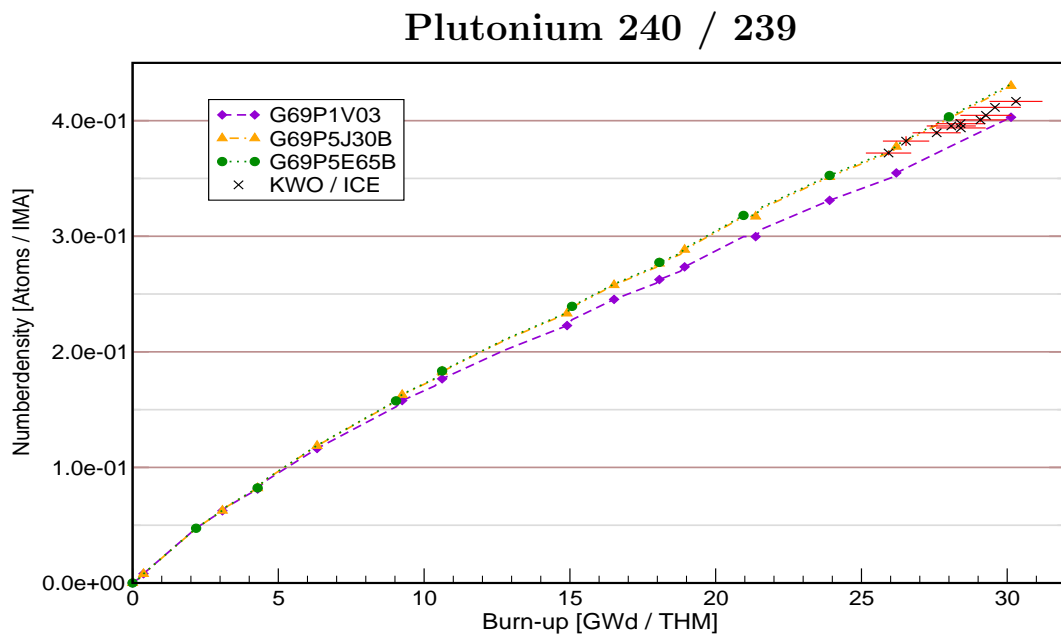


Figure A.19: Comparison of isotope ratio plotted against burn-up, KARBUS-calculations and KWO/ICE-Experiment for Pu^{240} to Pu^{239} ratio.

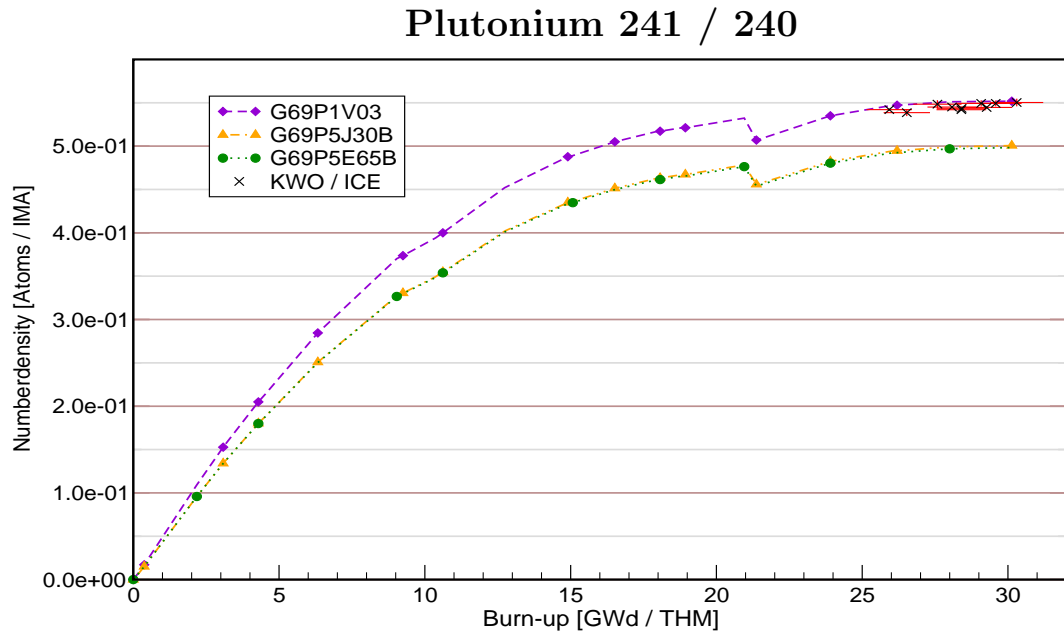


Figure A.20: Comparison of isotope ratio plotted against burn-up, KARBUS-calculations and KWO/ICE-Experiment for Pu^{241} to Pu^{240} ratio.

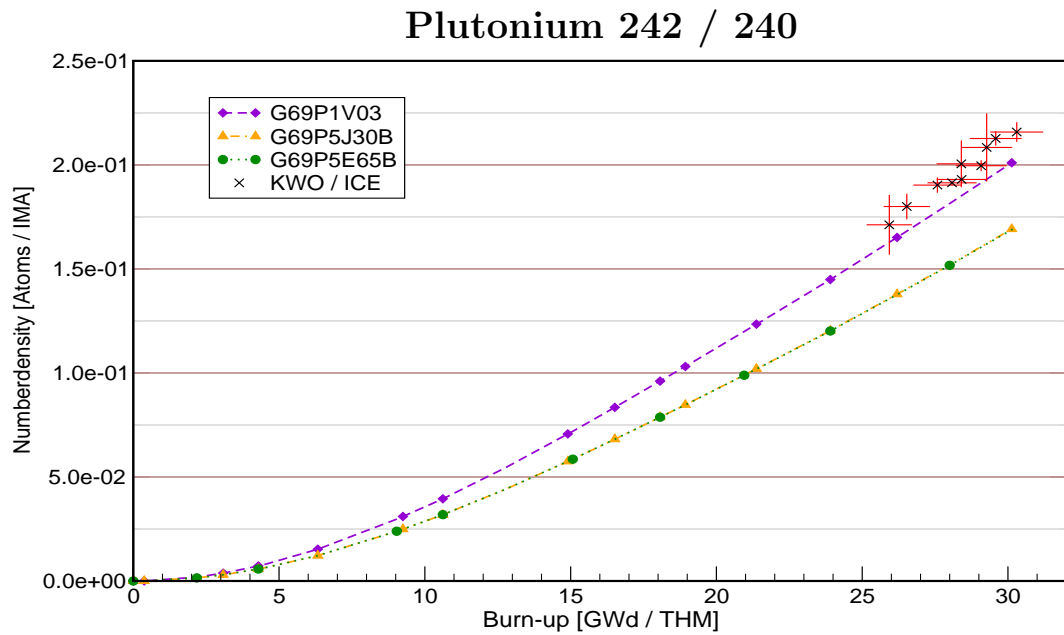


Figure A.21: Comparison of isotope ratio plotted against burn-up, KARBUS-calculations and KWO/ICE-Experiment for Pu^{242} to Pu^{240} ratio.

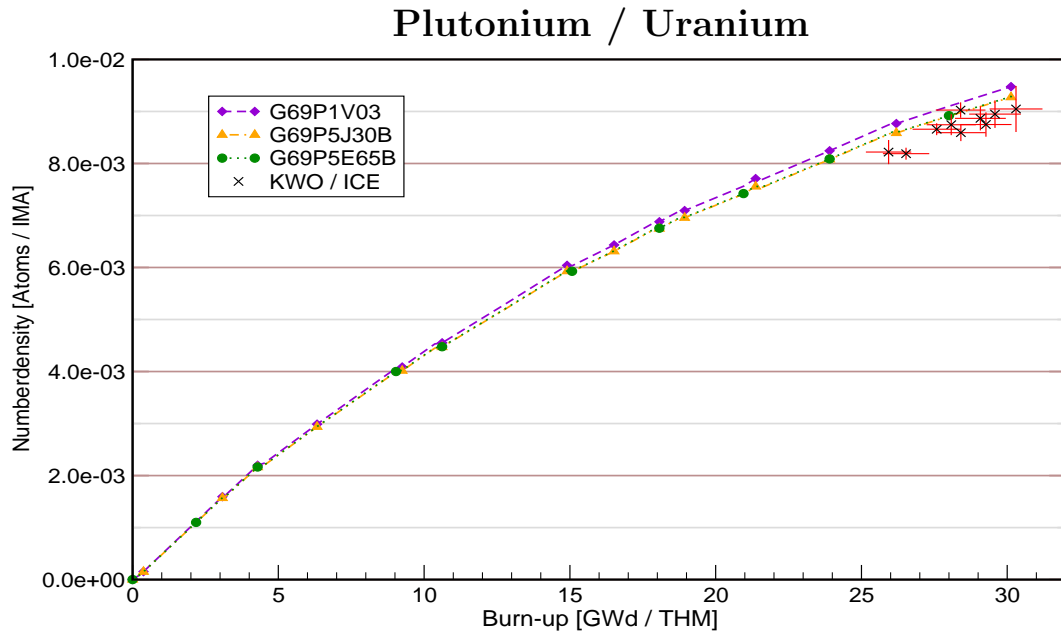


Figure A.22: Comparison of isotope ratio plotted against burn-up, KARBUS-calculations and KWO/ICE-Experiment for total contents Pu to U ratio.

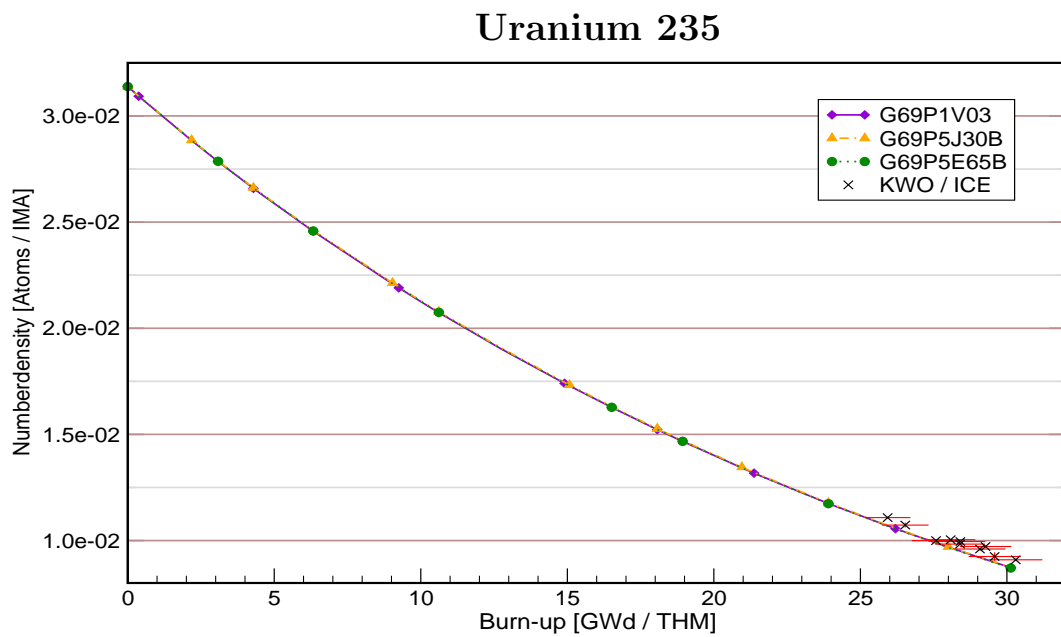


Figure A.23: Comparison of number densities plotted against burn-up, KARBUS-calculations and KWO/ICE-Experiment for U^{235} .

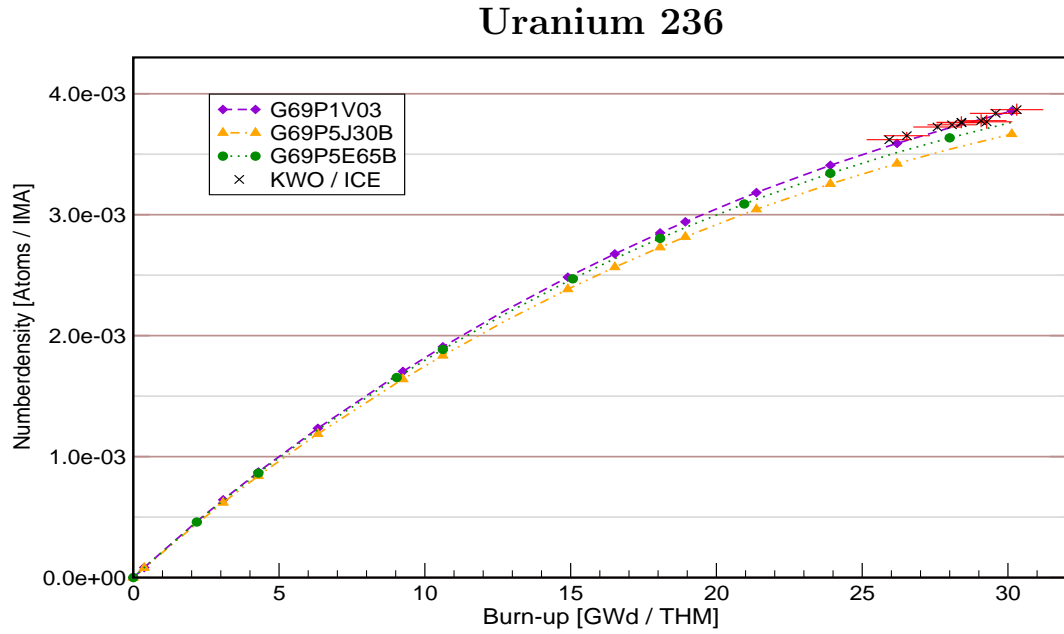


Figure A.24: Comparison of number densities plotted against burn-up, KARBUS-calculations and KWO/ICE-Experiment for U^{236} .

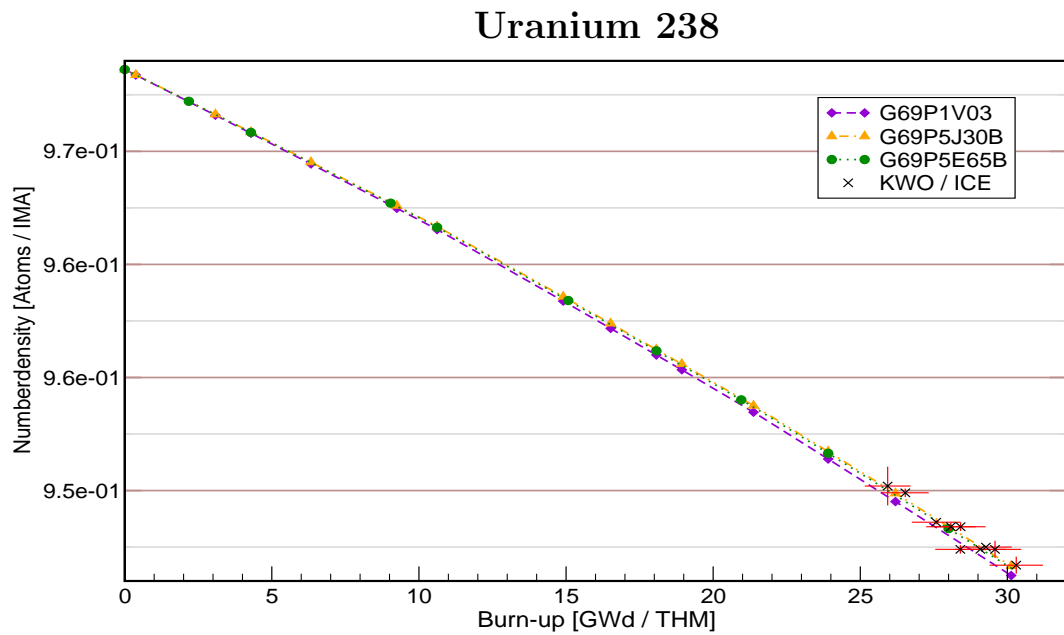


Figure A.25: Comparison of number densities plotted against burn-up, KARBUS-calculations and KWO/ICE-Experiment for U^{238} .

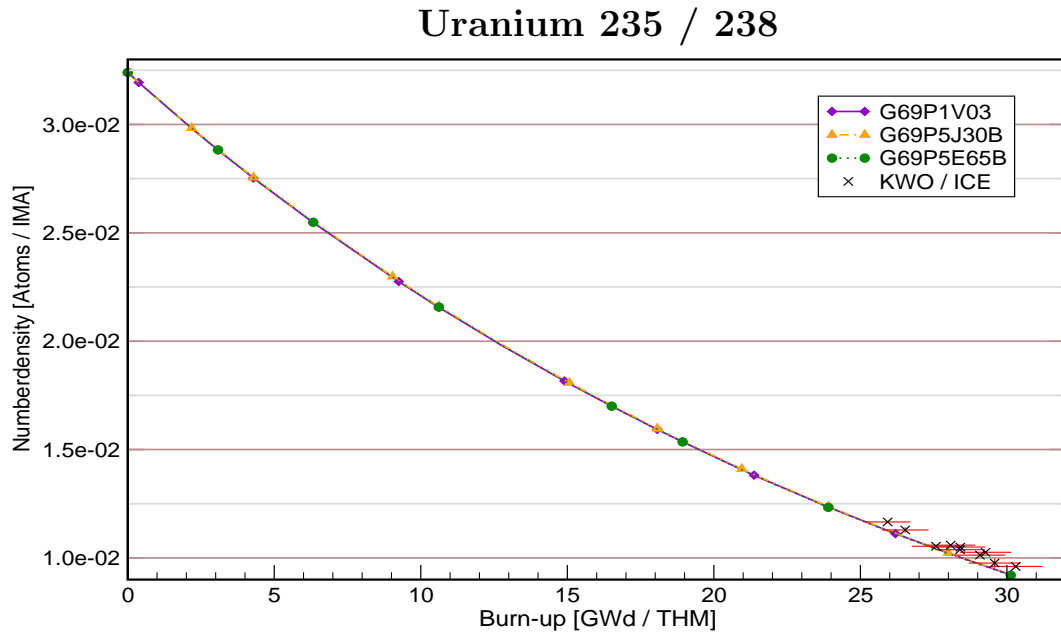


Figure A.26: Comparison of U^{235}/U^{238} isotope ratio plotted against burn-up, KARBUS-calculations and KWO/ICE-Experiment.

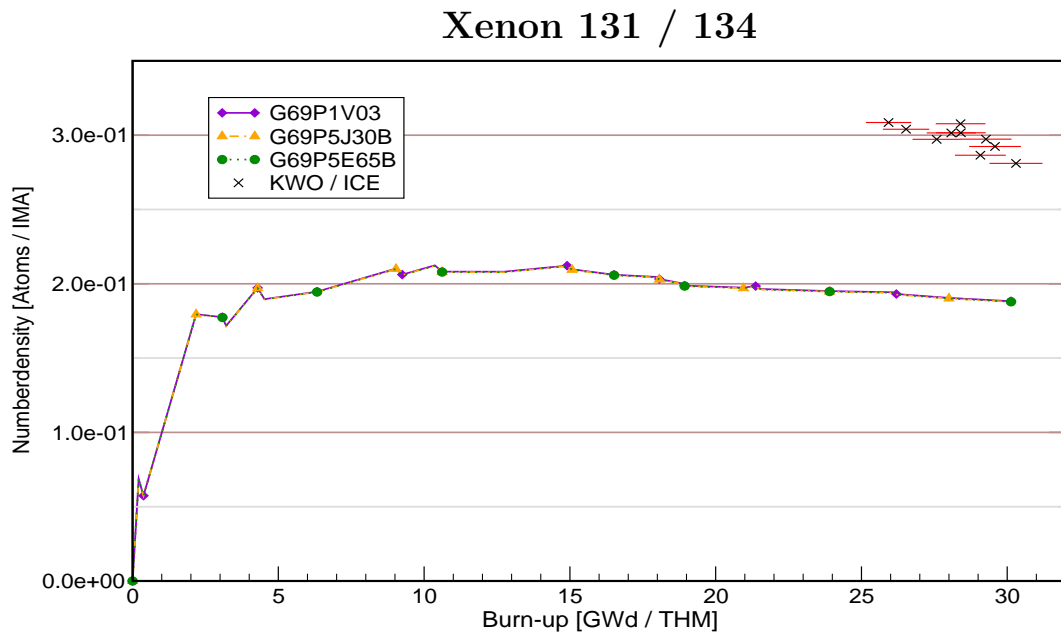


Figure A.27: Comparison of isotope ratio plotted against burn-up, KARBUS-calculations and KWO/ICE-Experiment for Xe^{131} to Xe^{134} ratio.

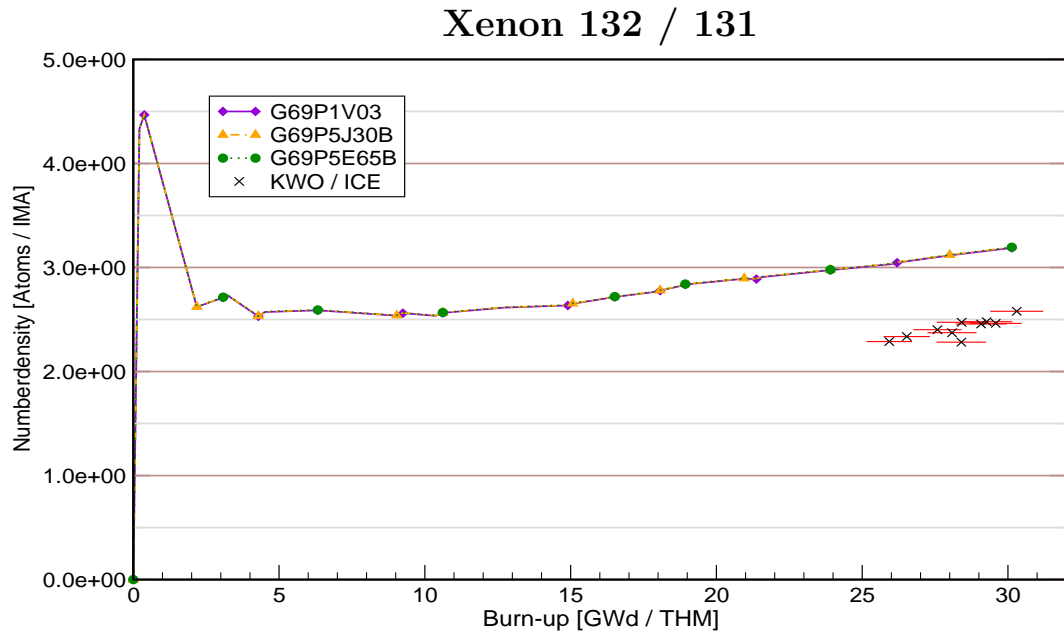


Figure A.28: Comparison of isotope ratio plotted against burn-up, KARBUS-calculations and KWO/ICE-Experiment for Xe^{132} to Xe^{131} ratio.

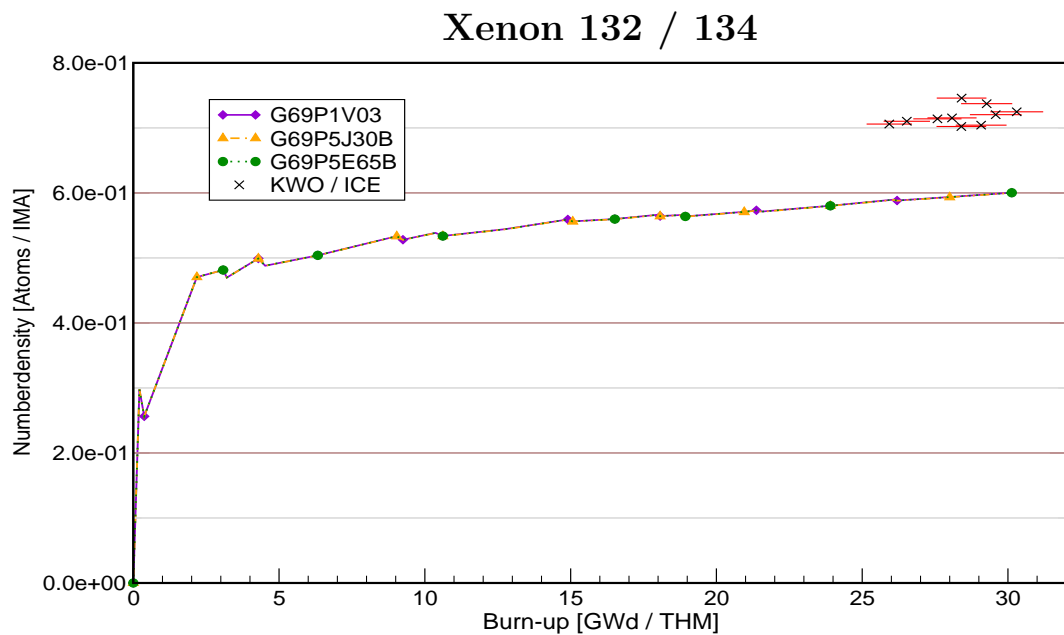


Figure A.29: Comparison of isotope ratio plotted against burn-up, KARBUS-calculations and KWO/ICE-Experiment for Xe^{132} to Xe^{134} ratio.

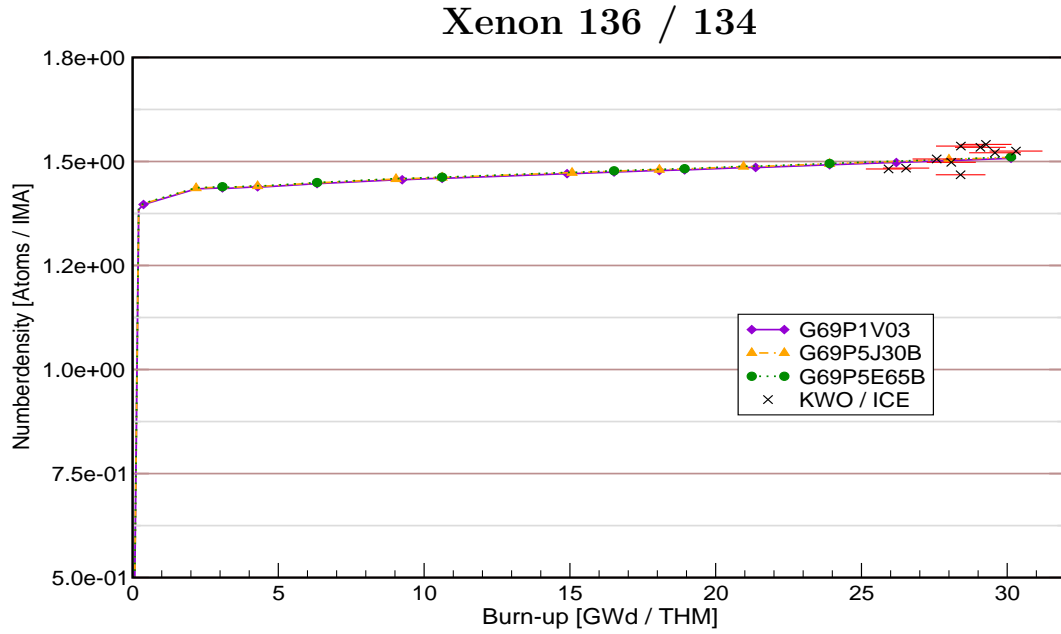


Figure A.30: Comparison of isotope ratio plotted against burn-up, KARBUS-calculations and KWO/ICE-Experiment for Xe^{136} to Xe^{134} ratio.

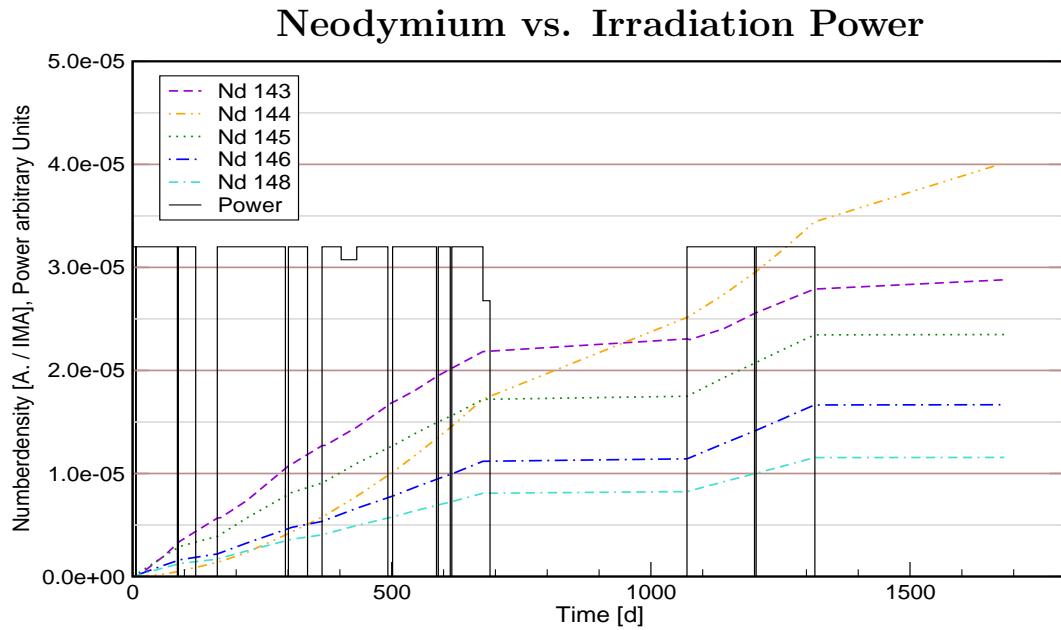


Figure A.31: *Nd* buildup in comparison with power history, *Nd* in Atoms per IMAs, power in arbitrary units. Maximum power 219.6 W/cm.

A.4 Additional ICE Charts, Calculations

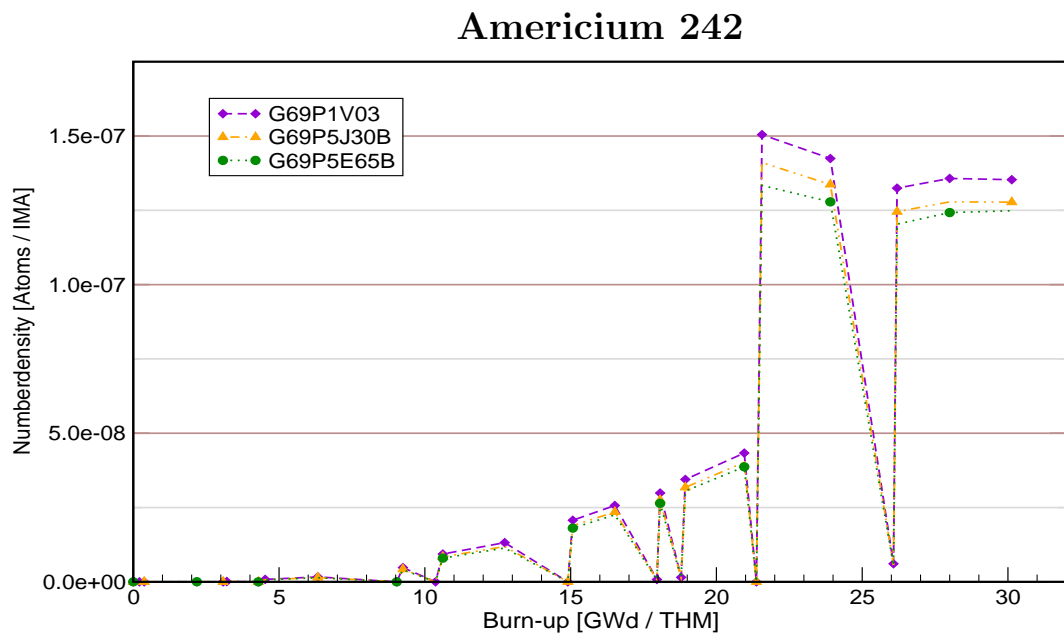


Figure A.32: Comparison of number densities plotted against burn-up, KARBUS-calculations for Am^{242} .

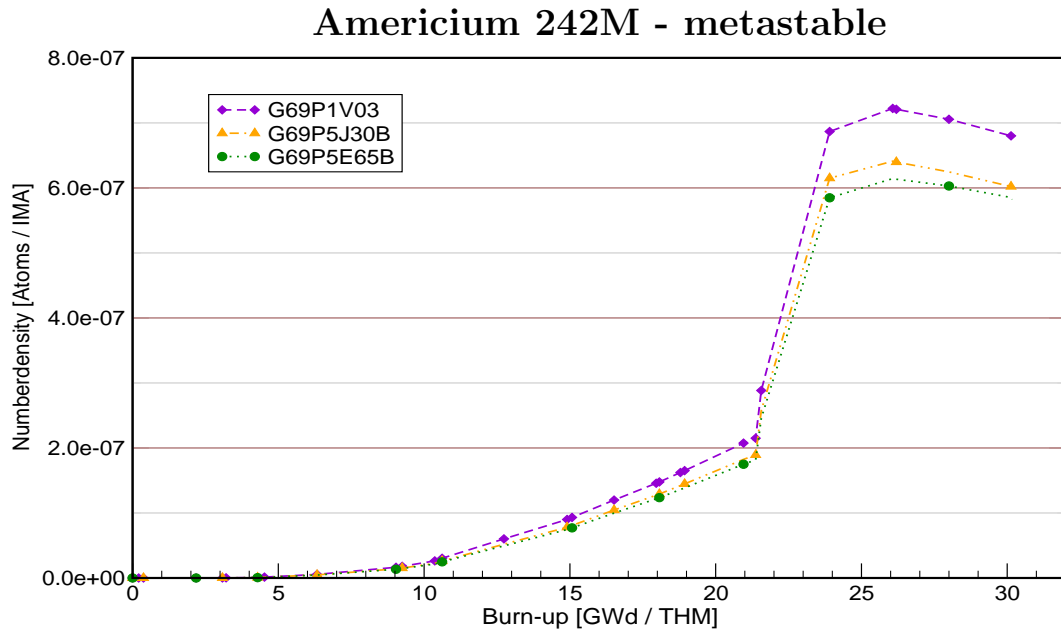


Figure A.33: Comparison of number densities plotted against burn-up, KARBUS-calculations for metastable Am^{242M} .

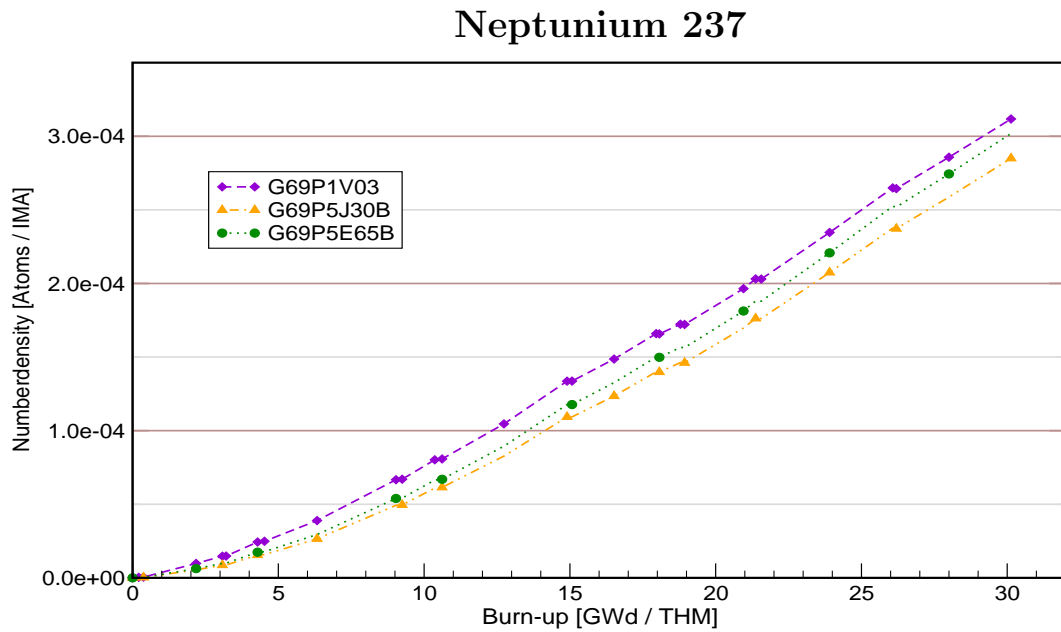


Figure A.34: Comparison of number densities plotted against burn-up, KARBUS-calculations for Np^{237} .

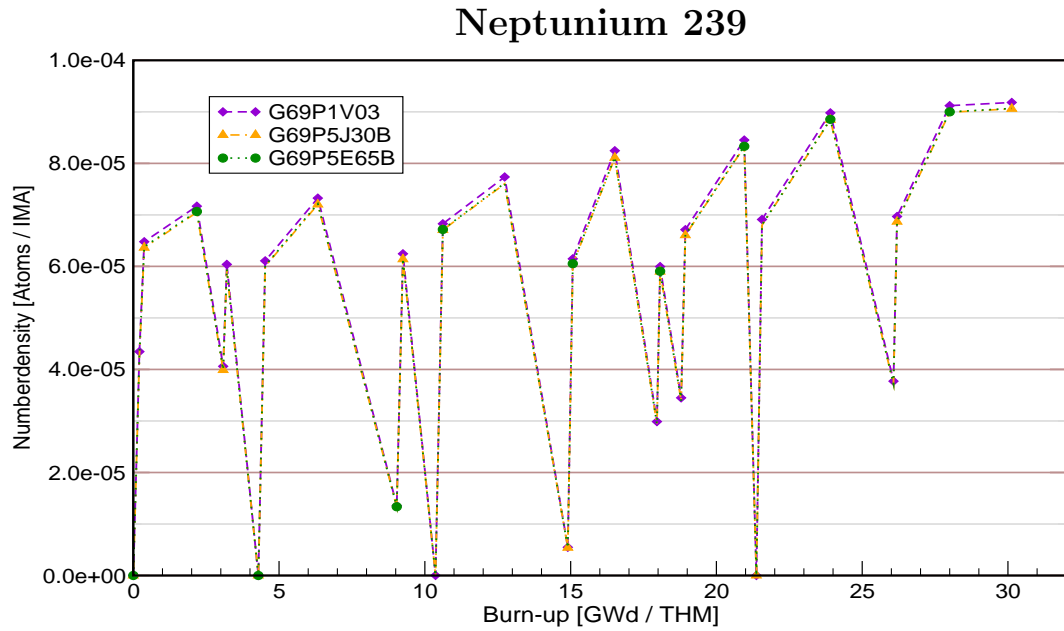


Figure A.35: Comparison of number densities plotted against burn-up, KARBUS-calculations for Np^{239} .

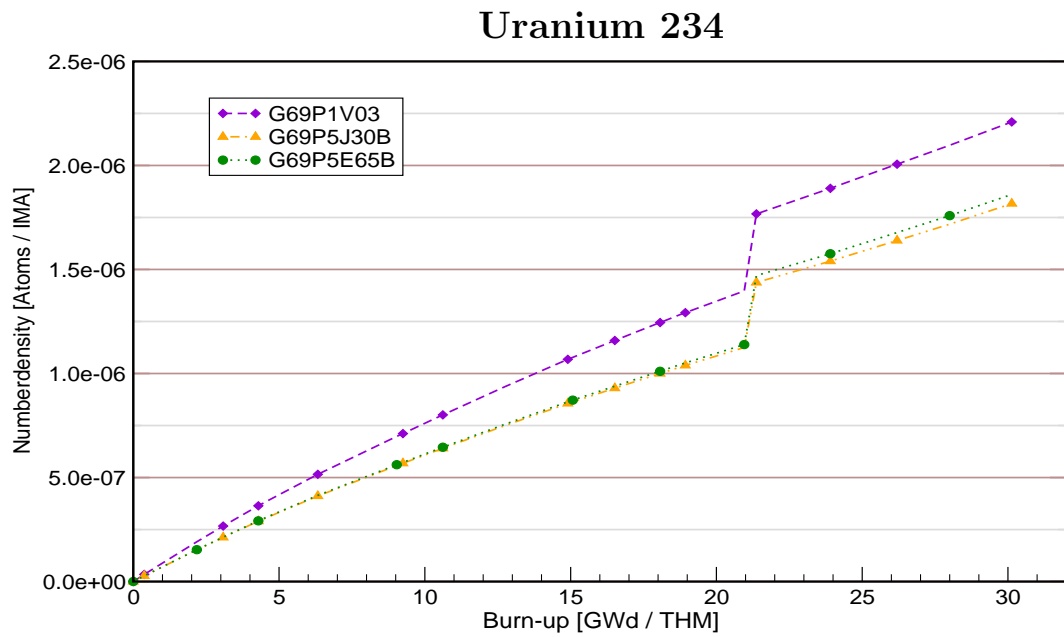


Figure A.36: Comparison of number densities plotted against burn-up, KARBUS-calculations for U^{234} .

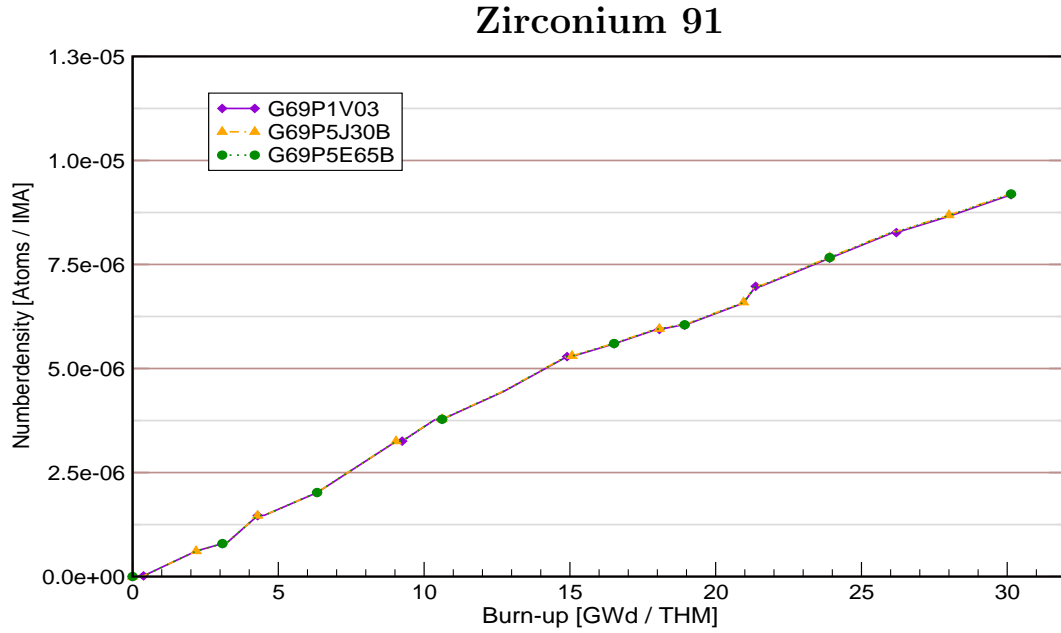


Figure A.37: Comparison of number densities plotted against burn-up, KARBUS-calculations for Zr^{91} .

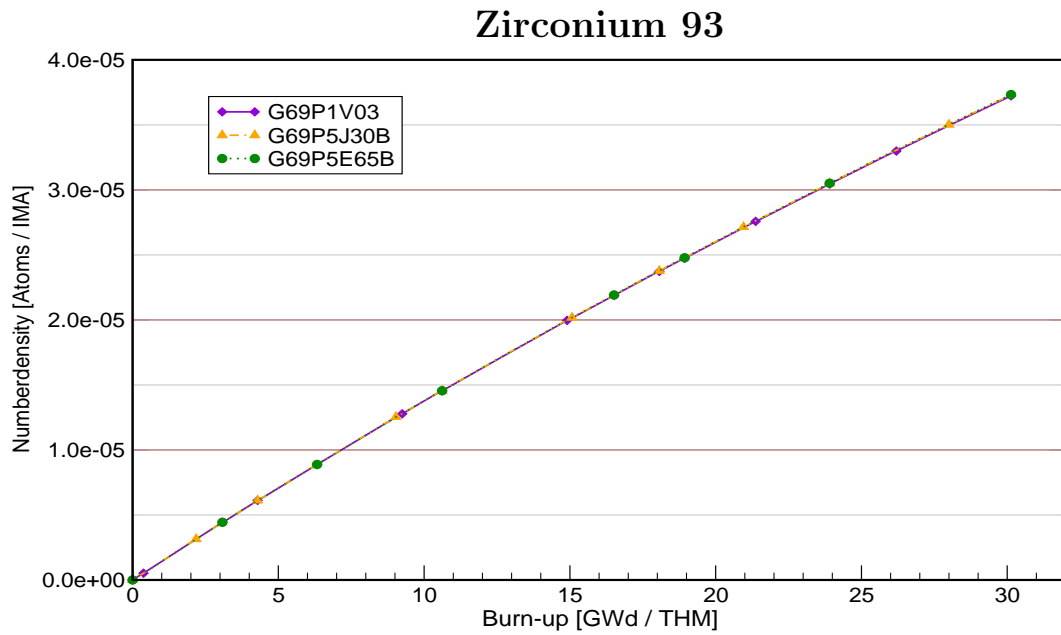


Figure A.38: Comparison of number densities plotted against burn-up, KARBUS-calculations for Zr^{93} .

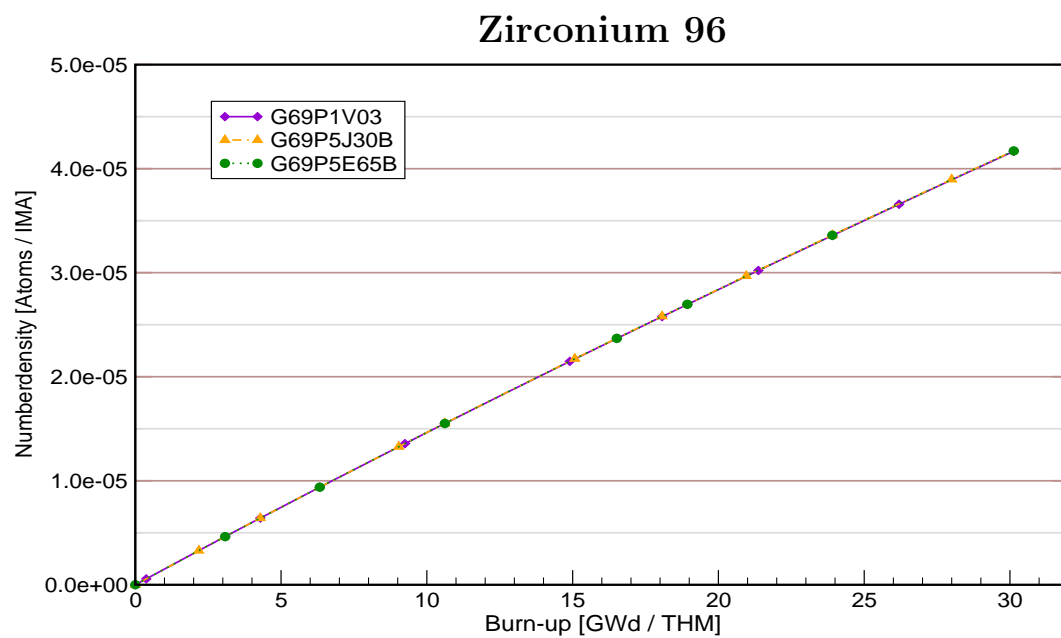


Figure A.39: Comparison of number densities plotted against burn-up, KARBUS-calculations for Zr^{96} .

Appendix B

Appendix of Chapter No.5

B.1 LWR High Burn-ups, Charts for Constant Boron Concentration

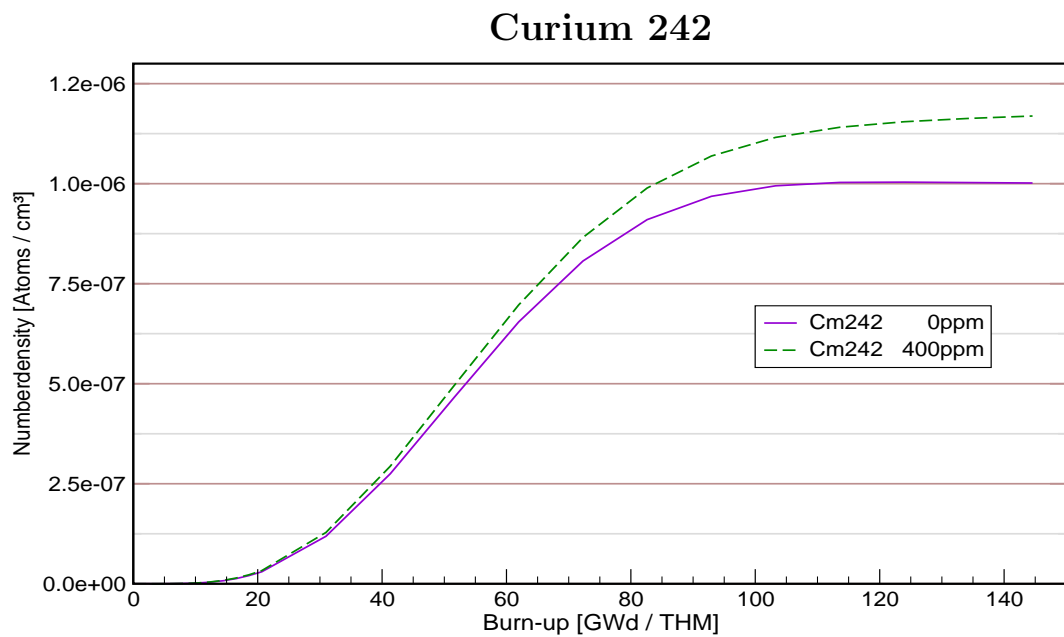


Figure B.1: Influence of constant soluble boron concentrations on Cm^{242} , curves plotted for two different concentrations.

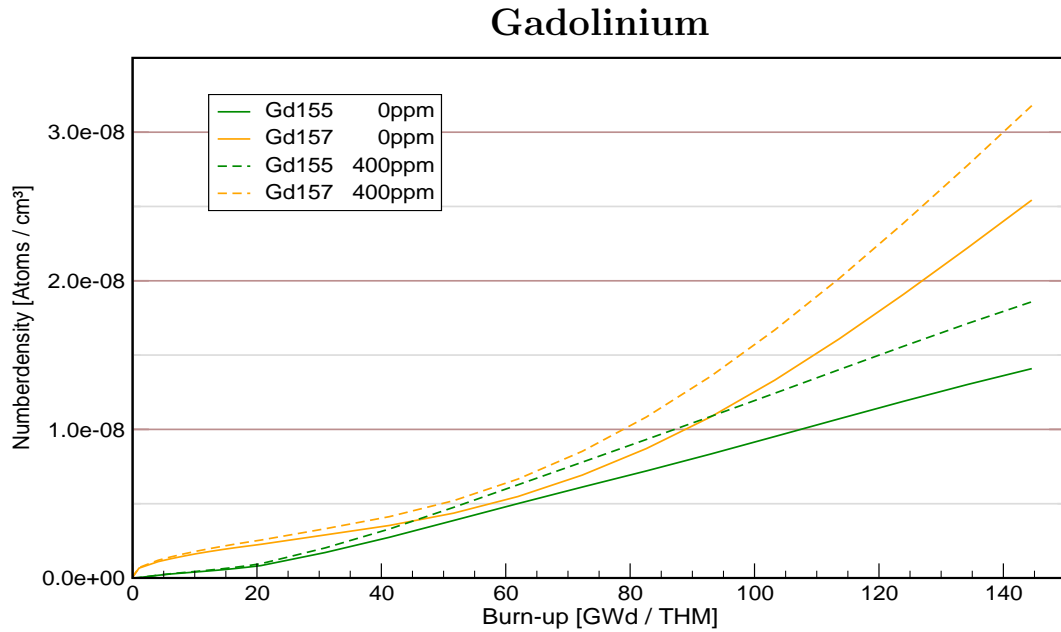


Figure B.2: Influence of constant soluble boron concentrations on Gd^{155} and Gd^{157} , curves plotted for two different concentrations.

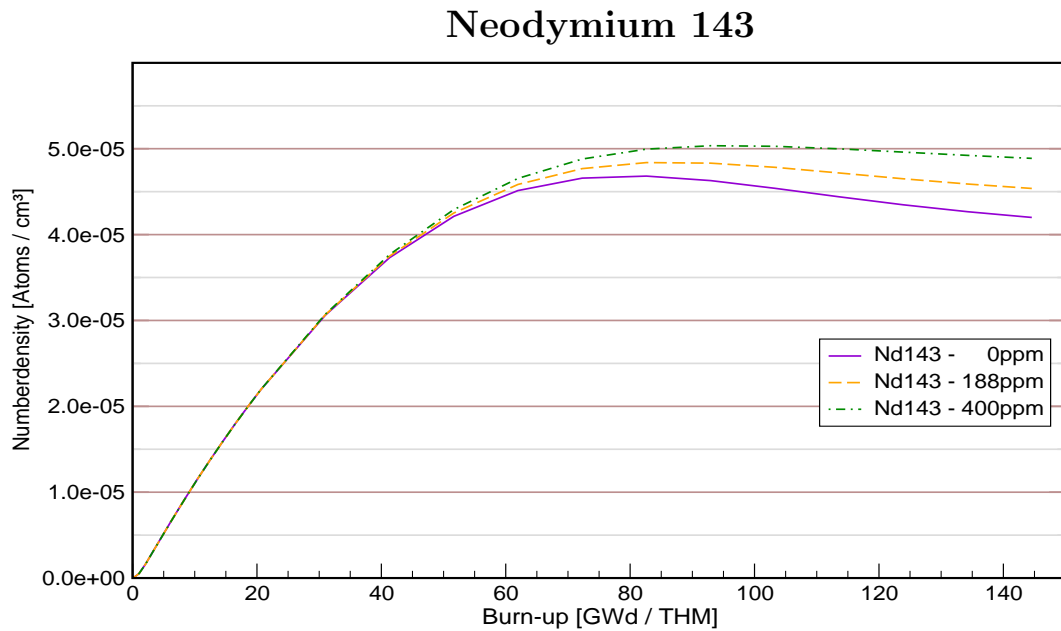


Figure B.3: Influence of constant soluble boron concentrations on Nd^{143} , curves plotted for three different concentrations.

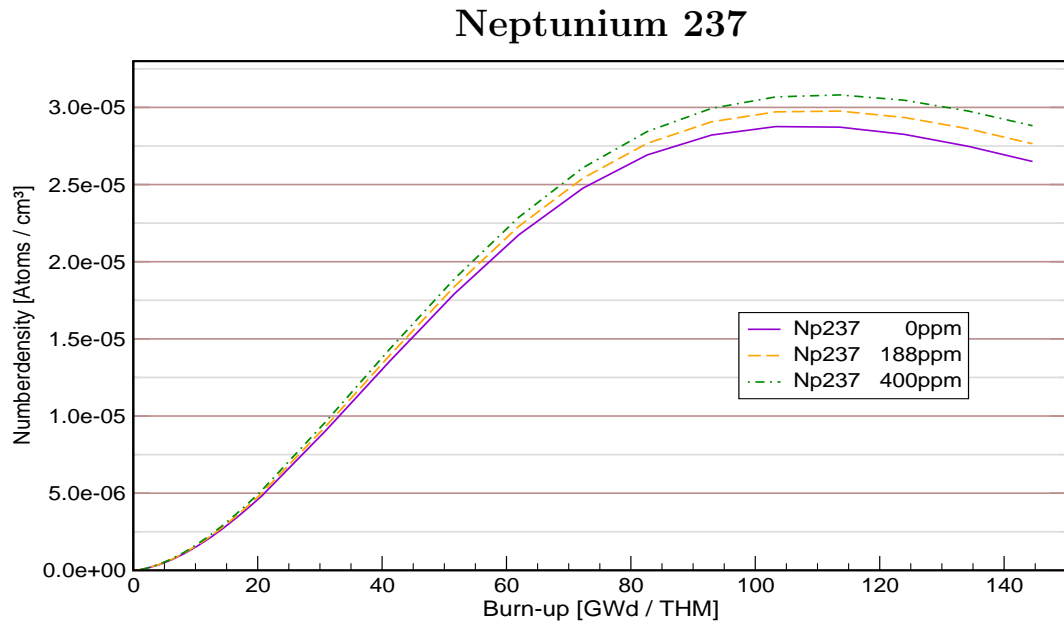


Figure B.4: Influence of constant soluble boron concentrations on Np^{237} , curves plotted for three different concentrations.

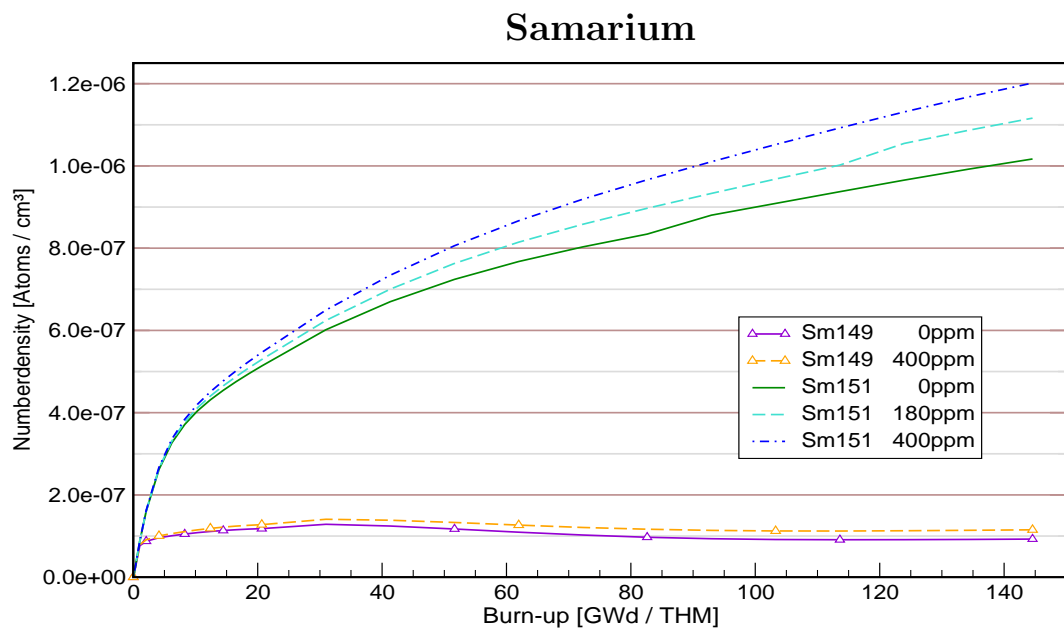


Figure B.5: Influence of constant soluble boron concentrations on Sm^{149} and Sm^{151} , curves plotted for different concentrations.

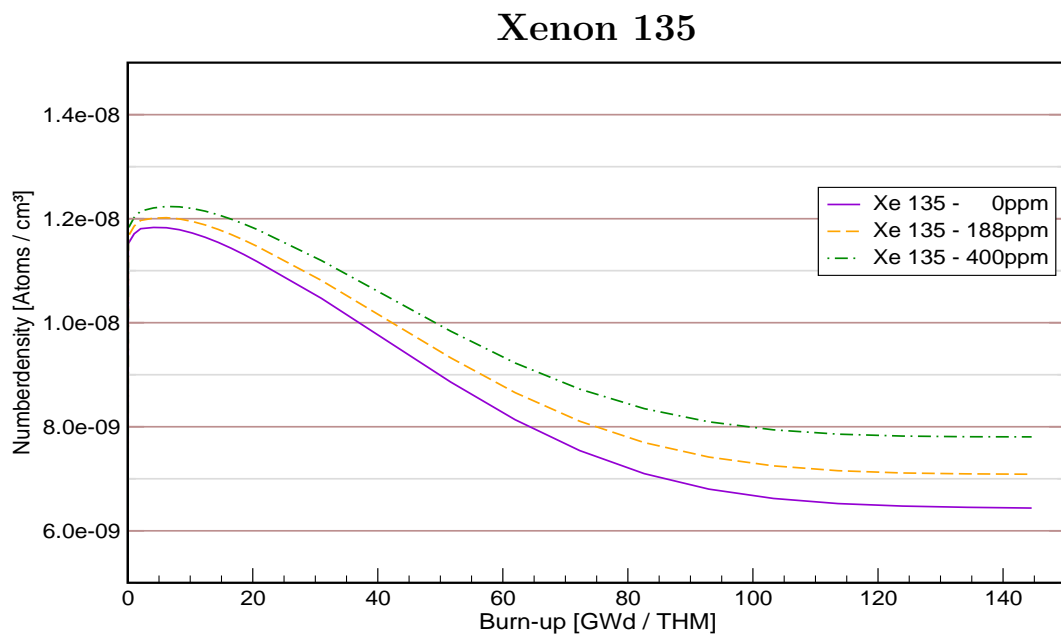


Figure B.6: Influence of constant soluble boron concentrations on Xe^{135} , curves plotted for three different concentrations.

B.2 LWR comparison of variable and constant 188 / 80 ppm boron modeling

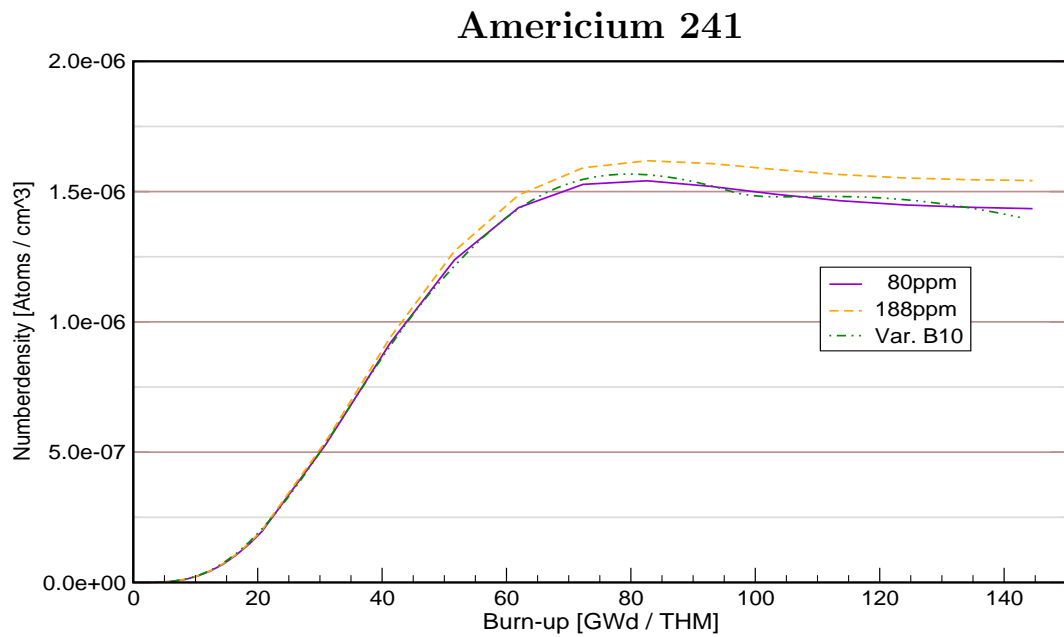


Figure B.7: Am^{241} : The chart shows curves for variable boron modeling (376...0 ppm) and constant concentrations, V_m/V_s : 1.283 .

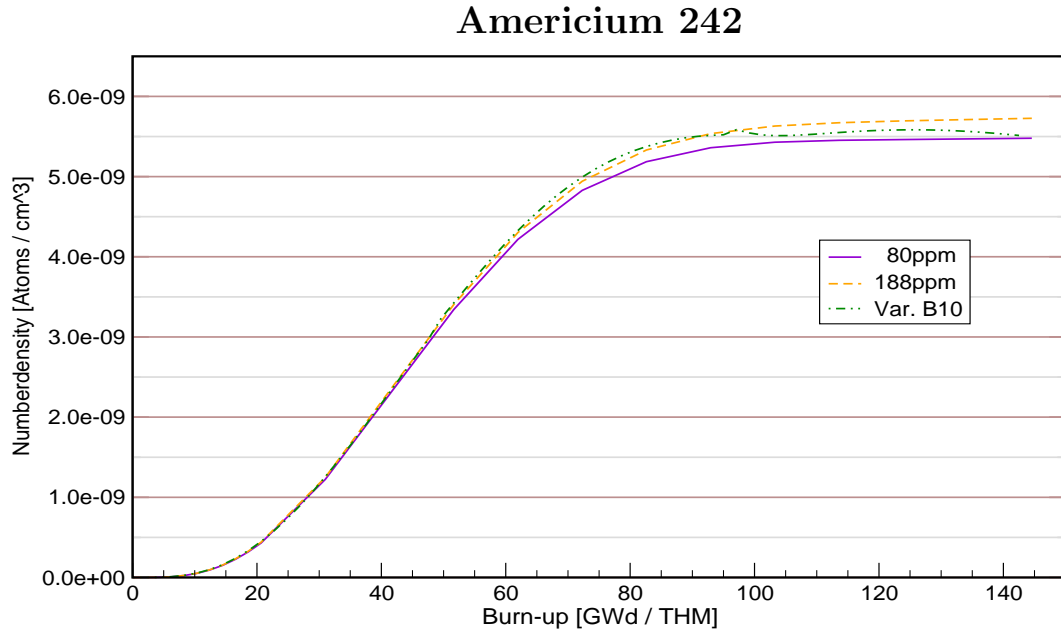


Figure B.8: Am^{242} : The chart shows curves for variable boron modeling (376...0 ppm) and constant concentrations, V_m/V_s : 1.283 .

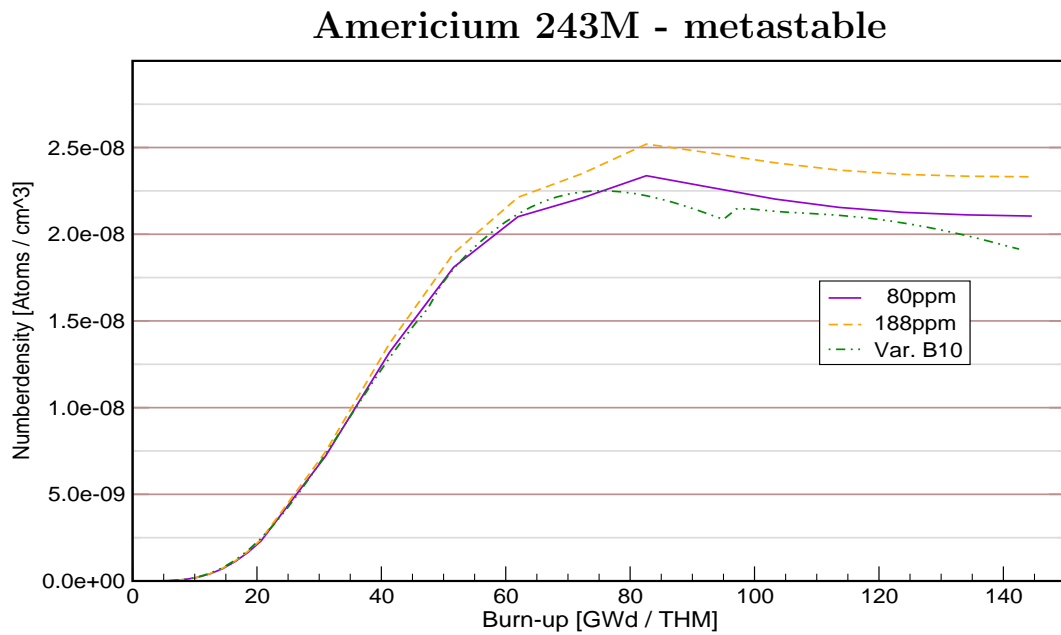


Figure B.9: Am^{243M} : The chart shows curves for variable boron modeling (376...0 ppm) and constant concentrations, V_m/V_s : 1.283 .

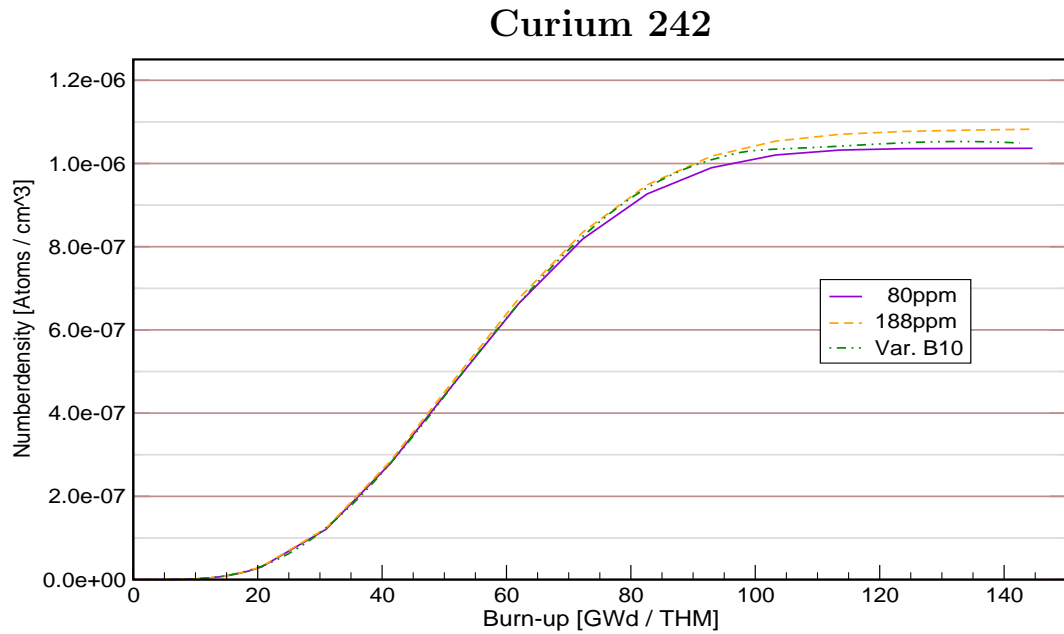


Figure B.10: Cm^{242} : The chart shows curves for variable boron modeling (376...0 ppm) and constant concentrations, V_m/V_s : 1.283 .

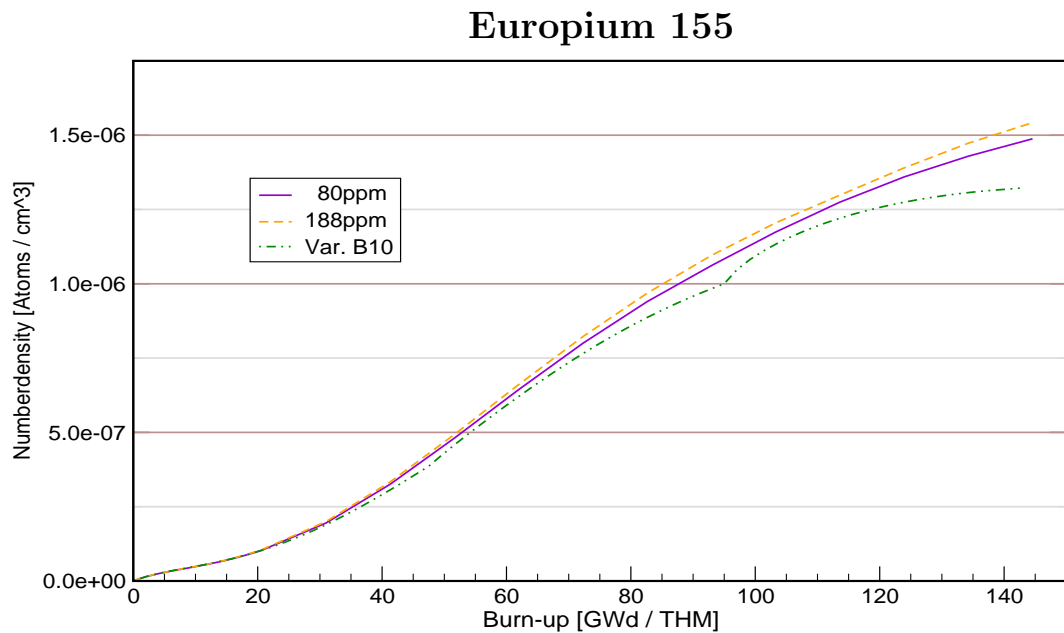


Figure B.11: Eu^{155} : The chart shows curves for variable boron modeling (376...0 ppm) and constant concentrations, V_m/V_s : 1.283 .

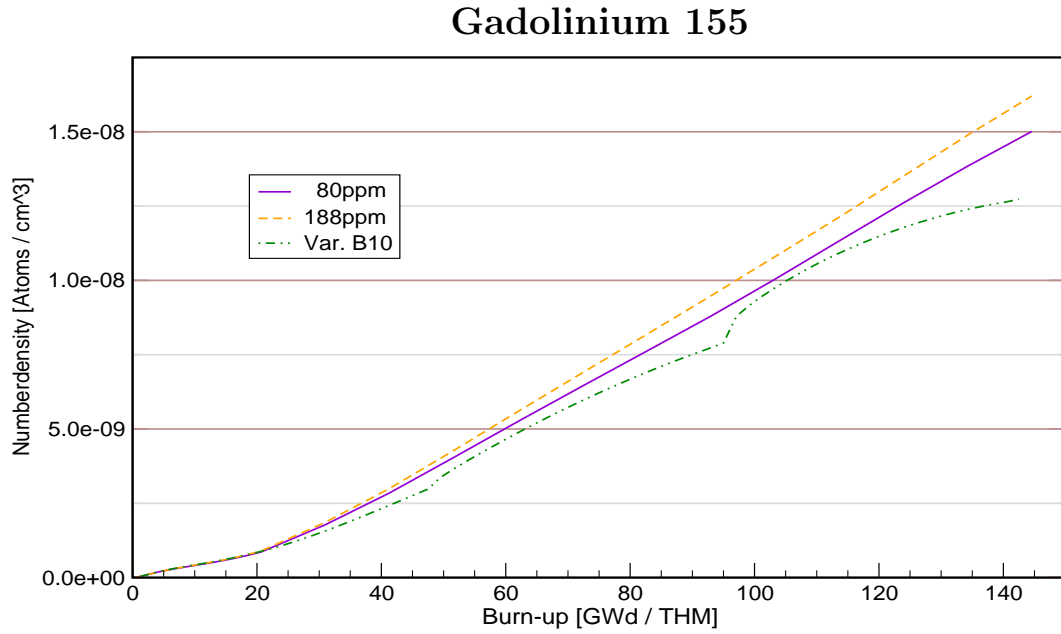


Figure B.12: Gd^{155} : The chart shows curves for variable boron modeling (376...0 ppm) and constant concentrations, V_m/V_s : 1.283 .

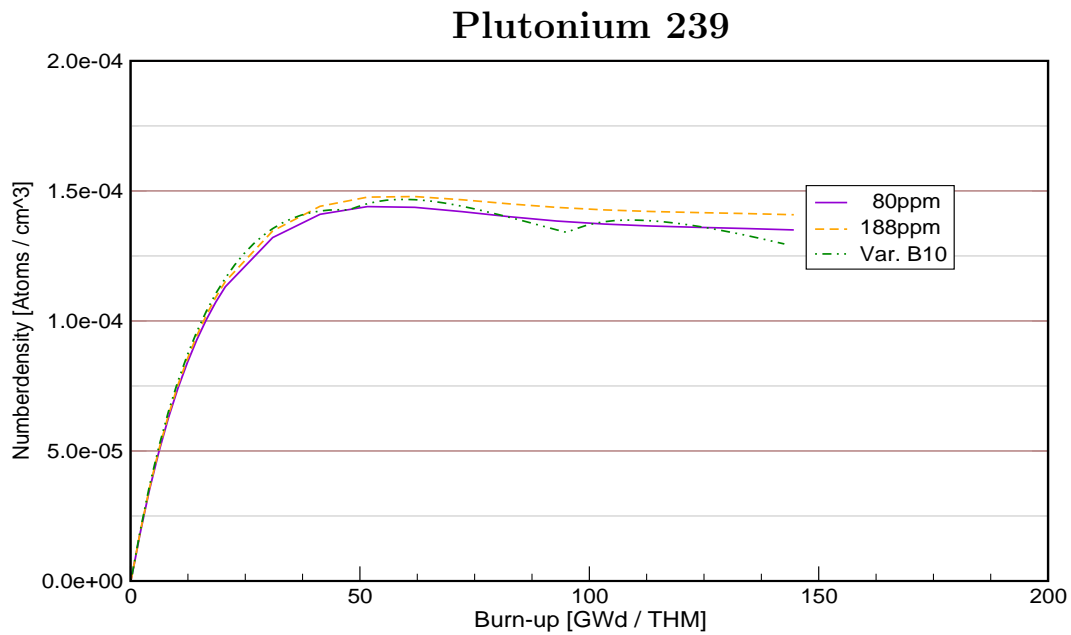


Figure B.13: Pu^{239} : The chart shows curves for variable boron modeling (376...0 ppm) and constant concentrations, V_m/V_s : 1.283 .

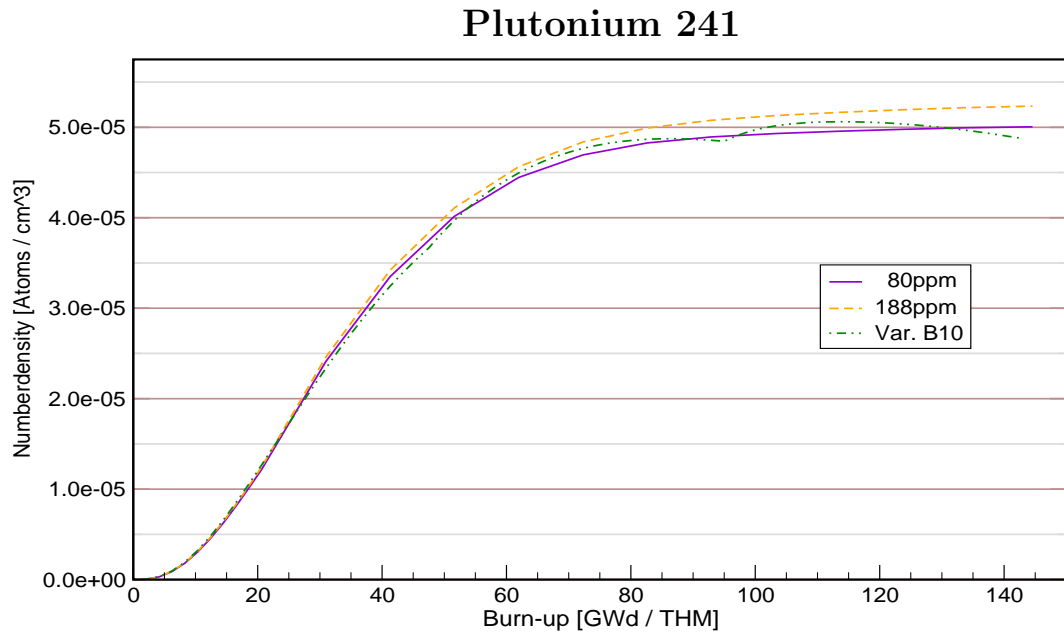


Figure B.14: Pu^{241} : The chart shows curves for variable boron modeling (376...0 ppm) and constant concentrations, V_m/V_s : 1.283 .

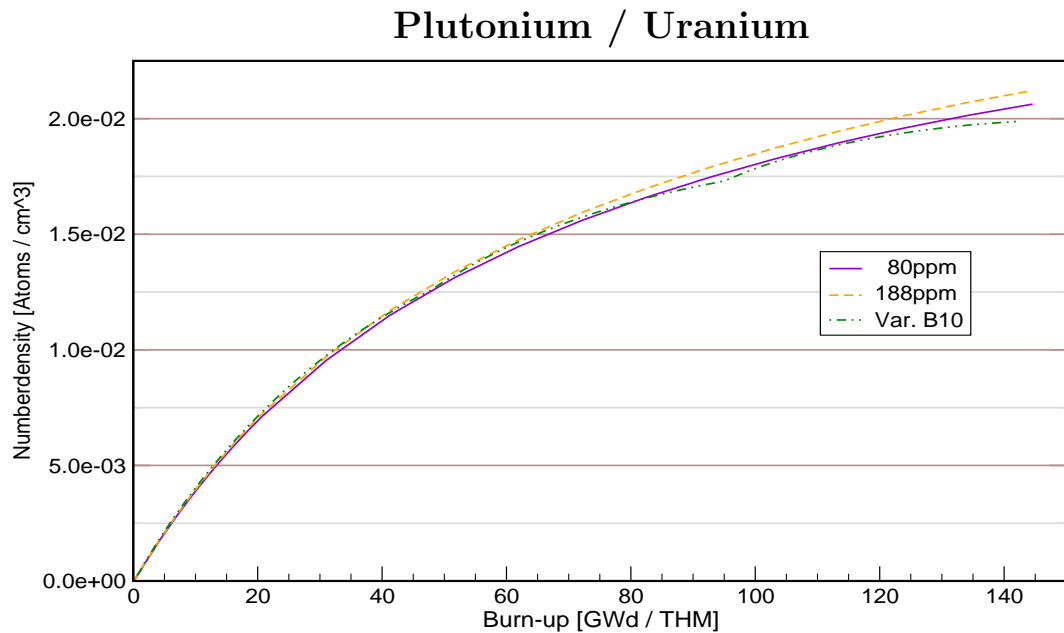


Figure B.15: Plutonium/Uranium ratio, the chart shows curves for variable boron modeling (376...0 ppm) and constant concentrations, V_m/V_s : 1.283 .

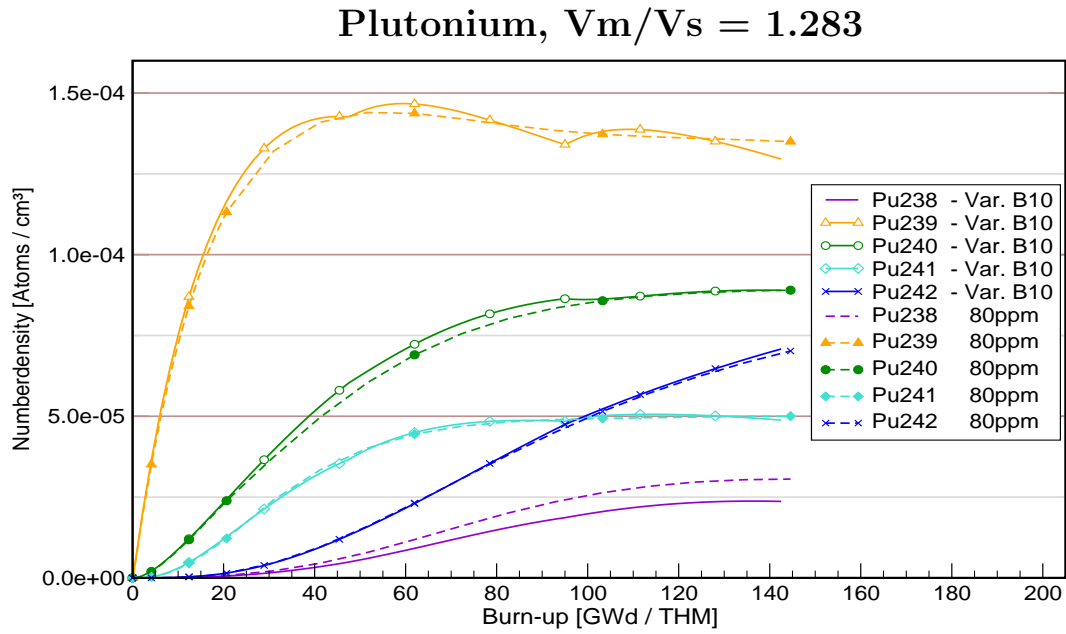


Figure B.16: Plutonium: the chart shows curves for variable boron modeling (376...0 ppm) and constant concentrations.

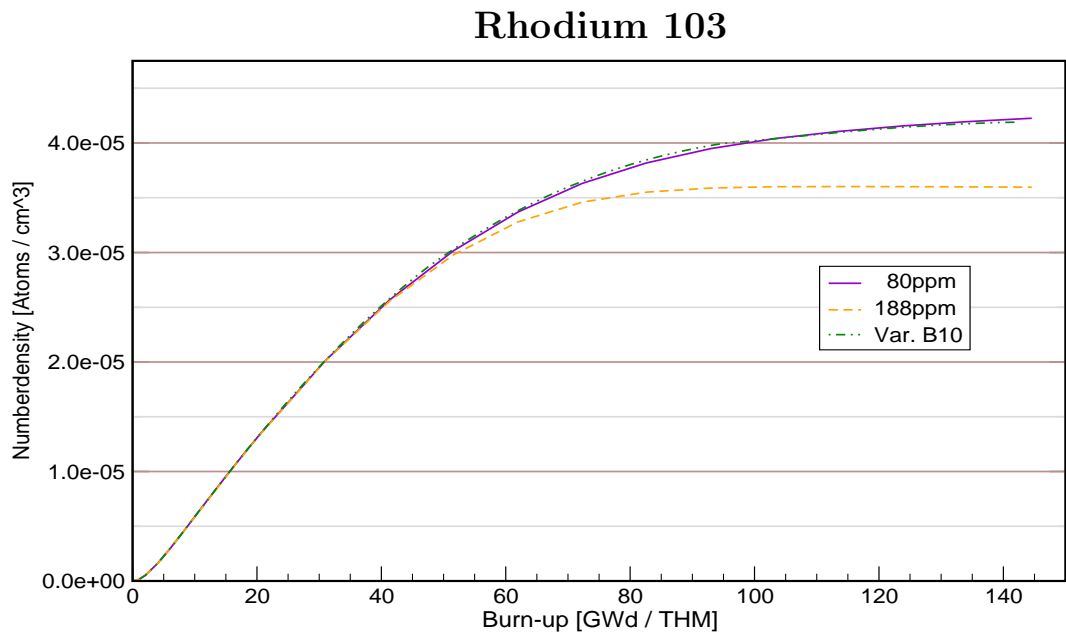


Figure B.17: Rh^{103} : The chart shows curves for variable boron modeling (376...0 ppm) and constant concentrations, $V_m/V_s: 1.283$.

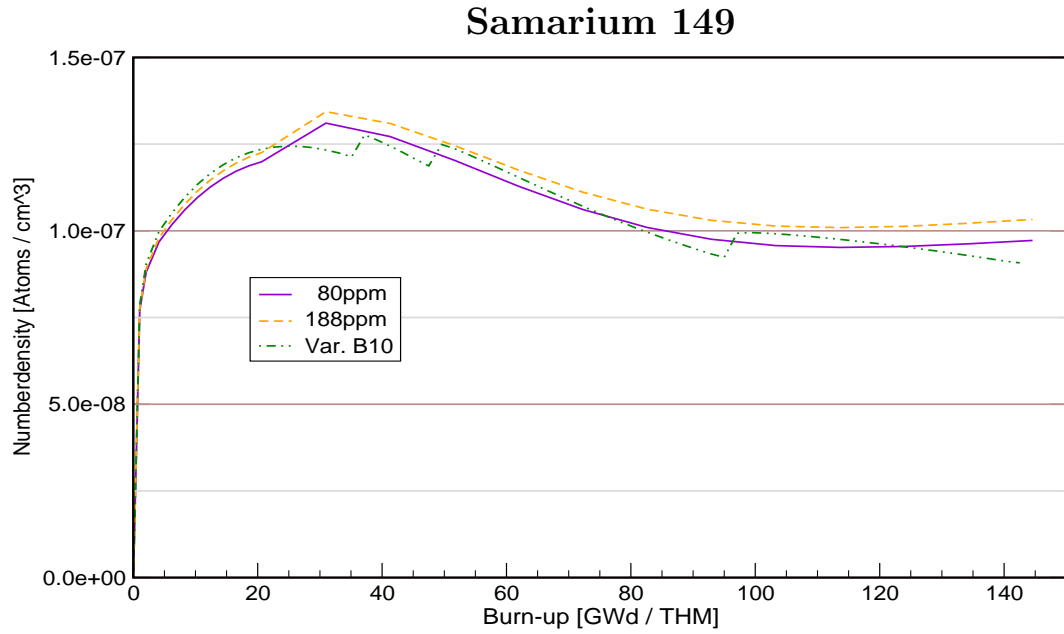


Figure B.18: Sm^{149} : The chart shows curves for variable boron modeling (376...0 ppm) and constant concentrations, V_m/V_s : 1.283 .

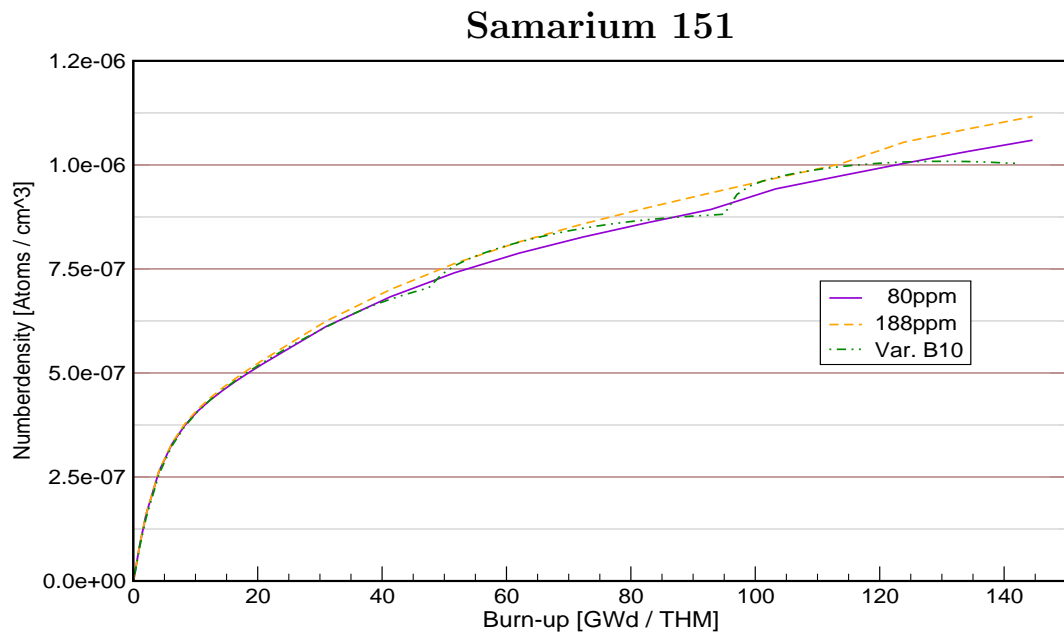


Figure B.19: Sm^{151} : The chart shows curves for variable boron modeling (376...0 ppm) and constant concentrations, V_m/V_s : 1.283 .

B.3 LWR comparison of variable and constant 188 / 80 ppm boron modeling, minor correlation

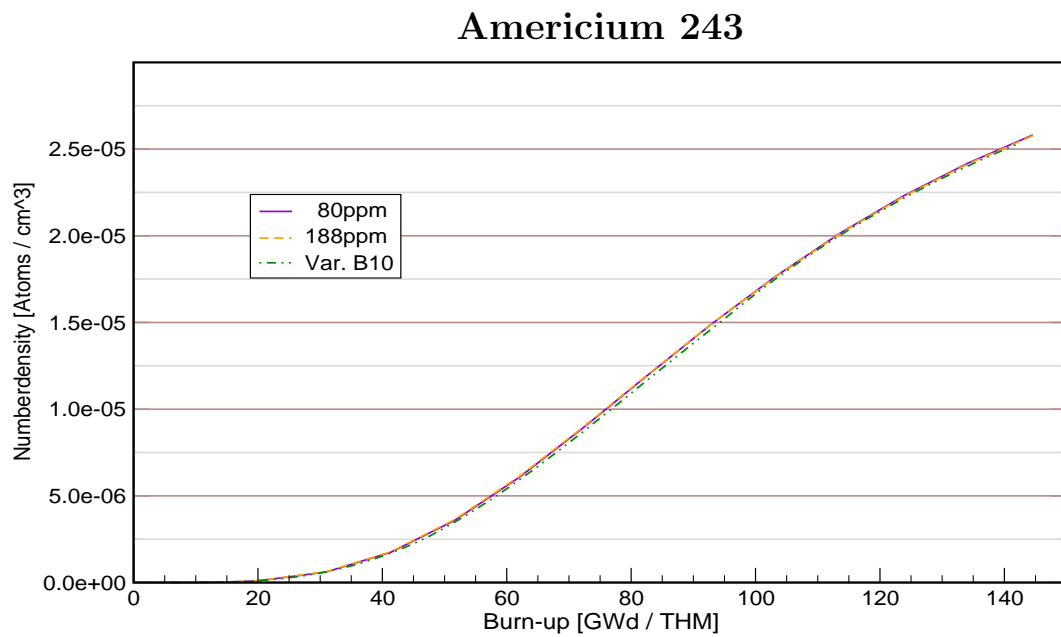


Figure B.20: Am^{243} : The chart shows curves for variable boron modeling (376...0 ppm) and constant concentrations, V_m/V_s : 1.283 .

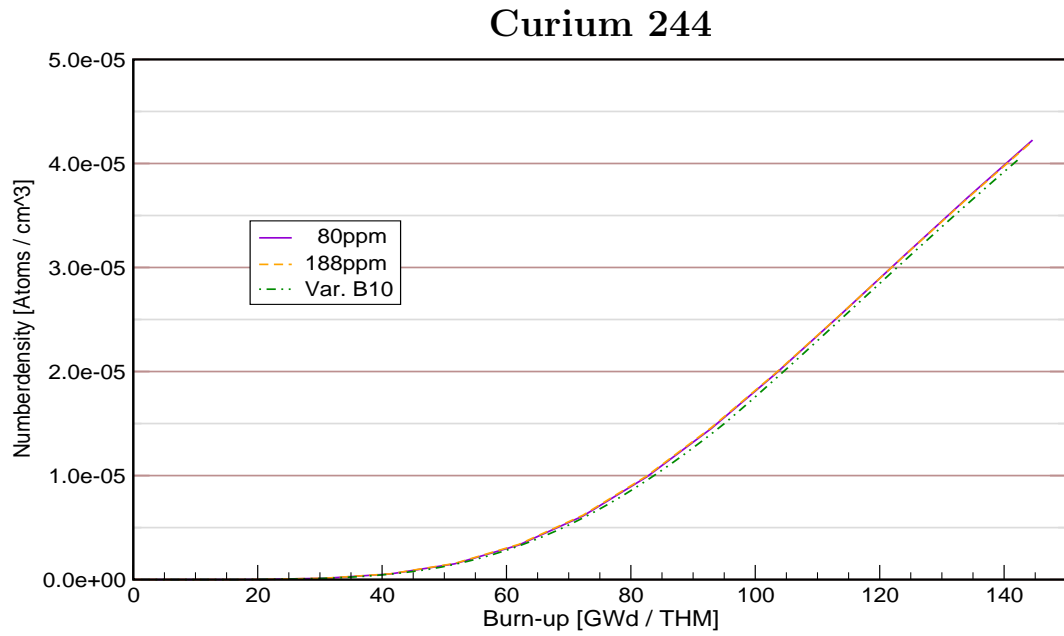


Figure B.21: Cm^{244} : The chart shows curves for variable boron modeling (376...0 ppm) and constant concentrations, V_m/V_s : 1.283 .

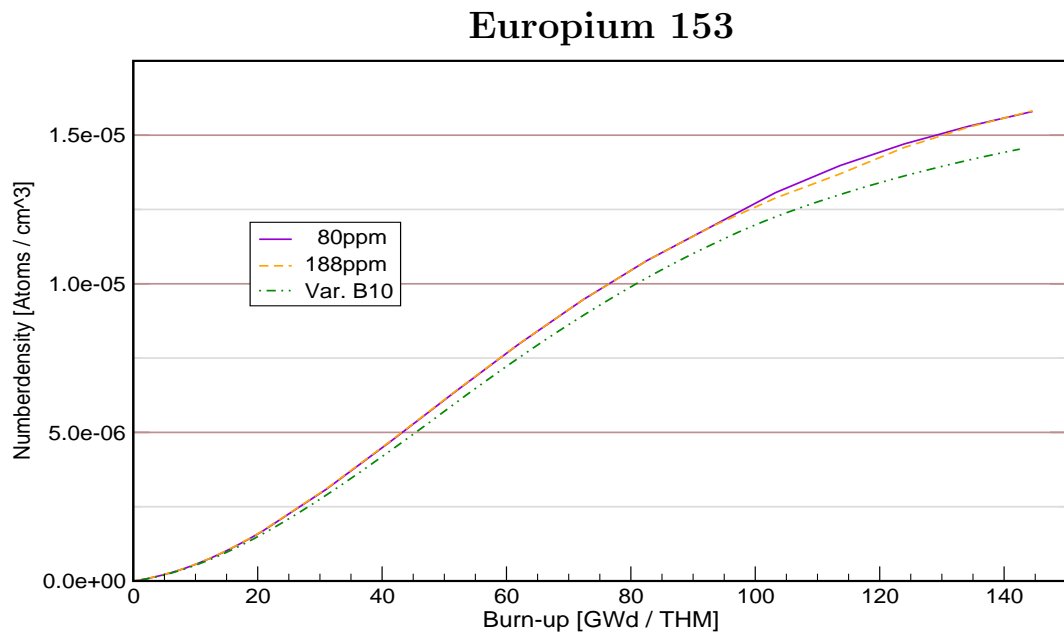


Figure B.22: Eu^{153} : The chart shows curves for variable boron modeling (376...0 ppm) and constant concentrations, V_m/V_s : 1.283 .

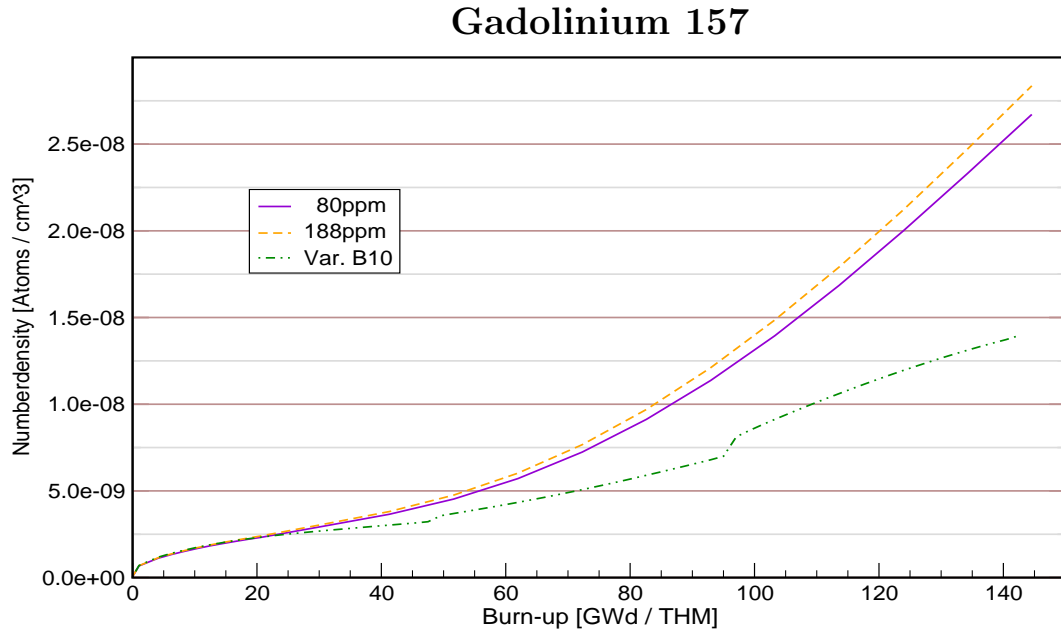


Figure B.23: Gd^{157} : The chart shows curves for variable boron modeling (376...0 ppm) and constant concentrations, V_m/V_s : 1.283 .

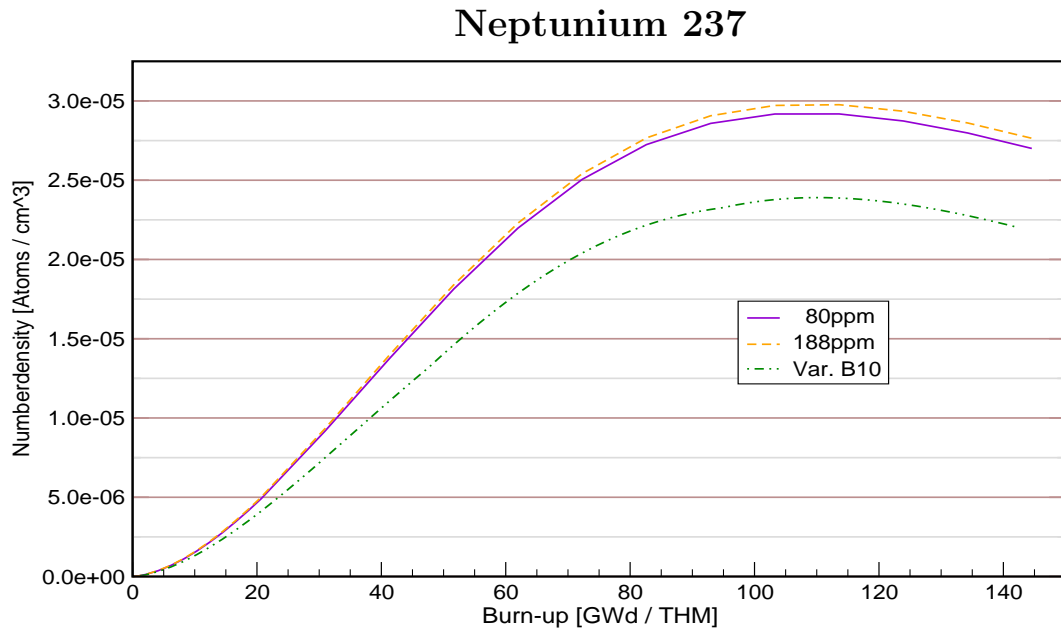


Figure B.24: Np^{237} : The chart shows curves for variable boron modeling (376...0 ppm) and constant concentrations, V_m/V_s : 1.283 .

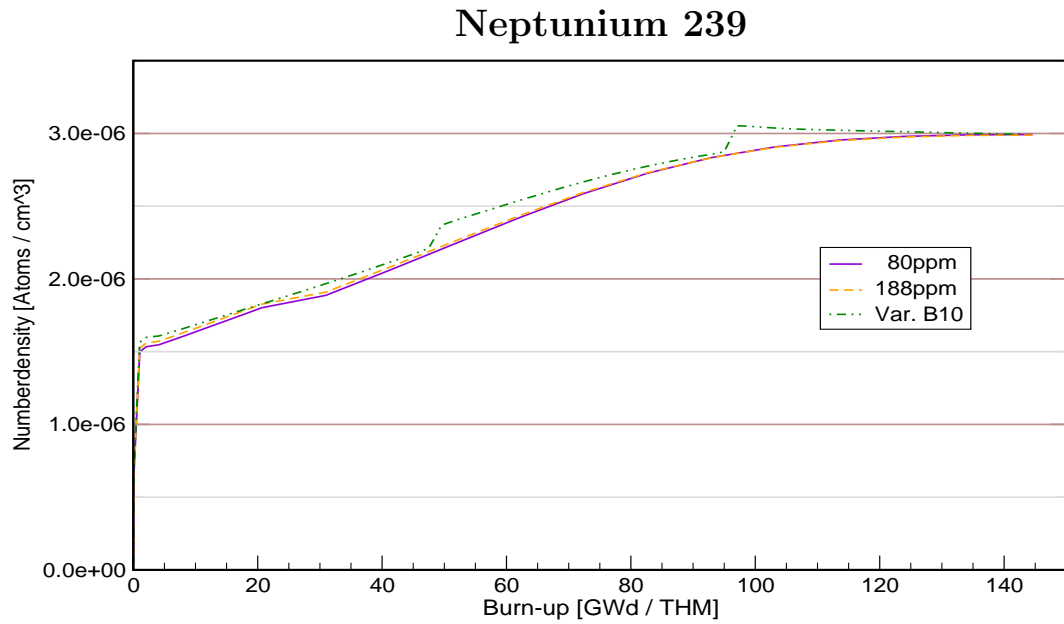


Figure B.25: Np^{239} : The chart shows curves for variable boron modeling (376...0 ppm) and constant concentrations, V_m/V_s : 1.283 .

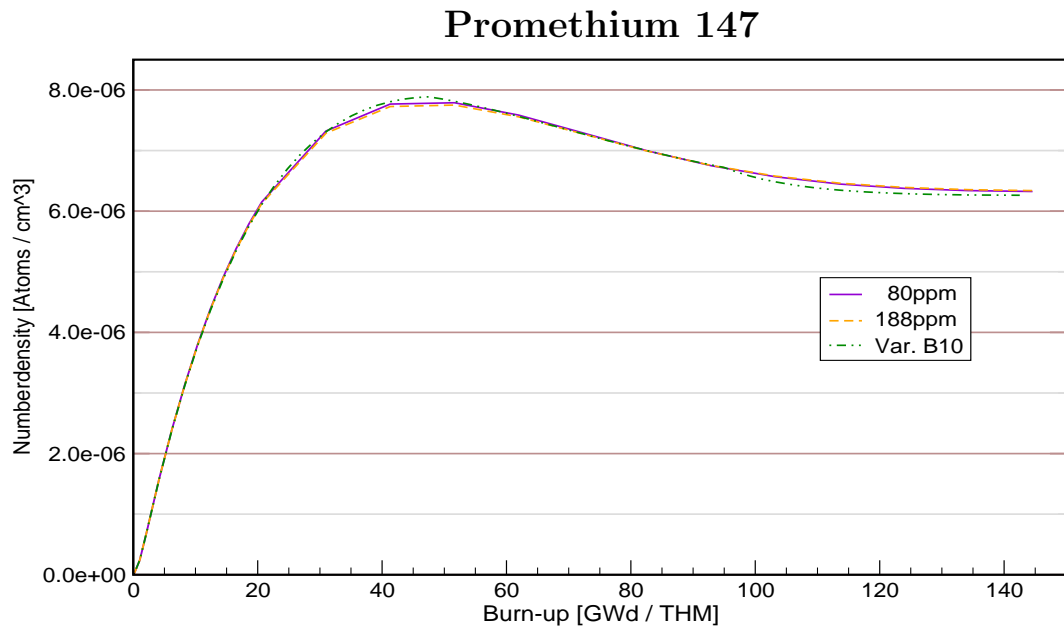


Figure B.26: Pm^{147} : The chart shows curves for variable boron modeling (376...0 ppm) and constant concentrations, V_m/V_s : 1.283 .

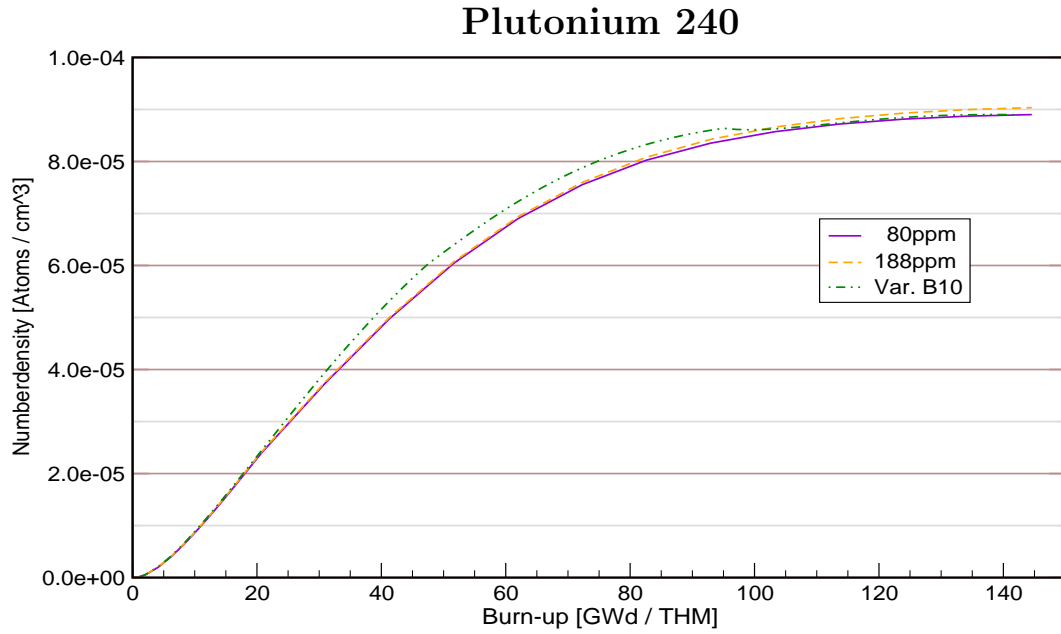


Figure B.27: Pu^{240} : The chart shows curves for variable boron modeling (376...0 ppm) and constant concentrations, V_m/V_s : 1.283 .

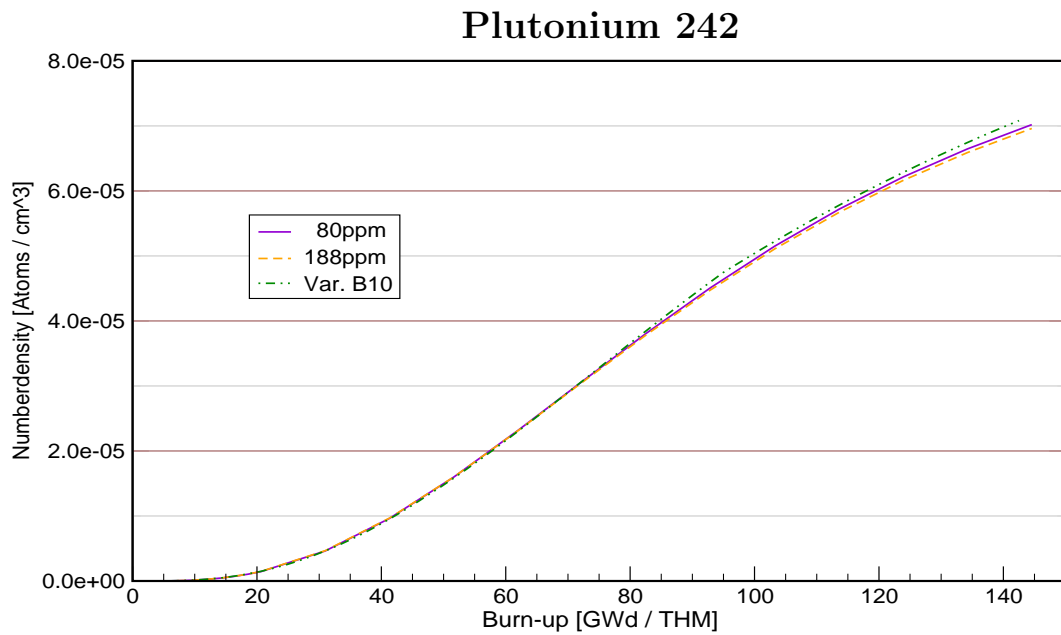


Figure B.28: Pu^{242} : The chart shows curves for variable boron modeling (376...0 ppm) and constant concentrations, V_m/V_s : 1.283 .

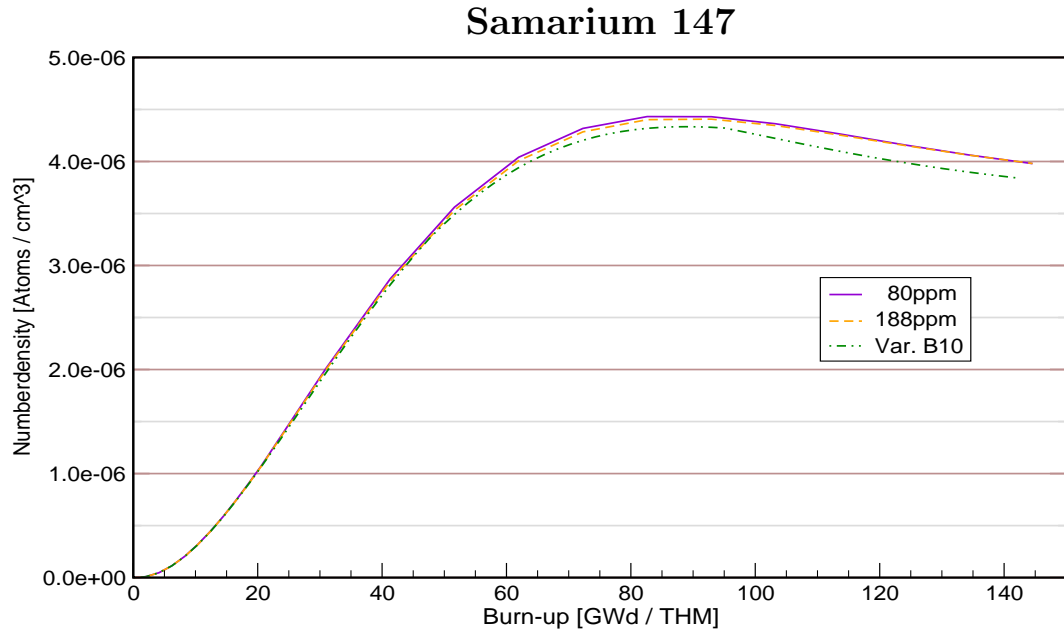


Figure B.29: Sm^{147} : The chart shows curves for variable boron modeling (376...0 ppm) and constant concentrations, V_m/V_s : 1.283 .

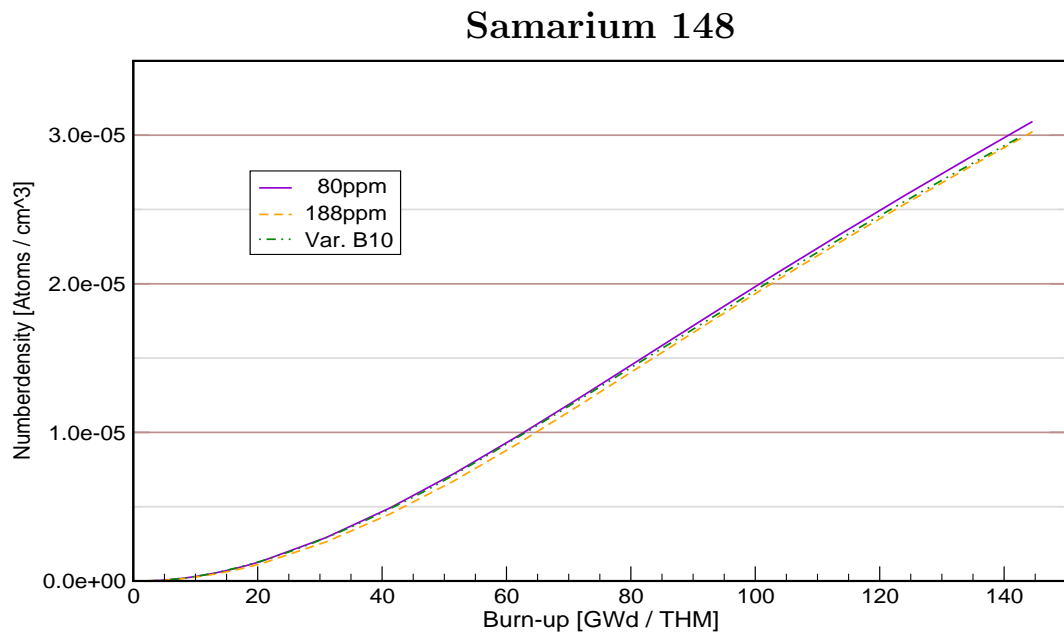


Figure B.30: Sm^{148} : The chart shows curves for variable boron modeling (376...0 ppm) and constant concentrations, V_m/V_s : 1.283 .

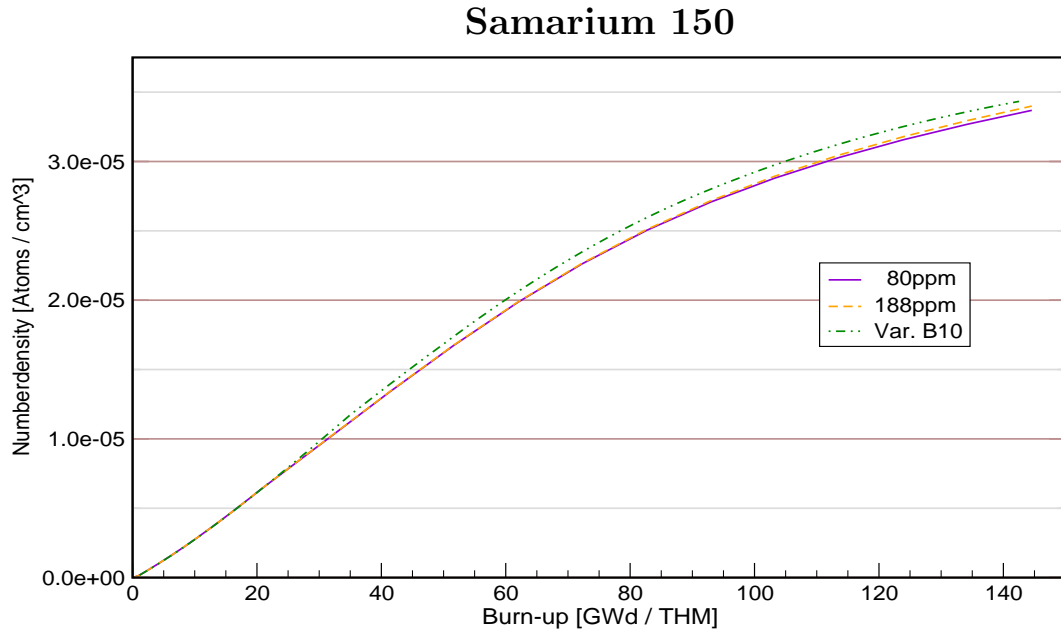


Figure B.31: Sm^{150} : The chart shows curves for variable boron modeling (376...0 ppm) and constant concentrations, V_m/V_s : 1.283 .

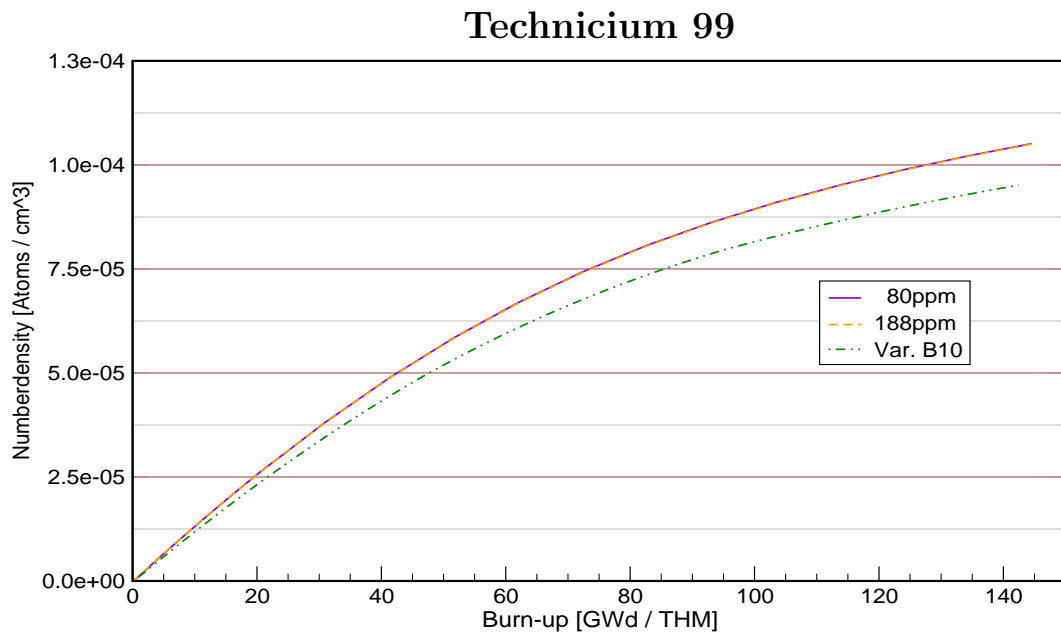


Figure B.32: Tc^{99} : The chart shows curves for variable boron modeling (376...0 ppm) and constant concentrations, V_m/V_s : 1.283 .

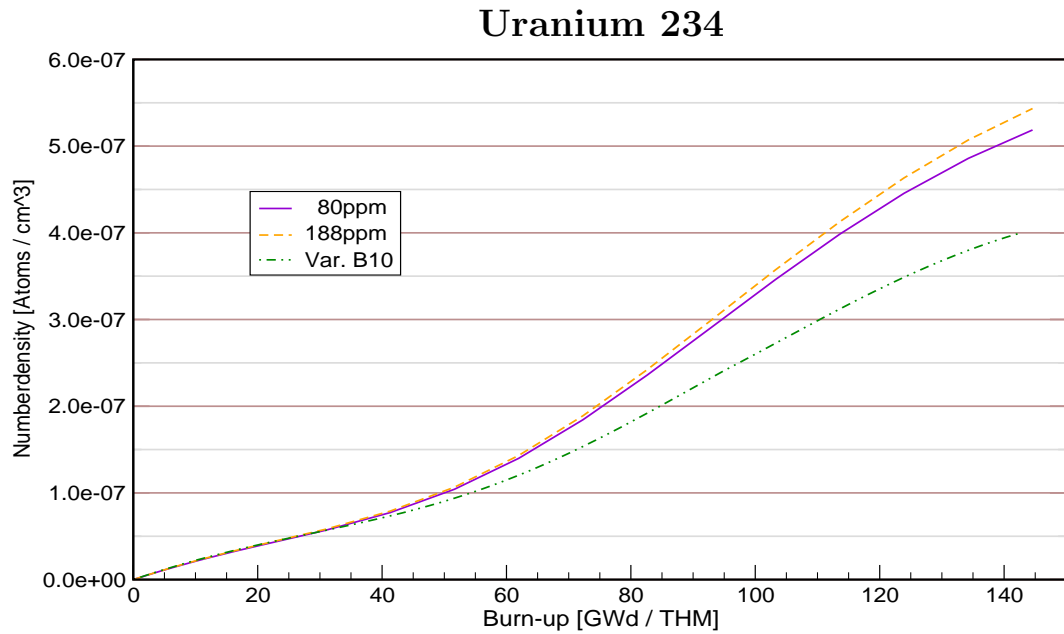


Figure B.33: U^{234} : The chart shows curves for variable boron modeling (376...0 ppm) and constant concentrations, V_m/V_s : 1.283 .

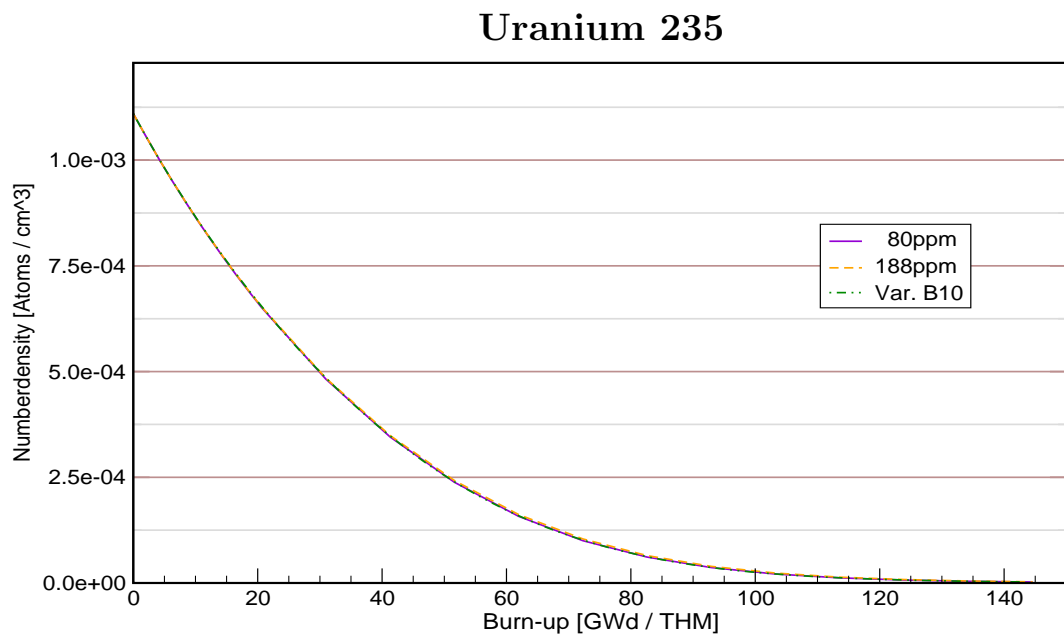


Figure B.34: U^{235} : The chart shows curves for variable boron modeling (376...0 ppm) and constant concentrations, V_m/V_s : 1.283 .

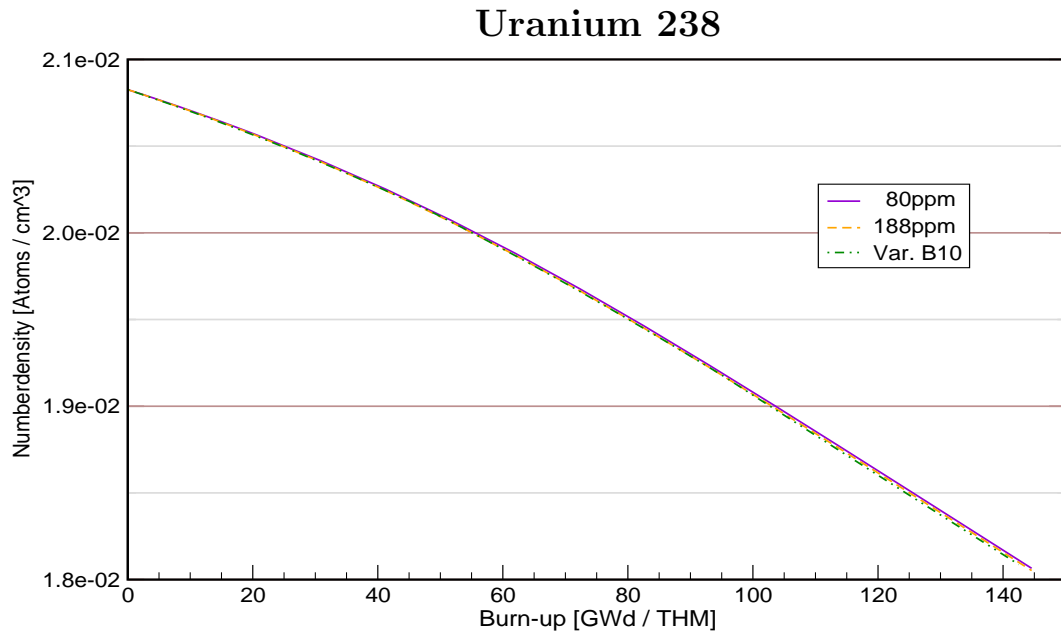


Figure B.35: U^{238} : The chart shows curves for variable boron modeling (376...0 ppm) and constant concentrations, V_m/V_s : 1.283 .

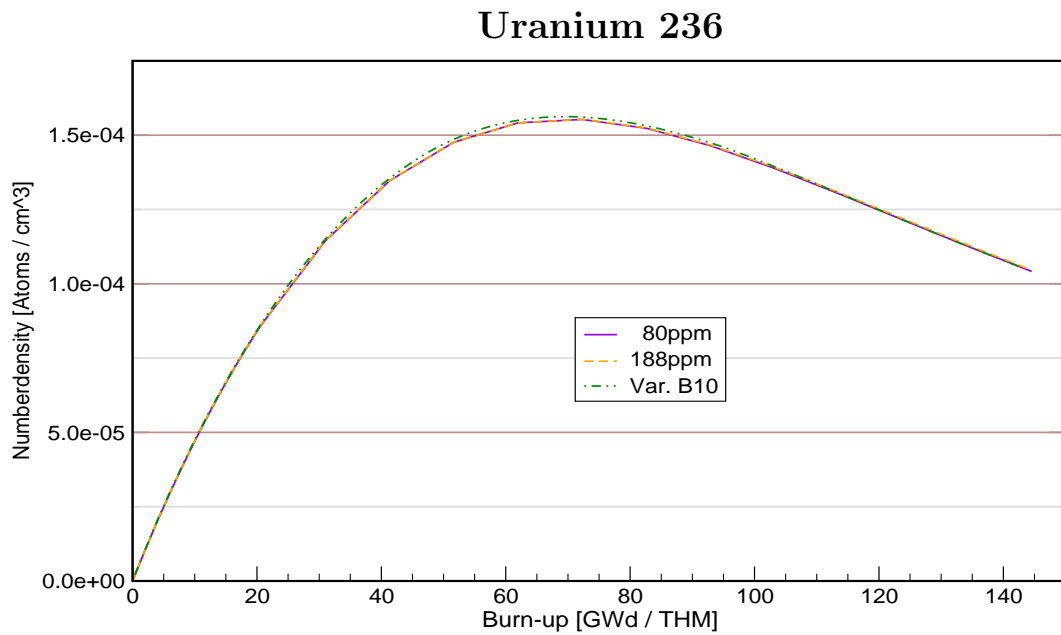


Figure B.36: U^{236} : The chart shows curves for variable boron modeling (376...0 ppm) and constant concentrations, V_m/V_s : 1.283 .

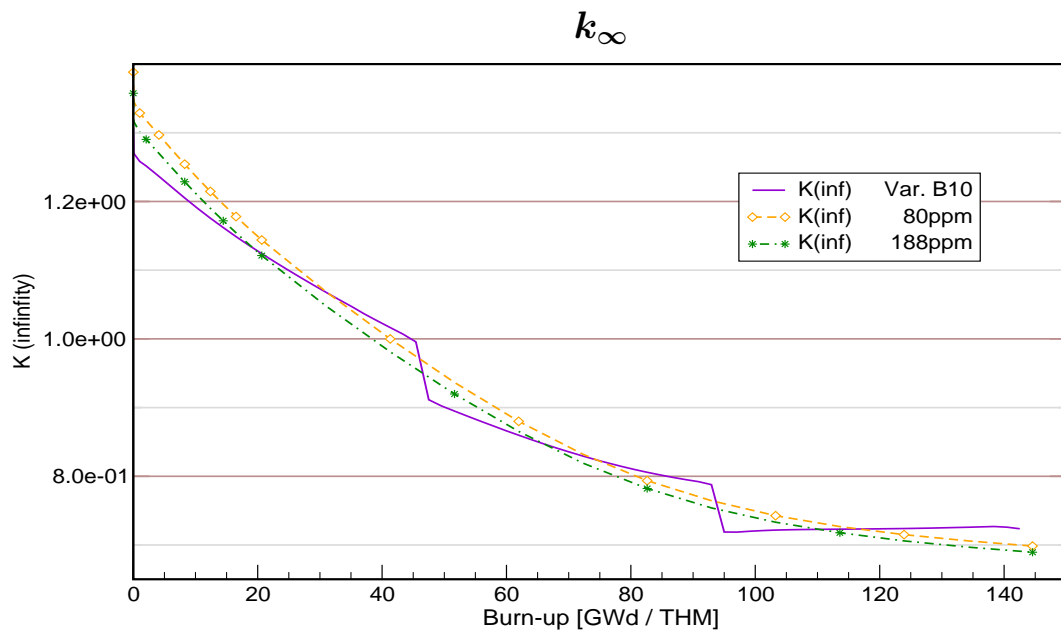


Figure B.37: The chart shows the k_{∞} curve for the variable and two constant concentrations, V_m/V_s : 1.283 .

B.4 LWR, comparison of three different lattices.

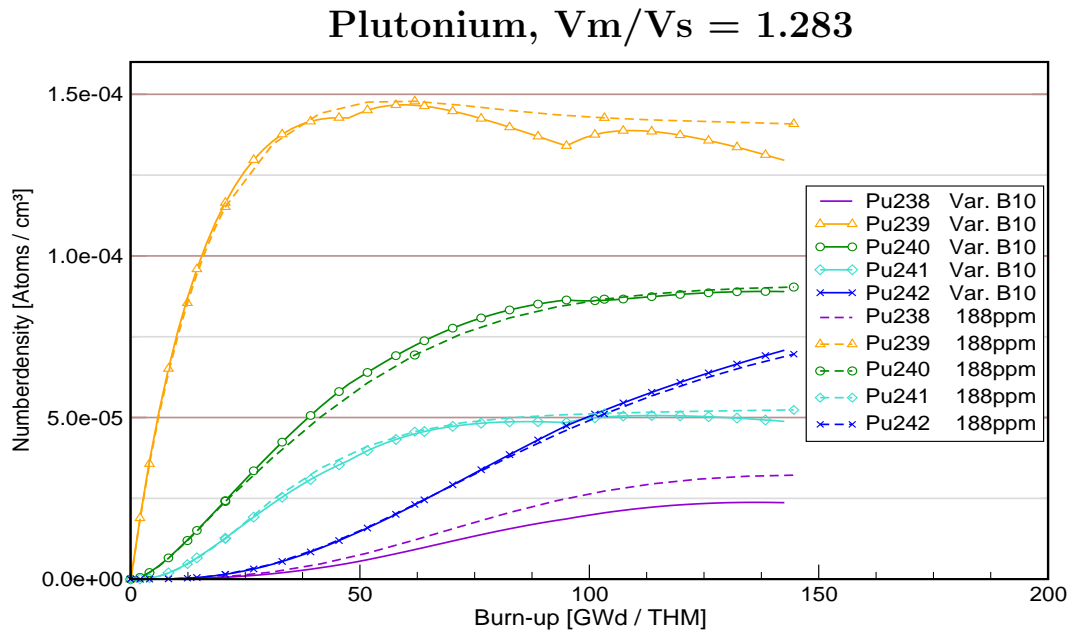


Figure B.38: Plutonium: the chart shows curves for constant 188 ppm and variable boron modeling (376...0 ppm) for $V_m/V_s = 1.283$.

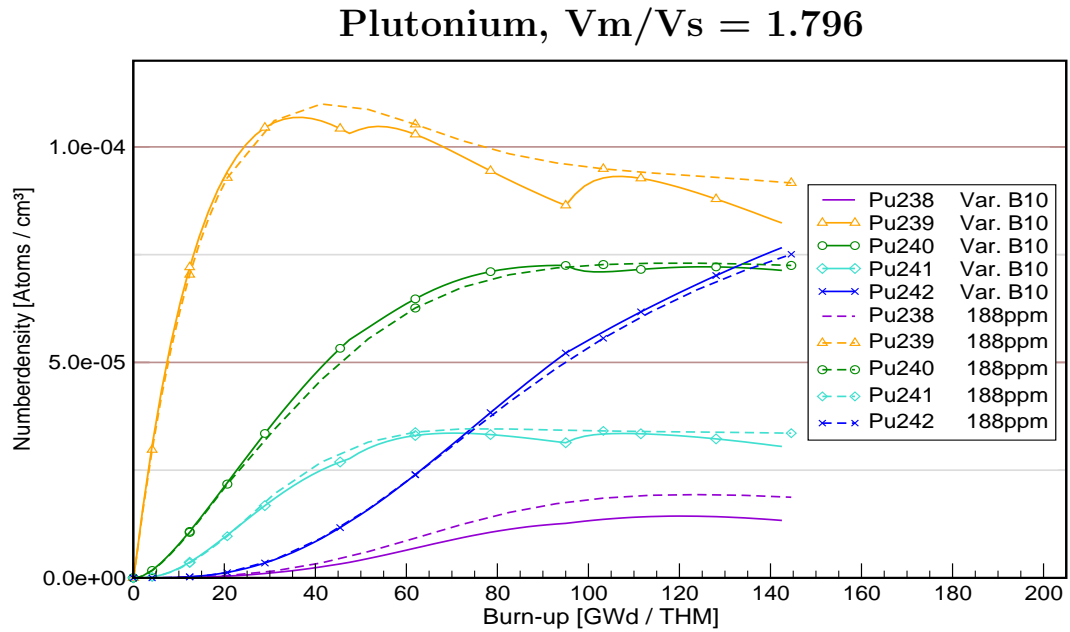


Figure B.39: Plutonium: the chart shows curves for constant 188 ppm and variable boron modeling (376...0 ppm) for $V_m/V_s = 1.796$.

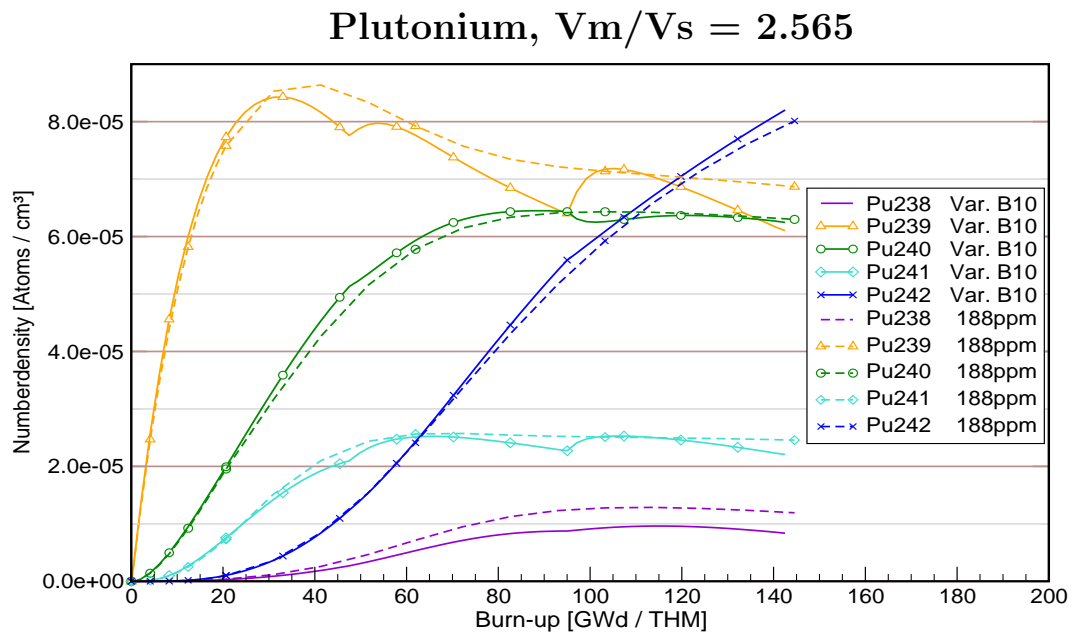


Figure B.40: Plutonium: the chart shows curves for constant 188 ppm and variable boron modeling (376...0 ppm) for $V_m/V_s = 2.565$.

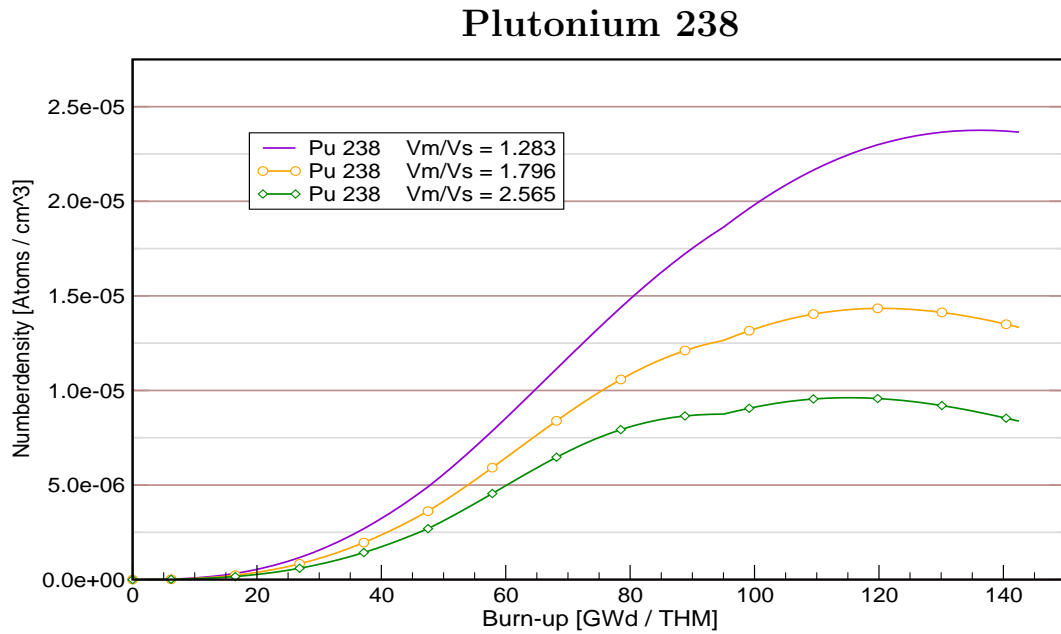


Figure B.41: Pu^{238} : The chart compares curves for variable boron modeling (376...0 ppm) for three different Vm/Vs ratios.

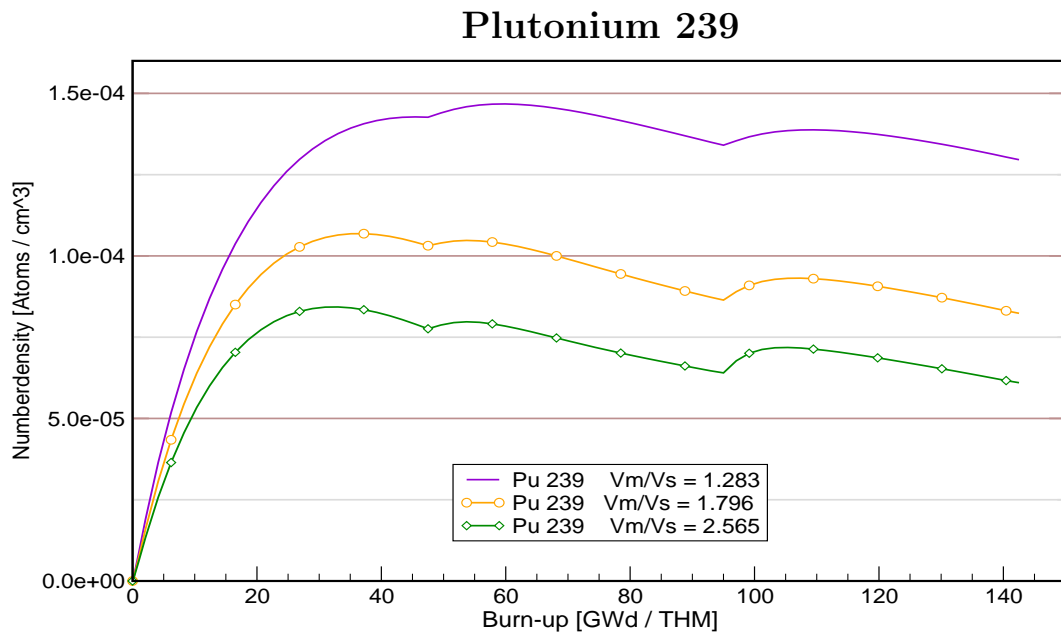


Figure B.42: Pu^{239} : The chart compares curves for variable boron modeling (376...0 ppm) for three different Vm/Vs ratios.

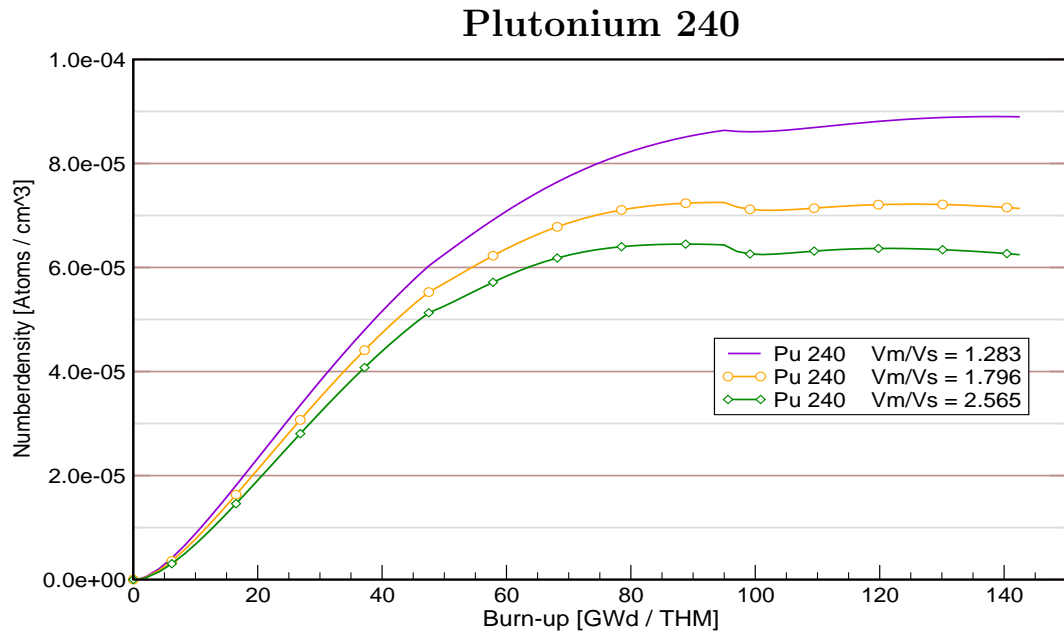


Figure B.43: Pu^{240} : The chart compares curves for variable boron modeling (376...0 ppm) for three different V_m/V_s ratios.

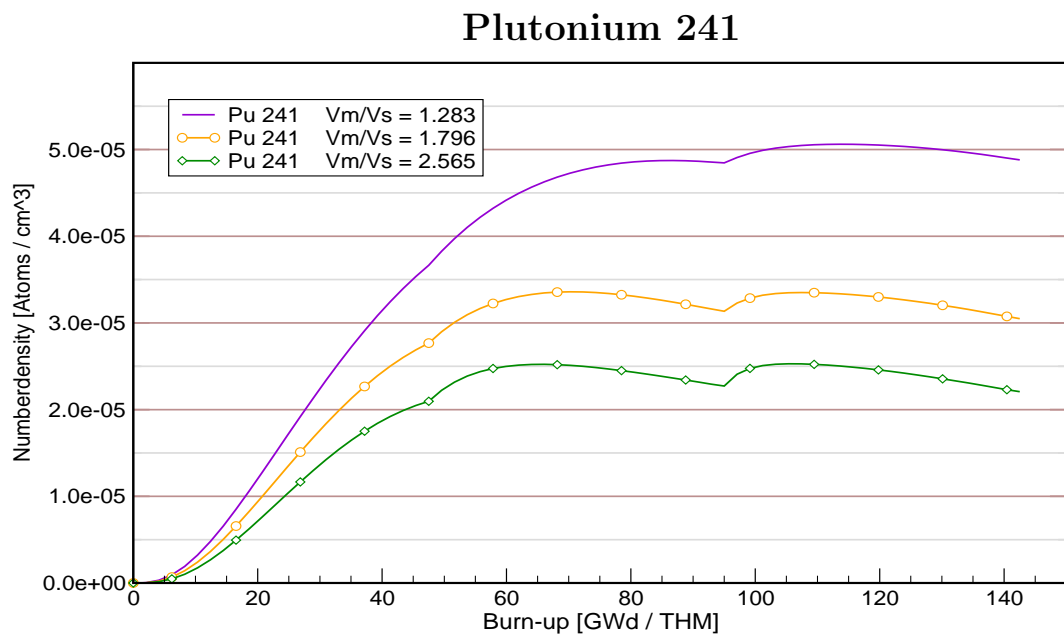


Figure B.44: Pu^{241} : The chart compares curves for variable boron modeling (376...0 ppm) for three different V_m/V_s ratios.

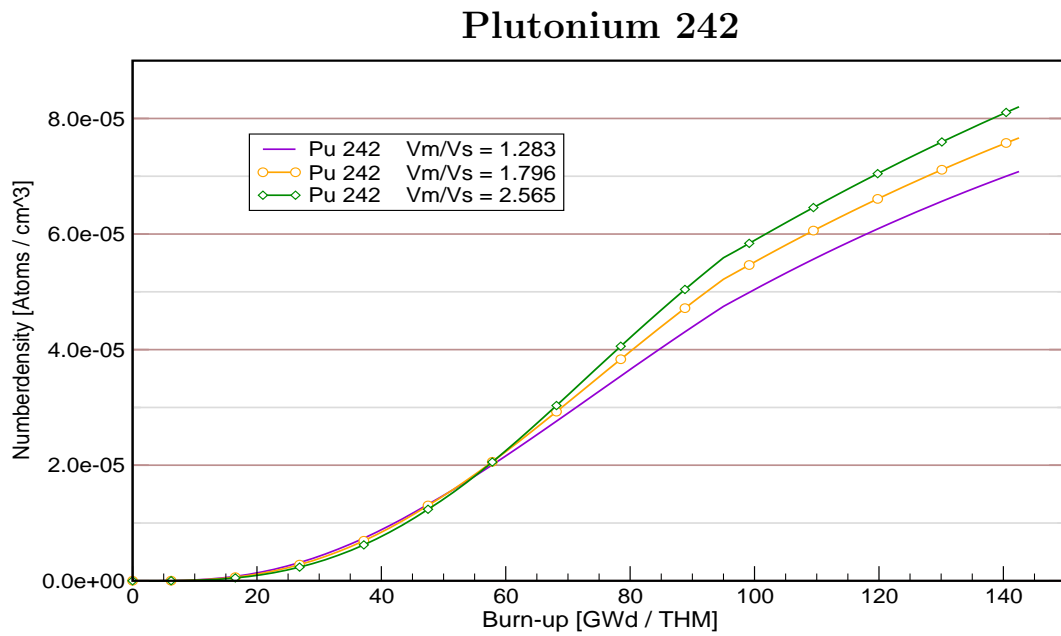


Figure B.45: Pu^{242} : The chart compares curves for variable boron modeling (376...0 ppm) for three different V_m/V_s ratios.

Bibliography

- [1] George I. Bell and Samuel Glasstone. *Nuclear Reactor Theory*. Van Nostrand Reinhold Company, 1970.
- [2] Michel Billaux. Frédéric Joliot / Otto Hahn Summer School. In *High Burn-up fuels for LWRs - Fuel Performance, Limits and Operational Safety Issues*, 2005.
- [3] C.H.M. Broeders. *Entwicklungsarbeiten für die neutronenphysikalische Auslegung von Fortschrittlichen Druckwasserreaktoren (FDWR) mit kompakten Dreiecksgittern in hexagonalen Brennelementen*. Technical report KfK 5072, Kernforschungszentrum Karlsruhe - Institut für Neutronenphysik und Reaktortechnik, 1992.
- [4] C.H.M. Broeders. Investigations related to the buildup of transurania in pressurized water reactors. Technical Report FZKA 5784, Forschungszentrum Karlsruhe - Institut für Neutronenphysik und Reaktortechnik, 1996. Version 26th March 1999.
- [5] Craig Brown et al. Extended power uprates and 2-yr cycles for BWRs - where do we go from here? *Nuclear Technology*, 151:120 et sqq., August 2005.
- [6] James J. Duderstadt and Louis J. Hamilton. *Nuclear Reactor Analysis*. John Wiley & Sons, Inc., 1976.
- [7] Ulrich Fischer and H.W. Wiese. Verbesserte konsistente Berechnung des nuklearen Inventars abgebrannter DWR-Brennstoffe auf der Basis von Zell-Abbrand-Verfahren mit KORIGEN. Technical Report KfK 3014, Kernforschungszentrum Karlsruhe, 1983.
- [8] Ministerium für Umwelt und Verkehr Baden-Württemberg. Abschlussbericht zu den Meldepflichtigen Ereignissen im Kernkraftwerk Phillipsburg, Block 2. Technical report, Ministerium für Umwelt und Verkehr Baden-Württemberg, 2003.

Bibliography 2

- [9] P.L. Frattini et al. Axial offset anomaly: coupling PWR primary chemistry with core design. *Nuclear Energy*, 2:123–135, April 2001.
- [10] Robert Gregg and Andrew Worrall. Effect of highly enriched / highly burnt fuels on fuel cycle costs, radiotoxicity, and nuclear design parameters. *Nuclear Technology*, 151:126 et sqq., August 2005.
- [11] M.L. Grossbeck et al. Development of improved burnable poisons for commercial nuclear power reactors. Technical report, Department of Nuclear Energy, University of Tennessee, September 2003.
- [12] Prof. Dr. h. c. mult. D. G. Cacuci. *Vorlesung Energiesysteme Teil 2*. Institut für Kerntechnik und Reaktorsicherheit an der Universität Karlsruhe (TH), 2003.
- [13] Kevin W. Hesketh. Frédéric Joliot / Otto Hahn Summer School. In *Principles of Reactor Economics*, 2001.
- [14] Kevin W. Hesketh. Frédéric Joliot / Otto Hahn Summer School. In *High Burn-up fuels for LWRs - Motivation and Physical Consequences*, 2005.
- [15] Michael J. Hignatsberger. IAEA Technical Committee Meeting. In *Utilisation of Thorium Fuel; Options in Emerging Nuclear Energy Systems*, November 1999.
- [16] Electric Power Research institute EPRI. PWR Primary Chemistry Update. *Radiation Control News*, Vol. 17, May 1993.
- [17] Forschungszentrum Karlsruhe. Karlsruher Nuklidkarte, December 1998.
- [18] L. Koch and S. Schoof. The isotope correlation experiment ICE - Final Report. Technical Report Nr. 2/81, ESARDA - European Safeguards Research and Development Association, 1981. Kernforschungszentrum Karlsruhe: KfK3337.
- [19] LexToday. <http://www.lextoday.de/bor>, September 2005.
- [20] LexToday. <http://www.lextoday.de/borsaeure>, September 2005.
- [21] Edwin S. Lyman. Public health risks of substituting mixed-oxide for uranium fuel in pressurized-water reactors. *Science & Global Security*, 9:1–47, 2000.
- [22] B. Merk. *Eine mehrskalige Näherungslösung für die zeitabhängige Boltzmann-Transportgleichung*. PhD thesis, Forschungszentrum Karlsruhe - Institut für Reaktorsicherheit, 2004.

- [23] Franz Mittelstaedt. *Elementarbuch der Kerntechnik*. Carl Hanserverlag München, 1968.
- [24] Francis Nordmann. Aspects on chemistry in french nuclear power plants. In *14th International Conference on the Properties of Water and Steam in Kyoto*, 2004.
- [25] P. Oberle. Erstellung einer 78-Gruppenkonstanten Bibliothek mit Energien bis 150 MeV für KAPROS. Master's thesis, Forschungszentrum Karlsruhe, Oktober 2004.
- [26] Patrick M. O'Leary and Michelle L. Pitts. Effect of burnable absorbers on PWR spent nuclear fuel. In *Framatom ANP*, March 2001.
- [27] Masahiko Osaka et al. Aspects of Pu-238 production in the experimental fast reactor JOYO. *Annals of Nuclear Energy*, 32:1024–1031, 2005.
- [28] Karl O. Ott and Robert J. Neuhold. *Introductory Nuclear Reactor Dynamics*. American Nuclear Society, 1985.
- [29] IAEA Safety-Standards. Design of the reactor core for nuclear power plants. Technical report, IAEA- International Atomic Energy Agency, 2005.
- [30] Hiroshi Sagara et al. Denaturing of plutonium by transmutation of minor-actinides for enhancement of proliferation resistance. *Nuclear Science and Technology*, 42:161–168, 2005.
- [31] Charlotta E. Sanders and John C. Wagner. Impact of integral burnable absorbers on PWR burnup credit criticality safety analyses. Technical report, Oak Ridge National Laboratory, 2001.
- [32] Jeffrey R. Secker et al. Optimum discharge burnup and cycle length for PWRs. *Nuclear Technology*, 151:109 et sqq., August 2005.
- [33] Eugen Shwageraus et al. Use of thorium for transmutation of plutonium and minor actinides in PWRs. *Nuclear Technology*, 147:53–68, 2004.
- [34] EaglePicher Technologies. Enriched boric acid for pressurized water reactors. inquiry.boron@eaglepicher.com, July 2002.
- [35] Fritz Ullmann. *Ullmann's Encyclopedia of Industrial Chemistry*. Wiley-VCH Verlag GmbH Weinheim, 7 edition, 2005.

Bibliography 4

- [36] J.C. Wagner and C.V. Parks. Parametric study of the effect of burnable poison rods for PWR burnup credit. Technical report, Oak Ridge National Laboratory, 2002.
- [37] John C. Wagner. Impact of soluble boron modeling for PWR burnup credit criticality safety analyses. In *American Nuclear Society: 13 International ANS/ENS 2003 Winter Meeting, "Nuclear Technology: Achieving Global Economic Growth While Safeguarding the Environment"*, 2003.
- [38] D. Woll. Introduction to the use of the UNIX-version of the karlsruhe program system "KAPROS". Technical report FZKA 6280, Forschungszentrum Karlsruhe, December 2001.
- [39] A. Ziegler. *Lehrbuch der Reaktortechnik*, volume 1. Springer-Verlag Berlin Heidelberg, 1983.